# Progress in thermoplasmonics for solar energy applications

Guohua Liu [a,*], Jinliang Xu [a,*], Ting Chen [b], Kaiying Wang [c]

[a] *Beijing Key Laboratory of Multiphase Flow and Heat Transfer for Low Grade Energy Utilization, North China Electric Power University, Beijing, 102206, China*
[b] *School of Chemical and Environmental Engineering, Jianghan University, Wuhan, 430056, China*
[c] *Department of Microsystems, University of South-Eastern Norway, Horten 3184, Norway*

## ARTICLE INFO

## ABSTRACT

Plasmonics offer unprecedented control over light and stimulate fundamental research and engineering applications in solar energy. The surface plasmon resonance is responsible for both enhanced light scattering and absorption. The plasmon excitations in nanostructures can be tuned to control the hot-carrier emission. The damping dissipation of the kinetic energy of surface plasmons releases heat at nanoscale, which can be used to create high-performance nano-heaters and/or radiators. Spectrally and/or thermally engineered plasmonic nanomaterials attract considerable attention for solar energy application due to their distinct thermoplasmonic properties. In light of these advances, this paper provides a critical review of current research in thermoplasmonics with focus on its physic mechanisms, structure tuning strategies and solar energy applications. Basic mechanism of thermoplasmonics is described from the photothermal conversion and heat transfer physics to thermal-induced processes. Structure tuning strategies including self-tunable plasmons, plasmon coupling strategies and active plasmons with tunable gap distances are then fully discussed in terms of their principles and structures. Based on the flourishing development of novel thermoplasmonic structures, potential applications ranging from solar collector, solar radiator, thermo-photovoltaic, solar desalination and sterilization, solar degradation and catalysis, to solar fuels, and solar fertilizers are additionally highlighted. The advantages of using plasmonics over the conventional technologies are identified, and the areas where important basics involved when the thermoplasmonics bringing into application are stressed throughout the text. Finally, we provide our views on future challenges in solar thermoplasmonics, together with a few suggestions for further developments of this technology. This work would bring new insights and inspire innovative works on designing thermoplasmonics for solar energy application.

## Contents

* Corresponding authors.
  *E-mail addresses:* liuguohua126@126.com (G. Liu), xjl@ncepu.edu.cn (J. Xu).

# 1. Introduction

Energy utilization with zero carbon emissions is critically important for increasing prosperity and economic growth of our society [1,2]. Burning fossil fuels for heat generation in energy sector is a major contributor to global carbon dioxide emissions. Heat accounts for half of global energy consumption, and currently 10% of which is produced from sustainable sources such as solar, wind, geothermal, and wave energy. Among which, solar energy is one of the most abundant renewable resources, and great efforts have been made on solar thermal and solar cell technologies to achieve energy and environmental sustainability. Solar thermal technology enables more efficient use of solar energy than in photovoltaics, accounting for 7% of the renewable thermal energy, which highlights significant need for development of solar-to-thermal conversion technologies [3,4].

Solar thermal technologies including trough collectors, linear Fresnel and dish reflectors, power tower systems normally operate in a local temperature of 300–1200 °C to produce electricity. These high local temperatures only can be gained by concentrating 100–1000 solar powers. This requires implanting large-scale solar plants that in turn needs large footprint investments [5]. Solar thermal technologies are critically important not only for producing heat and power, but also for the setup of chemical plants that use the heat to drive chemical reactions such as carbon dioxide conversion, water splitting, and chemical synthesis [3,6–11]. However, such high-temperature plants may only become market-competitive by the development of low-cost, compact solar absorbers to attain high operating temperature.

Plasmonic absorbers allow fantastic light control at nanoscale that is attractive for fundamental research and engineering applications of solar energy [12–14]. Metallic nanostructures interact with incident lights by photoexcitation of surface plasmon resonance (SPR), featuring with remarkable and unique optical responses. These plasmon resonances enable the structures to trap light energy, concentrate the energy near the structure surface and convert it into energetic electrons and heat [15–17]. For a long time, light absorption and consequent temperature increase are thought as detrimental
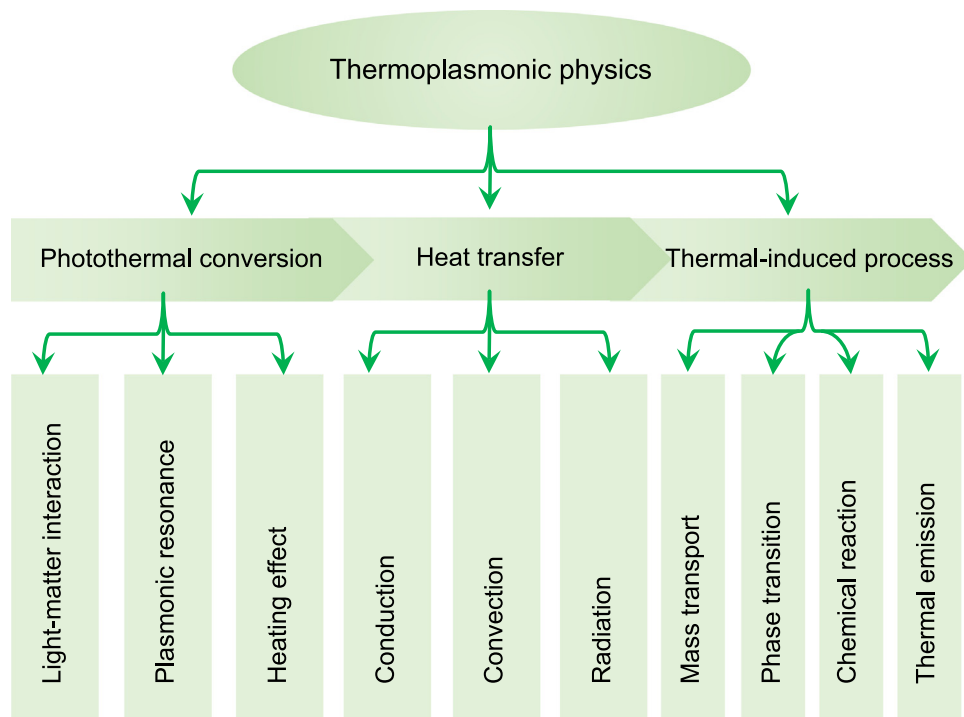
Thermoplasmonic physics

Photothermal conversion → Heat transfer → Thermal-induced process

Light-matter interaction

Plasmonic resonance

Heating effect

Conduction

Convection

Radiation

Mass transport

Phase transition

Chemical reaction

Thermal emission

**Fig. 1.** Overview of thermoplasmonic fundamentals covered in this article.

factors to optical plasmonics [18–21]. Recently scientists recognized that this enhanced energy absorption, turning plasmonic structures into nanoscale heat sources controlled by light, provides a unique way to tune the thermal-induced processes [22–25].

Thermoplasmonics exploit the damping loss of resonance as heat source that is natural to be used for transforming solar energy into heat [13,26,27]. Early demonstration has found applications in solar steam generation, sterilization and seawater desalination [10,28–31]. However, the particle-enabled systems are restricted by their low-stability upon solar irradiation, causing the particles to aggregate over time. Recently, thin-film plasmonic systems surmount this limitation and found wide applications in solar-driven interfacial evaporation, thermophotovoltaics, solar radiator etc [12,32–35]. Such improvements usually result from the improved charge separation and/or increased light absorption by the active layer. Another aspect of thermoplasmonics lies in solar chemistry for activating reactions. This includes $CO_2$ reduction into fuels and water splitting to produce hydrogen [8,36–42]. There has also been interest in using plasmon resonances to drive nitrogen transformations for producing ammonia or fertilizers [43–46]. Increased reaction yields as well as improved selectivity are the focus of these reactions. Although major breakthroughs in solar energy conversion are yet to be realized, the initial successes provide sufficient motivation to further explore the novelties of thermoplasmonics.

Herein, we discuss recent advances in solar thermoplasmonics that investigates the use of plasmonic nanostructures as heating sources for solar energy application. This paper is structured as follows: The basics of thermoplasmonics are revisited from light-to-heat conversion and heat transfer physics to thermal-induced processes (Section 2). Three categories of thermoplasmonics consisting of self-tunable structures, plasmon-coupling structures and active plasmon structures are then discussed in terms of their principles and configurations (Section 3). The development of novel thermoplasmonic structures thus opens access to the potential applications including solar desalination and radiator, thermo-photovoltaic, photothermal catalysis, solar sterilization and disinfection, solar fuels, and fertilizers (Section 4). The advantages of using plasmonics over conventional technologies are identified, and the areas where important basics involved when the thermoplasmonics bringing into application are stressed. Finally, the concluding remarks are made, and future challenges together with a number of suggestions are outlined for further developments of this technology (Section 5).

## 2. Thermoplasmonic fundamentals

An overview of thermoplasmonic fundamentals is shown in Fig. 1. The discussion begins with photothermal conversion, including an introduction to the light–matter interactions before proceeding to the most crucial plasmon resonances and their heating effects. Next, heat transfer is addressed in details on how the energy dissipation resulting in a local increase of
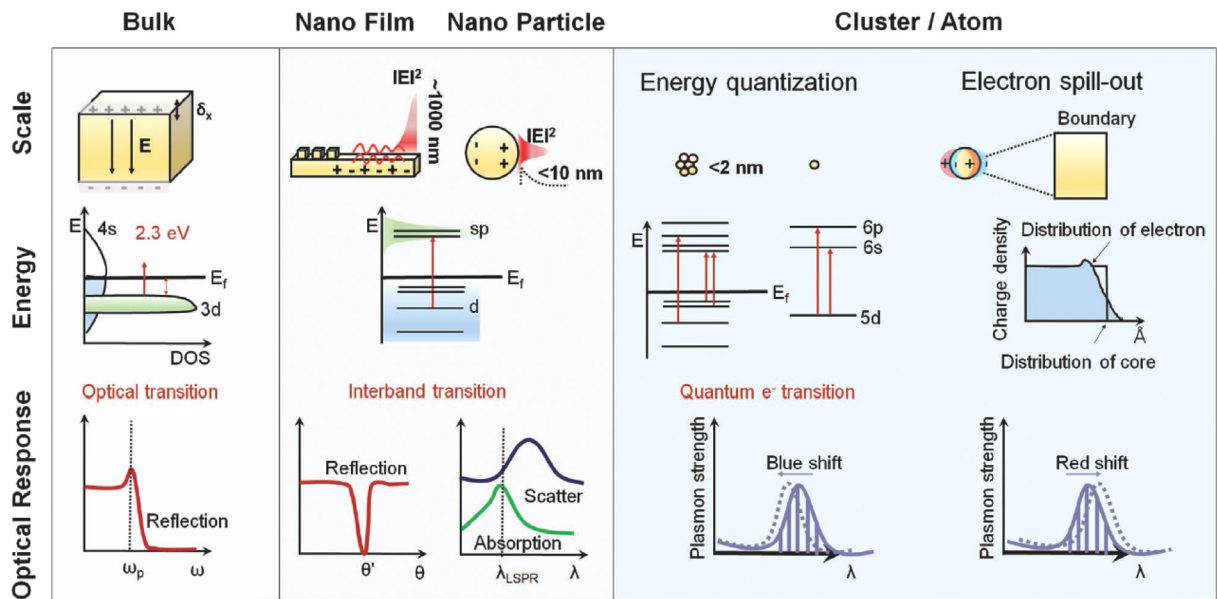
**Fig. 2.** Light–matter interaction in different structure sizes.
*Source:* Reproduced with permission [49].
© 2021 Wiley-VCH.

temperature. Moreover, the thermal-induced processes are discussed with emphasis on mass transport, phase transition and stress wave, chemical reaction, refractive index variation and thermal emission, which is relevant to solar energy application.

## 2.1. Photothermal conversion

### 2.1.1. Light–matter interaction

Light–matter interactions depend on the wavelength/frequency of incident light, material optical properties and the size of illuminated object [47,48]. Light is an oscillating wave of electromagnetic energy, consisting of a magnetic and electric field that is orthogonal to each other. In free space, the wave front moves forward at the speed of light $c = 3 \times 10^8$ m/s. The wavelength $\lambda$ is useful in denoting the size of wave and the oscillation frequency is denoted as $f$. One can define the wavelength and oscillation frequency via the relation $c = \lambda f$. Light–matter interaction is dominated by electric interactions, and the propagation of an oscillating electric field is described by:

$$\boldsymbol{E}\left(\boldsymbol{r}, t\right) = \boldsymbol{E}_0 \cos\left(-\omega t + \boldsymbol{k}\boldsymbol{r} + \phi\right) = Re\left\{\boldsymbol{E}_0 \exp(i\left[-\omega t + \boldsymbol{k}\boldsymbol{r} + \phi\right])\right\} \tag{1}$$

where $\boldsymbol{E}_0$ denotes the maximum amplitude of electric field, $\phi$ is a phase offset, $t$ and $\boldsymbol{r}$ are time and location, respectively. $\omega = 2\pi f$ is the angular frequency and $\boldsymbol{k}$ is the wave vector with a magnitude given by the wave number $k = 2\pi/\lambda$.

Optical response of a medium can be descried by a precise parameter of electric permittivity [47,51]. The permittivity $\varepsilon$ is the ratio of the amplitude $D$ of electric displacement field induced in the material and the amplitude of incident electric field, i.e. $\varepsilon = \varepsilon_r\varepsilon_0 = D/E$, here $\varepsilon_0$ refers to the free-space permittivity and $\varepsilon_r$ denotes the relative permittivity of material. The relative permittivity is a complex number. Its real part describes the energy stored within the medium, while the imaginary part is related to energy dissipation. Another optical property of matter is the refractive index $n = \sqrt{\varepsilon_r}$, which is helpful in normalizing the wavelength ($\lambda = \lambda_0/n$) and speed of light ($v = c/n$) that propagates through the material. The effective propagation speed will be reduced if the real component is large. The wave energy will be absorbed in the medium when the imaginary part is large, causing deconstructive interference.

The propagation wave interacts with the constituent atoms when light propagates through a bulk material. The energetic charged carriers are sensitively perturbed by the induced electric field from the wave. This carrier perturbation creates oscillating charges that scatters light anisotropically in the plane perpendicular to the wave polarization (Fig. 2). Because the impact of single atom is negligible, the net effect of a bulk medium is a secondary electromagnetic wave with the same frequency, but the phase delay and amplitude are determined by the material permittivity. The net field within the medium is thus defined by the superposition of the secondary and incident waves.

Nanostructures that is much smaller than the wavelength offer new possibilities for the excitation of plasmon resonances [21,52–56]. The interaction between light and nanostructure is described by Maxwell's equations, and the
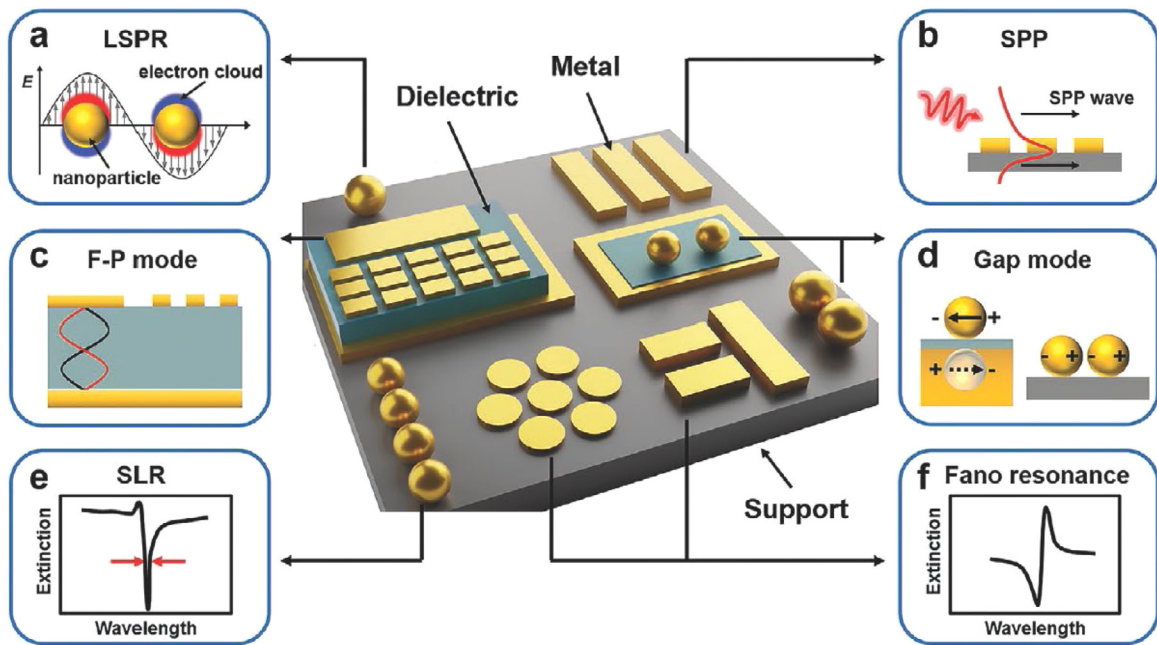
**Fig. 3.** Plasmonic resonances. (a) LSPR. (b) SPP. (c) F–P cavity mode. (d) Gap mode. (e) SLR mode. (f) Fano resonance.
*Source:* Reproduced with permission [50].
© 2021 Wiley-VCH.

induced electric field can be derived from Helmholtz equation [22,51]:

$$\nabla \times \mu_r^{-1} (\nabla \times \boldsymbol{E}) - \left(\frac{\omega}{c}\right)^2 \varepsilon_r (\omega) \boldsymbol{E} = 0 \tag{2}$$

here $\mu_r$ denotes the magnetic permeability, $\varepsilon_r (\omega)$ is the complex relative permittivity of media. This approach is appropriate to many nanostructures larger than 5 nm.

When the nanostructure is smaller than 10 nm as that of atom and cluster, quantum effects appear [49,57]. The distances between the occupied and unoccupied states increase as the decrease of structure size, resulting in discrete energy levels. Electronic transition between quantized states amplifies the uncertainty of resonance frequency, therefore reducing the plasmon lifetime. As a result, the smaller the particle is, the higher the peak plasmon frequency and the lower the plasmon lifetime, leading to a broadening of spectral linewidth. Moreover, the surface screening effect must be considered under this condition. The screening effect resulting from localized d-band electrons attenuates as the decrease of particle size, contributing to a further blue-shift. However, the spill-out effect of s-band electron reduces the quantum size effect on the d-band electron, increasing the resonance frequency. Nevertheless, the overall interaction is relatively weak due to the small volume.

*2.1.2. Plasmonic resonances*

Plasmon resonances refer to the excited oscillation of electrons upon external irradiation when the light frequency coincides with the oscillation frequency of electrons. Metallic nanostructures are the most common plasmonic materials since they have large electron densities [58,59]. The optical and photothermal performances are greatly dependent on their plasmonic modes (Fig. 3). There are two basic modes, including propagating surface plasmon polaritons (SPP) and local surface plasmon resonance (LSPR). Besides, plasmon coupling modes support the nanostructures with more desired optical properties to enhance their performance [56,60–63]. Due to the flexible design, the plasmon-hybrid metasurfaces demonstrated for the simultaneous excitation of the above modes [64–66]. They also underpin new resonances including Fabry–Pérot (F–P) cavity plasmon mode, surface lattice plasmon resonance (SLR), and Fano resonance [50,62,67,68]. These modes together endow the plasmonic structures with interesting properties unattainable by the basic mode.

The individual nanostructure normally supports LSPRs in which the free electrons oscillate with the incident photon at a specific frequency (Fig. 3a). The light–matter interactions include scattering and absorption. Scattering is the process in which the object radiates that light back into the surrounding medium. Absorption occurs when the incident light causes either an electronic or vibrational transition within the object, and the photon energy is retained within the object. LSPR of a particle can be roughly described by the particle's polarizability. The dipole moment is given [27]:

$$\boldsymbol{p} = \alpha \boldsymbol{E}_0 \quad \text{where} \quad \alpha (\omega) = (1 + \psi) V \varepsilon_0 \frac{\varepsilon (\omega) - \varepsilon_m}{\varepsilon (\omega) + \psi \varepsilon_m} \tag{3}$$

here, the term $\alpha$ is the polarizability of sphere, $\varepsilon_m$ and $\varepsilon(\omega)$ denote the permittivity of medium and nanostructure, respectively, $\psi$ is shape factor with a value of 2 for sphere. Surfaces with high curvature or sharp features have large values. To a polarized sphere of radius $R$, the light absorption also can be characterized by the extinction cross section $C_{ext}$ that is the sum of absorption ($C_{abs}$) and scattering ($C_{sca}$) cross sections [23,69]:

$$C_{ext} = C_{sca} + C_{abs} = \frac{k^4}{6\pi}|\alpha|^2 + kIm(\alpha) \tag{4}$$

$$C_{sca} = \frac{k^4}{6\pi}|\alpha|^2 = \frac{8\pi}{3}k^4R^6\left|\frac{\varepsilon - \varepsilon_m}{\varepsilon + 2\varepsilon_m}\right|^2 \tag{5}$$

$$C_{abs} = kIm(\alpha) = 4\pi kR^3 Im\left(\frac{\varepsilon - \varepsilon_m}{\varepsilon + 2\varepsilon_m}\right) \tag{6}$$

The absorbed energy is then released by either heat generation and/or photon emission. Quantum yield of photon emission is usually below 1% [70], highlighting all the absorbed energy is converted into heat.

SPP normally occurs at the interface linking metal and dielectric with assistance of grating structure or refractive index prism (Fig. 3b) [51,71]. Momentum and energy conservation must be satisfied in order to excite SPPs. The period arrangement of plasmonic structures inducing momentum mismatch between light wave and SPP wave is often used to design SPP mode, because such mismatch can be easily tailored by the morphology and period of structures, as well as incident angle of irradiation. Moreover, the decay length of SPP is found to be ∼50 times larger than that of LSPR. This propagation characteristic makes it possible to spatial separation of the electron collection sites and optical excitation, preventing the background interference.

F–P cavity mode presents in the plasmonic array with multiple stacks. Fig. 3c shows a sandwich structure with two metal mirrors and an optical dielectric medium, in which the electromagnetic wave interference may occur in the dielectric cavity. The plasmon wavelength is highly dependent on the cavity thickness. The internal electric field and plasmon bandwidths can thus be tuned by selecting appropriate materials and rational designing of the nanostructures [50,62,64]. Effective plasmonic coupling of the structures to a photonic cavity has been achieved by use of a plasmon element with large linewidth to replace one of the mirrors [72]. This coupled photonic–plasmonic system can concentrate surface plasmons, and thus the radiative damping can be significantly decreased.

Gap mode is induced by the near-field coupling when a plasmonic structure is close to another plasmonic element (film or particle) (Fig. 3d) [60]. A red-shift of resonance wavelength is observed as the presence of a neighboring film due to the nanostructure reduces the restoring force acting on the excited electrons. In addition, the near-field electromagnetic in the gap is strongly enhanced due to high light concentration in the small space. The interaction strength of different plasmonic structures increases with the decrease of the spacing. Therefore, precise control of the gap distance is critical important for gap mode. For particle–film system, an image dipole will be created in the film with an opposite charge distribution. These anti-symmetric dipole oscillations enable a magnetic resonance that is favorable for solar absorption.

Strong near-field and far-field coupling will be initiated if the arranging plasmonic structures in periodic arrays, leading to SLRs (Fig. 3e). The collective resonance of SLRs can suppress the radiative damping [62]. The nature property of SLR can be disclosed by assistance with the dipole approximation model. Each plasmonic element in this approximation is assumed as a dipole. For an infinite array, spectral width of the plasmon is determined by Im($\alpha^{-1}$-S), where $\alpha$ is the polarizability of an isolate particle, S is the retarded dipole sum from other particles. SLR mode thus can be easily modulated since the $\alpha$ and dipole sum S are determined by the structure parameters such as particle size, morphology as well as the period [50]. However, SLR cannot be excited if the particle size is too small. This is because the dipole sum may not offset the particle relaxation effect. Otherwise, out-of-plane plasmon resonances can promote SLR generation with high quality.

The multi-pole resonance and radiative dipolar coupling in complex hybrid nanostructures cause Fano resonance, which exhibits distinctly asymmetric spectral profiles (Fig. 3f) [62,67]. Fano resonances are normally occurring on the symmetry-breaking nanostructures with or nanoparticle clusters, in which the sharp sub-radiant and broad super-radiant plasmon modes typically show high-order and dipole feature modes [50,73]. Line-shape engineering in Fano resonance can produce narrow asymmetric resonance profiles with a sharp spectral contrast. Furthermore, the near-field of electric field is also greatly amplified at the resonance frequency.

An important characteristic of plasmon resonance lies in its ability to localize electromagnetic fields. Plasmonic particle can squeeze light to nanoscale size, leading to great enhancement of the electric field near particle surface [74,75]. In a dipolar limit, the field enhancement (**E/E**$_0$) is given by [27]:

$$\left(\frac{\boldsymbol{E}}{\boldsymbol{E}_0}\right)_s = \frac{(1+\psi)\varepsilon_m}{\varepsilon + \psi\varepsilon_m} \tag{7}$$

Experimental measurement and numerical calculation for 110 nm silver sphere show a near-field intensity about 20 times of the incident field (Fig. 4). For bowtie structures with small gap, the enhancements above 1000 can be predicted [21]. Such enhancement is of great interest in solar energy harvesting owing to the enhancement location is closest to the structure surface, which is the primary interface for solar energy harvesting or chemical reactions.
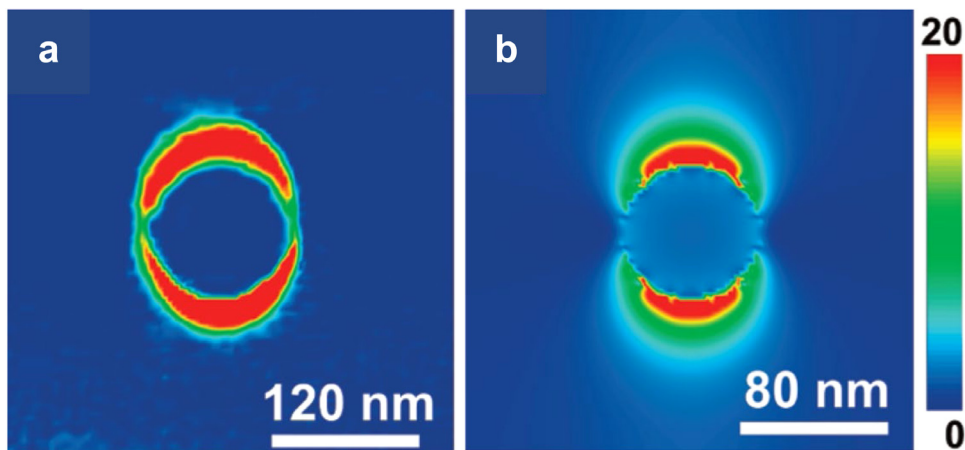
**Fig. 4.** Electric-field enhancements around Ag particle. Experimentally measured (a) and FDTD calculated (b) electric field-intensity maps.
*Source:* Reprinted with permission [74].
© 2010 American Chemical Society.
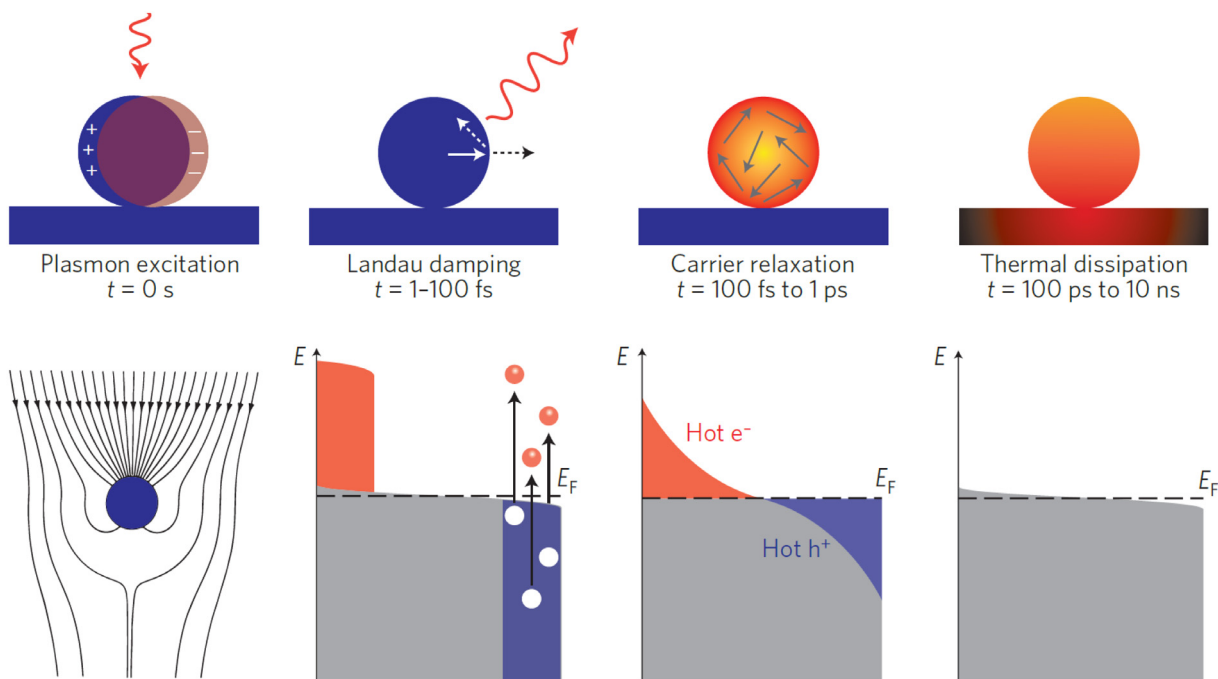


**Fig. 5.** The dominant processes involved in heat generation: Photoexcitation and relaxation of plasmon resonance with typical time scales.
*Source:* Reproduced with permission [15].
© 2015 Nature Publishing Group.

### 2.1.3. Heating and collective effect

A basic understanding of plasmon heating is illustrated in Fig. 5. Following energy transfer from the photons to electrons, and from the hot carriers to material lattice, the energy dissipation in lattices delivers energy as heat to the surrounding media. The whole process typically occurs at timescale of nanosecond [76,77]. From microscale point, LSPR is the coupled oscillation of electrons. The coherent oscillation lasts for a very short time in the order of a few femtoseconds [78]. The excited plasmons then decay either radiatively by photon re-emission (scattering) or nonradiatively by creation of hot carriers (absorption) to relax plasmonic energy [15,79]. The radiative and nonradiative dephasing routes are two competing mechanisms, and the branching ratio of these two decay is determined by radiance of the plasmon mode. It is not possible to entirely turn off the radiative decay because that would prevent the efficient light-based excitation of the plasmon in the first place. In the radiative damping, energy is dissipated by elastic scattering

of incident photons, and is a preferred pathway for large particles with size above 20 nm. The far-field scattering efficiency as a function of wavelength is determined by the dark-field scattering spectra of particles. In non-radiative decay, the particle directly absorbs photon energy, producing highly energetic non-thermal carriers (hot carriers) through Landau damping, which is the favorable path for small nanoparticles. Such charge carriers have a transient, non-thermal energy distribution with approximately flat shape up to the excitation photon energy [80]. The non-thermal electron–hole pairs scatter with other carriers to form high-temperature Fermi–Dirac thermal distribution within ∼100 fs. These hot carriers are then relaxed to thermal energy by electron–electron scattering on a time scale from 100 fs to 1 ps [51,58]. Finally, the heat is diffused to the surrounding by thermal conduction following a long timescale at 100 ps–10 ns, leading to global temperature increase. The timescale of the eventual heat diffusion to environment depends on multiple factors that including the particle composition, size and geometry, surface states, and metal–adsorbate interactions, etc.

From macroscale point, the electronic oscillation results in energy dissipation via Joule effect. Based on Poynting's theorem, this energy dissipation is written as [23,47,51]

$$Q = \iiint q dV = \iiint \frac{1}{2} Re \left( \boldsymbol{J}^* (\boldsymbol{r}) \cdot \boldsymbol{E} (\boldsymbol{r}) \right) dV = \iiint \frac{1}{2} \varepsilon_0 \omega \mathrm{Im} \left( \varepsilon (\boldsymbol{r}) \right) \cdot |\boldsymbol{E} (\boldsymbol{r})|^2 dV \tag{8}$$

where $q$ is the loss density of electromagnetic power and $\boldsymbol{J}$ is the current density. This heat generation also can be facile calculated using the absorptive cross-section [22,26]:

$$Q = C_{abs} I = C_{abs} \frac{c \varepsilon_0}{2} |\boldsymbol{E}_0|^2 \tag{9}$$

here $I$ denote the light irradiance. Dividing the dissipated energy rate by the light intensity, then derives another expression of the absorptive cross-section:

$$C_{abs} = \frac{Q}{I} = \frac{1}{c \varepsilon_0 |\boldsymbol{E}_0|^2} \iiint \varepsilon_0 \omega \mathrm{Im} \left( \varepsilon (\boldsymbol{r}) \right) \cdot |\boldsymbol{E} (\boldsymbol{r})|^2 dV \tag{10}$$

The absorptive cross-section is a quantity of interest to determine plasmonic heating. Analytical and numerical methods are often used to calculate the values.

For a sphere particle, the temperature increase in particle and surrounding is estimated as [23,24]:

$$\delta T = \begin{cases} \delta T_P \frac{R}{r} & r > R \\ \delta T_P & r \leq R \end{cases} \quad \text{where} \quad \delta T_P = \frac{C_{abs} I}{4 \pi \kappa R} \tag{11}$$

where $R$ is particle radius and $\kappa$ is thermal conductivity of medium. Fig. 6 a–e show the calculated field profiles of a gold particle with radii of 100 nm in water. The temperature increase reaches ∼50 K when the absorption power is 1 $\mu$W. A uniform electric field inside particle is observed under the resonance wavelength, while the retardation effect brings an obvious non-uniformity in energy absorption (Fig. 6c). Nevertheless, the temperature is uniform distributed over the whole particle (Fig. 6d).

The heating effect is amplified in presence of several particles or particle arrays [83,84]. Accumulative effect and Coulomb interaction between particles account for the collective heating. The scalar temperature fields from individual particle are added to generate the overall temperature profile. The more particles, the stronger the temperature increases. However, this total heat is different from the sum heat of all particles due to the partial screening of fields inside particles or the plasmon shift driven by Coulomb interaction between particles. So the resultant heat depends on not only the inter-particle distance, but also particle number $N$ and arrangements. The temperature increase of particle $j$ coupled with the neighboring particle $i$ heating is written as [12,23,85]:

$$\delta T_j = \frac{C_{abs,j} I}{4 \pi \kappa R} + \sum_{i \neq j} \frac{C_{abs,i} I}{4 \pi \kappa |r_i - r_j|} \tag{12}$$

The last term may dominant even for a sparse particle array [86]. This originates from the long-range temperature diffusion effect (Fig. 6f). The significance of collective effect can be evaluated by a dimensionless number $\xi = p^2/3R\varnothing$ [23, 81], where $p$ is an average neighboring interparticle distance, and $\varnothing \sim p \sqrt{N}$ is the feature size of particle distribution. The collective effects play dominate role when $\xi < 1$ (Fig. 6 g). In practice, ignoring the collective effect will lead to an underestimation of plasmonic heating.

### 2.2. Heat transfer

As the temperature increases within a control volume, heat inevitably dissipates into the surroundings. This process is referred to heat transfer [87]. The extent to which the temperature increase depends on how the heat can be dissipated efficiently. There are three mechanisms to be consideration: conduction, convection, and radiative as in Fig. 7 [82,88,89]. We are interested in the heat transfer rate $Q$ that is the same amount of absorbed energy. So the total heat transfer rate is the sum of the heat transfer forms $Q = \sum_i Q_i$. While it should be noted that the conductive heat transfer is dominant in nanoplasmonic systems [47,51,90].
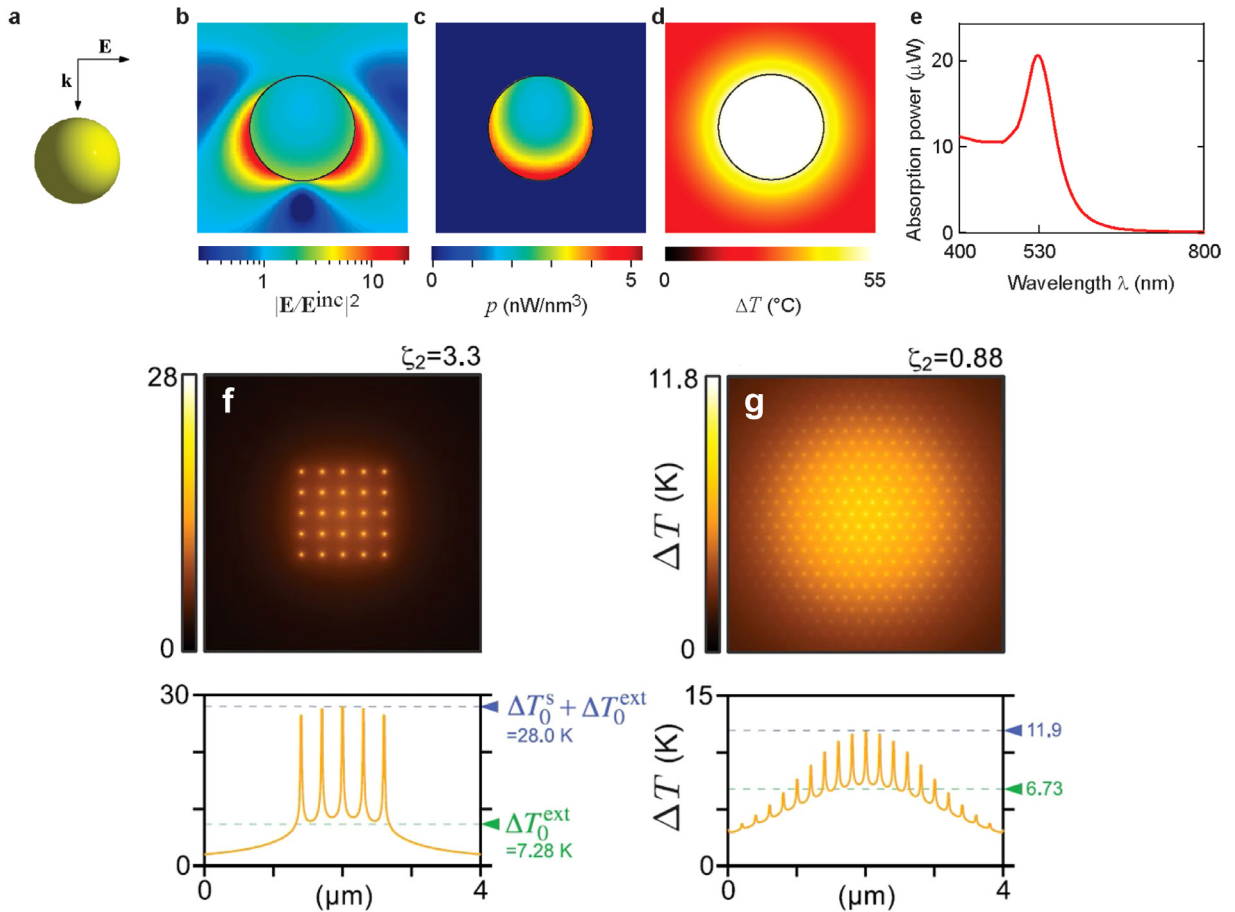
**Fig. 6.** Photothermal heating of gold particle in water. (a) Schematic, (b) Electric near-field intensity, (c) heat generation density, and (d) equilibrium distribution of the increase temperature. (e) Absorption power as a function of wavelength. Reproduced with permission [24]. © 2010 American Chemical Society. (f) Low sparsity characterized by the temperature rise around heat source. (g) the collective effect with an overall temperature offset. Reproduced with permission [81]. © 2013 American Chemical Society.
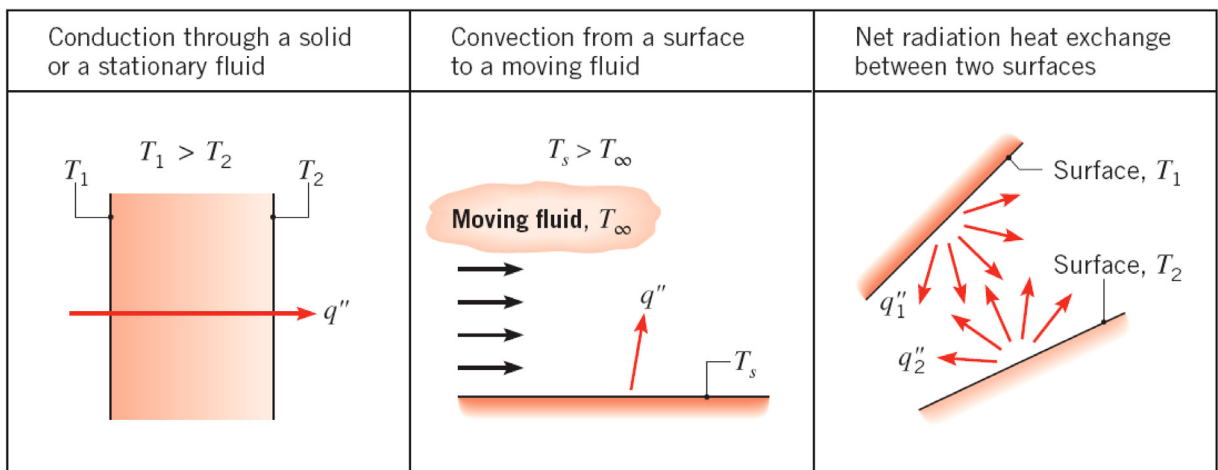


**Fig. 7.** Conduction, convection and radiation heat transfer.
*Source:* Reproduced with permission [82]
© 2017 Wiley-VCH.

### 2.2.1. Heat conduction

Thermal conduction occurs by direct collision of adjacent atoms/molecules that transfers the heat energy from one atom to another [82]. Such energy transfers from high-temperature region to low-temperature region when a temperature gradient exists in a body. The conductive heat flux in response to the temperature gradient is described by Fourier's law:

$$\boldsymbol{q}_{cd}\left(\boldsymbol{r}, t\right) = -\kappa \nabla T\left(\boldsymbol{r}, t\right) \quad \text{e.g.} \quad q_{cd} = \kappa \frac{T_1 - T_2}{L} \text{ for a one-dimensional slab} \tag{13}$$

where $L$ is the medium thickness. By considering energy balance for a control volume around the plasmonic heater, we can derive the temperature field via the equation [22,91]:

$$\rho C_p \frac{\partial T\left(\boldsymbol{r}, t\right)}{\partial t} = \nabla \cdot \left[\kappa \nabla T\left(\boldsymbol{r}, t\right)\right] + q_{cd}\left(\boldsymbol{r}, t\right) \tag{14}$$

Two key intrinsic quantities determine the heat dissipation in solving this equation: the thermal conductivity and the specific heat capacity $C_p$. Thermal conductivity denotes the heat conductive ability of a medium. The specific heat capacity is the required energy to increase the temperature of a medium normalized by the mass. We can do a lot with mathematical tools to linearize the equation or let it becomes an ordinary equation [47,82,91,92]. Then we can calculate the temperature distribution and/or heat flux in bodies.

### 2.2.2. Heat convection

Heat convection is driven by the temperature difference between hot surface and adjacent fluid [82,93]. Change of phase also belong to this case since the heat transfer flow comes from bubble emission or vapor condensation. Considering fluid flow over a hot surface, conductive heat flows from the surface into a laminar fluid layer, then proceeds into the neighboring fluid that is moving. Therefore, heat convection is the superposition of heat conduction and thermal transport into the flowing fluid. The total heat transfer is equal to a combination of the both energy transport. There are two types of convection, e.g. forced and free convection. The forced convection flow is driven by external fan or pump. While for the free convection, a buoyancy-driven flow is enabled by density differences upon temperature variations. The convective heat transfer is described by Newton's cooling law [82,94]:

$$q_{cv} = h_c\left(T_s - T_\infty\right) \tag{15}$$

where $T_s$ and $T_\infty$ are the surface and fluid temperature, respectively. $h_c$ is the convective coefficient that impacted by the fluid thermodynamic properties, and nature of fluid motion as well as the surface geometry. Convection is often the dominant heat transfer in macroscopic fluid systems. But it is useful to estimate if conduction or convection dominant in microscopic plasmonic systems. Rayleigh number is often used to identify the transition that denotes the time-scale ratio of convection of diffusion to convection [47,95]:

$$Ra = \frac{g\beta\Delta T R^3}{vD} \quad \text{where} \quad D = \frac{\kappa}{\rho C_p} \tag{16}$$

where $\beta$ is thermal expansion coefficient, $v$ denotes the fluid kinematic viscosity, $D$ is the thermal diffusivity. So for the nanoscale heating sources $Ra \ll 1$, the conduction is dominant, and then conversely convection is dominant for larger heat sources.

### 2.2.3. Thermal radiation

Radiation originates from the motion of charged particles, and the energy is emitted as photons. All surfaces emit thermal radiation, and the radiation rates depend on the absolute temperature and surface characteristics [96]. The near-field radiative heat transfer becomes dominant between nano-objects that can surpass the physic limits of far-field radiation [97]. The total power emitted by a sphere particle via radiative heat transfer is given by [47]

$$Q_{rd} = 4\pi R^2 \epsilon C_{sb} T^4 \tag{17}$$

where $\epsilon$ is the particle emissivity and $C_{sb}$ is the Stefan–Boltzmann constant. The net heat transfer rate between a heating surface and a large isothermal surface completely surrounding the heater are usually interested, which can be described by [82,93,98]

$$q_{rd} = \epsilon C_{sb}\left(T_s^4 - T_{sur}^4\right) \tag{18}$$

where $T_{sur}$ is the surrounding temperature. For the nano-heater, radiative heat transfer is generally inefficient. This is because the heat source is normally in physical contact with medium that has high thermal conductivity, which leads to the media has the same temperature as the heater.

### 2.3. Thermal-induced processes

Heat dissipation to surrounding medium is associated with thermal-induced processes. This is interest in solar energy application since a variety of processes are also likely to appear in the surrounding of solar absorber where the increased

temperatures cause an intensive heating or chemical reaction. Specifically, heat and mass transport normally occurs in solar collector and desalination process. Intensive heating and phase transition with stress wave propagation are beneficial for solar evaporation and sterilization. The knowledge of thermodynamic reaction is useful to support solar thermal chemistry. The content of refractive index variation and thermal emission underpin the design of solar radiator and thermophotovoltaic etc. In this section, the theoretical backgrounds are introduced to understand these processes.

*2.3.1. Mass transport*

Plasmonic heating induced mass transport includes Brownian motion, thermophoresis, and flow induced transport. Brownian motion refers to the nanoparticles in fluid random collided with molecules due to thermal disturbance from adjacent fluid. This is characterized by a simple relation [23,47,99]:

$$\langle \boldsymbol{r}^2 \rangle = 2dD_f t = \frac{dk_B T}{3\pi \eta R} t \tag{19}$$

where $\langle \boldsymbol{r}^2 \rangle$ represents the Mean Squared Displacement (MSD) in particle diffusion, $D_f$ denotes the diffusion coefficient, $k_B$ is Boltzmann constant, $\eta$ the fluid viscosity, $d$ the motion dimensionality and $t$ is the elapsed time. This equation indicates that the particle displacement is a function of its radius, the temperature, the nature of fluid and the timescale under consideration. This requires the particles in a thermal equilibrium state, but plasmonic heating unavoidably induces distinct gradients in thermal and viscous aspects. Diffusion with effective temperature and viscosity describes such dynamics known as hot Brownian motion, in which the induced diffusion coefficient may account for translational or rotational motion.

There also exists a kind of active Brownian motion [99,100], in which the dynamic can be decomposed into self-propelled motion and Brownian motion with a combined feature of active swimming and random fluctuations. Active particles take up energy from the external environment and use the energy to drive them out of equilibrium for active motion. MSD of such motion shows different behaviors upon distinct time scales (Fig. 8a) [101]. On short time scales, the inertia of particle is dominated, exhibiting ballistic motion. For long time scales, the inertial force is negligible and the particle exposed to an over-damped regime, in which the particles feature characteristic of Brownian motion, active motion, or effective Brownian motion. The magnitude of driving force and rotational diffusion coefficient determine the specific time scales for these regimes. The key factors including particle size and/or aspect ratio can be tuned to extend the regime of active motion and increase the effective diffusion coefficient.

In general, thermal gradients alter the particle dynamics at particle and fluid level with distinct features [12,110]. In the former case, thermophoresis drive the object motion in fluid along or away upon thermal gradient, inducing short-range motion. Thermophoresis is known as Ludwig–Soret effect that refers to the particle migration due to the existence of temperature gradients [12,23,111]. This can be used to manipulate nanoparticles in solution (Fig. 8b). Such motion is given by the equation [112,113]

$$v_T = -D_T \nabla T \tag{20}$$

where $v_T$ is the solute thermophoretic velocity, and $D_T$ is known as the thermophoretic mobility. The specific interactions at nanoparticle-solution interface determine the thermophoretic mobility, and its magnitude can be positive or negative in the light of solvent salinity [102,114]. The directional migration of nanoparticles under the external temperature gradient can be described as a mass flow,105:

$$\boldsymbol{J}_{\zeta,net} = \boldsymbol{J}_{\zeta,thermal} + \boldsymbol{J}_{\zeta,diffusive} = -\zeta D_T \nabla T - D_f \nabla \zeta \tag{21}$$

The former term of thermophoretic flux $\boldsymbol{J}_{\zeta,thermal}$ describes the migration of particles driven by temperature gradient, whereas the latter diffusion flux $\boldsymbol{J}_{\zeta,diffusive}$ gives the particle flow driven by concentration gradient. Here $\zeta$ is the local concentration. The significant of thermophoresis and diffusion can be examined by the Soret coefficient $S_T = D_T/D_f$, which judges the extent of depletion or accumulation of particles. This coefficient is a very sensitive term and its sign and magnitude can be altered by environmental temperature, surface chemistry of the objects, surface charge, and solvent properties. Under the steady state, the net flux vanishes. When $S_T > 0$, the objects move from hot to cold, showing a thermophobic behavior, while when $S_T < 0$, the objects migrate from cold to hot, exhibiting a thermophilic manner.

In the fluid level, the thermal gradients cause not only short-range motion of the particles driven by thermo-osmotic flow, but also long-range motion by either convection or thermoviscous flow. Convection is a bulk movement of fluid molecules, driving the particles towards the center of hot regions. This magnitude depends on the size of heat source, the temperature increase and the space confinement along vertical direction. To enhance convective flow, thermoplasmonic structures on substrate and coating of indium-tin-oxide on a substrate containing heat sources have been studied (Fig. 8c) [95,103]. Temperature gradients also contribute to variations in local viscosity. This has been verified by use of a moving heating spot to guide thermoviscous motion of particles [115]. The surface tension gradient enabled by temperature gradient intrinsically drives thermo-osmotic flows [116,117]. Due to the high temperature concentrated at interfacial region, a thermo-osmotic flow can be initiated with speeds above 100 $\mu$m/s, driving the surrounding particles gathering towards the heating source (Fig. 8d) [102,118,119].

*2.3.2. Phase transition and stress wave*

Phase transitions around plasmonic heater include particle reshaping/melting of absorber and/or phase-changes of the surrounding media [23,120–122]. Solar absorber with good thermal stability is thus important for large-scale applications.
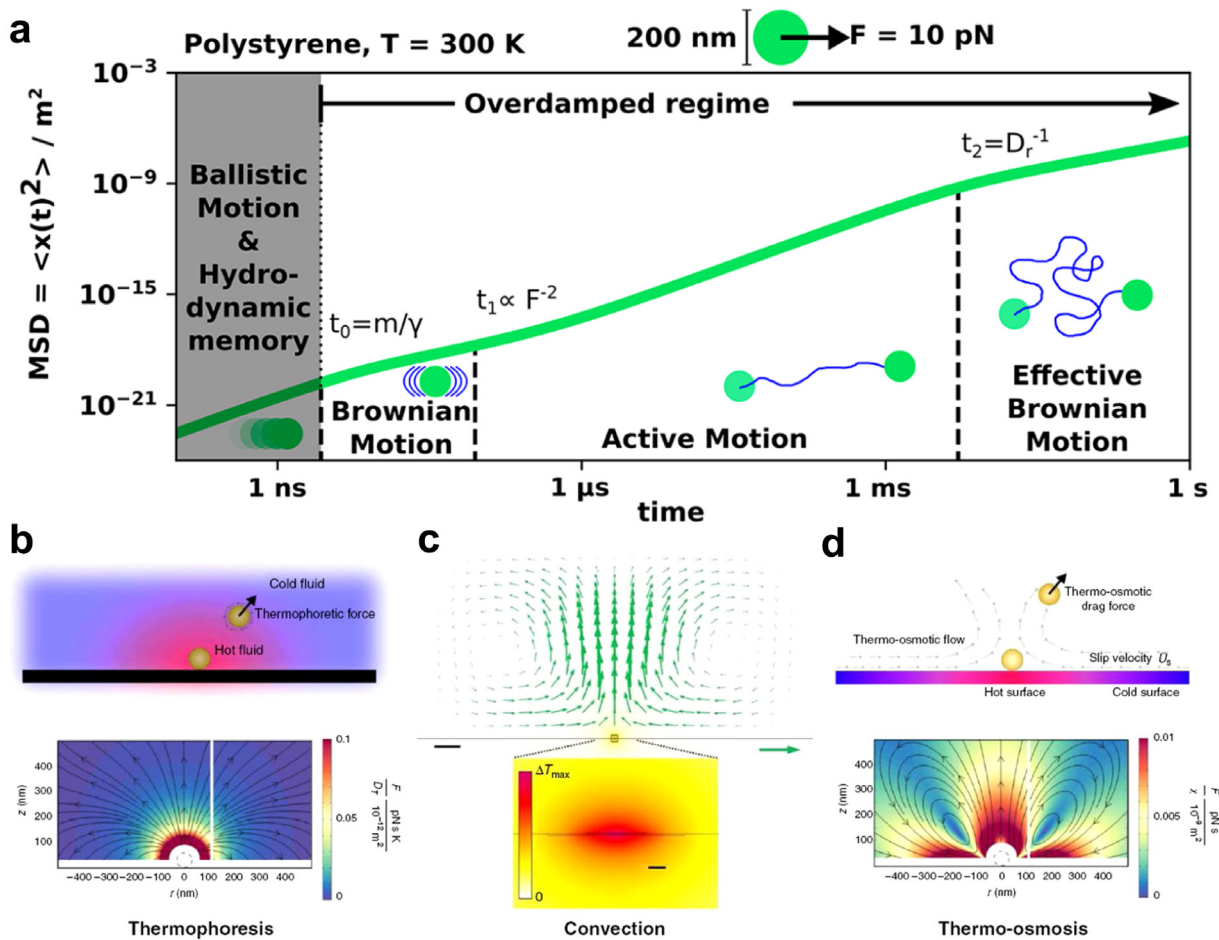
**Fig. 8.** (a) Four distinct regimes of active Brownian particle. Reproduced with permission [99]. © 2020 American Chemical Society. (b) thermophoresis, (c) convection and (d) thermo-osmosis. Reproduced with permission [102]. © 2017 American Chemical Society and [103] © 2014 Nature Publishing Group.

Due to insufficient stability, few state-of-the-art absorbers are qualified for operation over a wide range of temperature. For gold absorbers, the temperature must be controlled below 500 °C to prevent the thermal damage. To avoid reshaping, plasmonic elements can be embedded in $SiO_2$ matrix [123]. Recently, all-ceramic plasmonic absorbers based on TiN and $Al_2O_3$ demonstrated an unprecedented structural stability and an exceptional thermal stability at 1400 °C [124,125]. These findings put a key step towards fabricating thermally stable devices for harsh environments.

Phase transformations of surrounding media include water vaporization, melting of polymer and ice matrices, etc [28,120,126,127]. Liquid–vapor transition is the most typical example in solar steam generation. The simplest geometry of such device is often realized with particle arrays on substrate [128]. The liquid should be superheated before boiling initiated at the solid/liquid interface. Such a metastable state is very likely to occur around plasmonic particles. Temperatures as high as 230 °C have been evidenced around gold particles on a glass substrate. If the water is degassed, this temperature limit can even reach 300 °C. Bubbles will be nucleated via vaporization after approaching to a critical temperature threshold [129].

Fig. 9a shows the key processes of plasmonic bubble generation and dissipation [104]. The light absorption in metallic structure increases the surface temperature that promotes superheating in adjacent liquid. Once a bubble created, the dynamics is governed by a subtle interplay between various pressure forces, inertia of the fluid and surface tension, which can be described by Rayleigh–Plesset equation [130]:

$$\rho_L \left( R_b \ddot{R}_b + \frac{3}{2} \dot{R}_b^2 \right) + \frac{2\gamma}{R_b} + 4\eta \frac{\dot{R}_b}{R_b} = P_i(t) - P_\infty(t) \tag{22}$$

Where $R_b$ is the bubble radius, $P_i$ and $P_\infty$ are the internal and external pressures, respectively, and $\gamma$ is the fluid surface tension. $\rho_L$ is the mass density of liquid far from the particle. The overheated water drives the bubble growth by an influx of vapor into bubble. The formed bubble will contract without delay after turning off the heating laser. This is a result of
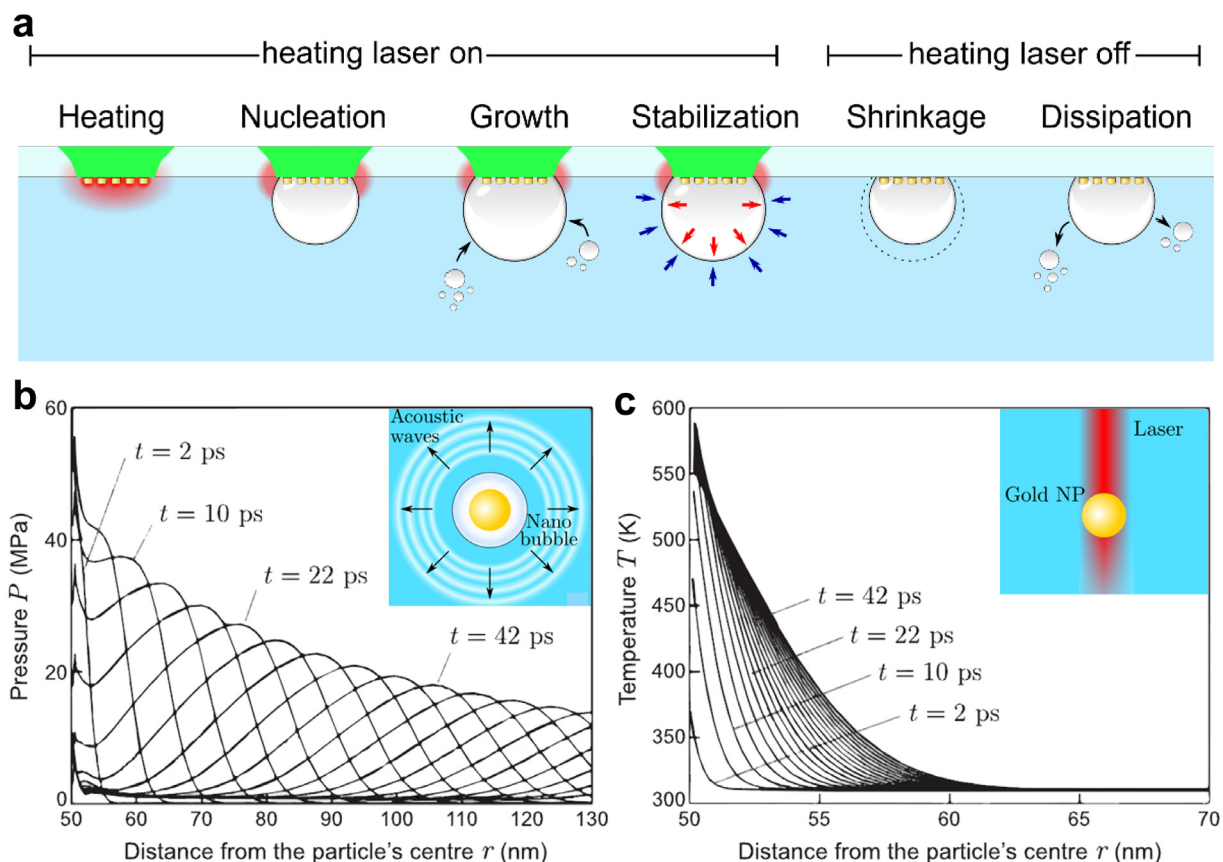
**Fig. 9.** Bubble dynamics and stress wave. (a) The bubble life cycle. Reproduced with permission [104]. © 2020 American Chemical Society. (b) Distributions of pressure and (b) temperature in water. Simulations are performed with a fluence of 60 J m$^{-2}$, a pulse duration of 200 fs, and a particle radius of 50 nm. Reproduced with permission [105]. © 2007 Elsevier and [106] ©2021AIP.

a drop in internal pressure caused by vapor condensation. Further vapor condensation into surrounding fluid is a process controlled by diffusion, and therefore the bubble dissipation process is very slow for a large bubble [131]. The bubble formation around plasmonic structure can substantially increase the structure temperature. This is particularly true for bubble formation around the particles in homogeneous media since the bubble is fully enveloping the nanostructure [132–134]. When investigating the bubble formation around a particle array on substrate, the particle–substrate contact area becomes important in determining the overall temperature [128,135]. Heat dissipating ability of the substrate has important implications for the structural integrity.

Plasmonic particles in water undergo a quick liquid-to-vapor phase change as the local temperature approaching to 300 °C. In this situation, vapor generation shares some similarities with that of explosive boiling [136,137], in which the transition are governed by ballistic vapor transport and Kapitza resistance, leading to the propagation of strong pressure waves and fast thermal diffusion at nanoscale (Fig. 9b and c) [105,135,137]. The term shock wave is common used in literature [138,139], which is a pressure wave of large amplitude that forms when some molecules constituting the medium happen to move faster than the sound speed. Its prominent feature lies in discontinuity in velocity, density and pressure. The pressure increase $\delta P$ can be expressed as function of the absorbed energy $Q$ by defining a Grüneisen parameter $\Gamma$ [23,106]:

$$\delta P = \Gamma Q \tag{23}$$

The wave emission concomitant to bubble generation paves a new way to destroy bacteria at a subcellular level [12,31]. This is because not only the thermal denaturation or the bubble formation is deleterious, but also the stress wave itself can induce mechanical damages.

### 2.3.3. Chemical reaction

Plasmon-driven solar chemistry is an important research area as that contributes to clean energy [14]. Solar catalytic reactions combined both the advantages of solar and thermal activation, the thermal effect has to be carefully considered
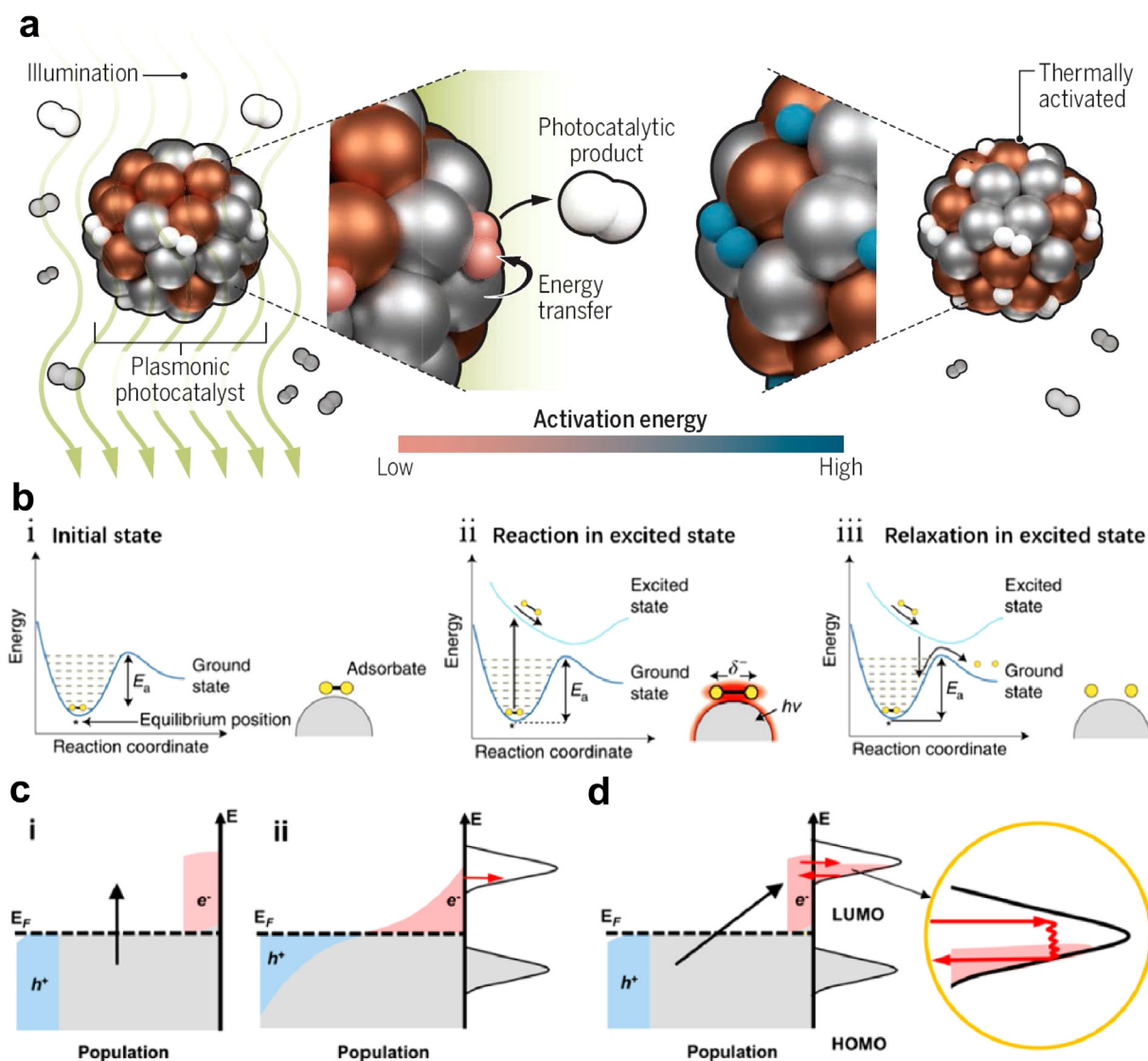
**Fig. 10.** Thermoplasmonic-activated chemistry. (a) Hot carriers in reducing the activation barrier of chemical reaction. Reproduced with permission [107]. © 2018 AAAS. (b) Plasmon-induced dissociation reaction, showing (i) the initial state and (ii) reaction and (iii) relaxation in the excited state of the molecule. Reproduced with permission [108]. © 2018 Nature Publishing Group. (c) Indirect hot electron transfer from metals to adsorbates: (i) nonthermalized distribution of hot carriers; (ii) Fermi–Dirac distribution of thermalized hot carriers. (d) Direct electron transfer. Reproduced with permission [109]. © 2017 American Chemical Society.

for understanding the underlying mechanism [36,140]. Thermoplasmonics controlling of light and heat at nanoscale can be used to promote chemical reactions. Behind mechanism for the improved reaction mainly comes from a local variation of temperature, near-field enhancement of electromagnetic field and hot-carrier injection [109,141,142]. The nonequilibrium states of hot-carriers resulted from plasmon decay can trigger reactions via thermal and/or nonthermal pathways, modifying the landscape of chemical reaction that is otherwise kinetically hindered (Fig. 10a) [107,143].

In thermo-catalytic systems, the reaction conditions are constrained by kinetic activity of catalyst and thermodynamics of reaction. The reaction involves several sub-processes such as adsorption of reactant molecules, activation of chemical bonds, formation of intermediates, conversion of intermediates into products, and desorption of product molecules [36,78]. The overall reaction is thus consisted of the above elemental steps and each step should surmount a specific $E_a$ value (Fig. 10b). The reaction rate constant $K$ and its molar activation energy $E_a$ are related via Arrhenius law [12,36]:

$$K \propto exp\left(-\frac{E_a}{RT}\right) \tag{24}$$

where $R$ is gas constant. This law depicts the thermal-enhancement of reaction rates since the plasmonic heating creates a temperature increase of the reactant under thermal equilibrium. Such heating undoubtedly lowers the $E_a$ that is beneficial to the overall reaction [108,144]. But the high temperature may reversely shift the thermal equilibrium towards product decomposition. Therefore, in consideration of the contradicting temperatures desirable for kinetics and thermodynamics, realization of higher yields beyond this thermal-equilibrium limit, which in turn reduces pressure and energy consumption, is highly desired [145].

Two categories of catalyst have been designed including pure plasmonic structures and plasmon-hybrid systems [109,146]. Plasmonic catalysis over pure metallic catalyst can be understood from plasmon decay to chemical bond activation and intermediate conversion. Hot electron is widely accepted as key role in the catalysis rather than the thermal effect. The plasmon decay of excitation promotes the hot carriers transferred to adsorbed molecules via direct or indirect energy transfer, creating adsorbate–metal complex states to promote redox processes (Fig. 10b c and d) [11,78,109,147]. The direct electron transfer contributes to the formation of hybridized surface states. This process has low transfer efficiency due to the relatively small transition dipole moments of molecule–metal composites. While the indirect electron transfer has a high transfer efficiency owing to the continuous distribution of hot-electrons near Fermi level, which is thus the primary excitation pathway.

Plasmon-hybrid systems are potential platforms for solar chemistry. The main advantage of this system lies in facilitating charge separation across the interfacial Schottky barrier [109,148]. The carrier lifetimes can be extended by spatially separation of hot electrons from holes over metal–semiconductor interface [149]. Besides, the depletion region built within semiconductor can sweep hot-electrons away from the metal–semiconductor interface, further reducing the charge recombination [150]. The hot-electron accumulation in semiconductor thus provides new opportunities to tune their energy levels. Moreover, active sites over semiconductor also prompt catalytic reactions. Therefore, these hybrid catalysts create synergetic effect in reducing the activation barrier of chemical reaction [151,152].

However, there are some limitations in using hot-electron pairs for chemical reactions [153]. These limitation origin from (1) fast relaxation time of excited carriers with large kinetic energies that restricts their mean free paths, and limits the effective volume to generate injectable carriers; (2) relatively low rate of excited carriers with high energies due to the constraint imposed by momentum conservation; and (3) constraints on magnitude and direction of the carrier momentum to avoid reflection at the interface. Moreover, the interplay between thermoplasmonic and catalytic properties, as well as the carrier transport in such systems has not been thoroughly investigated. It is also difficult to disentangle the thermal contribution from other effects in such systems. [140]

*2.3.4. Refractive index variation and thermal emission*

Temperature increase in plasmonic structure naturally diffuses over the surrounding medium. This would create variation of refractive index in the surrounding medium. Such variation can be expressed as a function of temperature variation using the coefficient *dn/dT* [23]:

$$\delta n = \frac{dn}{dT} \delta T \tag{25}$$

The temperature coefficient of refractive index for gas and solids are usually negligible, and only liquids feature appreciable values (e.g. at room temperature and normal pressure, BK7 glass :-0.125 · $10^{-4}$, water: $-0.9 \cdot 10^{-4}$, air: $-1 \cdot 10^{-6}$). Water is a common surrounding medium. The refractive index of water is often given up to 100 °C, which has a strong nonlinear variation of not only the temperature but also the wavelength. The coefficient values typically are small, but they are actually large enough to create measurable plasmonic effects, such as modification of plasmon resonance, building a thermal lens effect and an increase of scattering [154–159].

Thermal emission radiates electromagnetic energy in both space and time [50,160], which leads to broadband, omnidirectional photon emission towards far-field, with a spectral density related to the emitter temperature by Planck's law (Fig. 11a) [161,162].

$$I_{\lambda,b} (\lambda, T) = \frac{2hc^2}{\lambda^5 [exp (hc/\lambda k_B T) - 1]} \tag{26}$$

where $h = 6.626 \times 10^{-34}$ J is Planck's constant. According to Kirchhoff' law, the material emissivity is equal to its absorptivity for an arbitrary reciprocal object (Fig. 11b) [96].

$$\epsilon_\lambda = \alpha_\lambda < 1 \tag{27}$$

Metallic structures can be used for thermal emission due to the increased energy absorption at plasmon wavelength (Fig. 11c). The near-field radiative heat transfer is prominent in nanoscale systems where the size is much smaller than the emitted wavelength. When the particle assembling in close vicinity, the collective effect occurs and the heat power radiated by the structure is read [165,166]

$$Q_{rd} = 4\pi \int_0^\infty \epsilon_\lambda (\lambda) I_{\lambda,b} (\lambda, T) d\lambda = 4\pi \int_0^\infty \epsilon_\lambda (\lambda) \frac{2hc^2 C_{geo}}{\lambda^5 [exp (hc/\lambda k_B T) - 1]} d\lambda \tag{28}$$
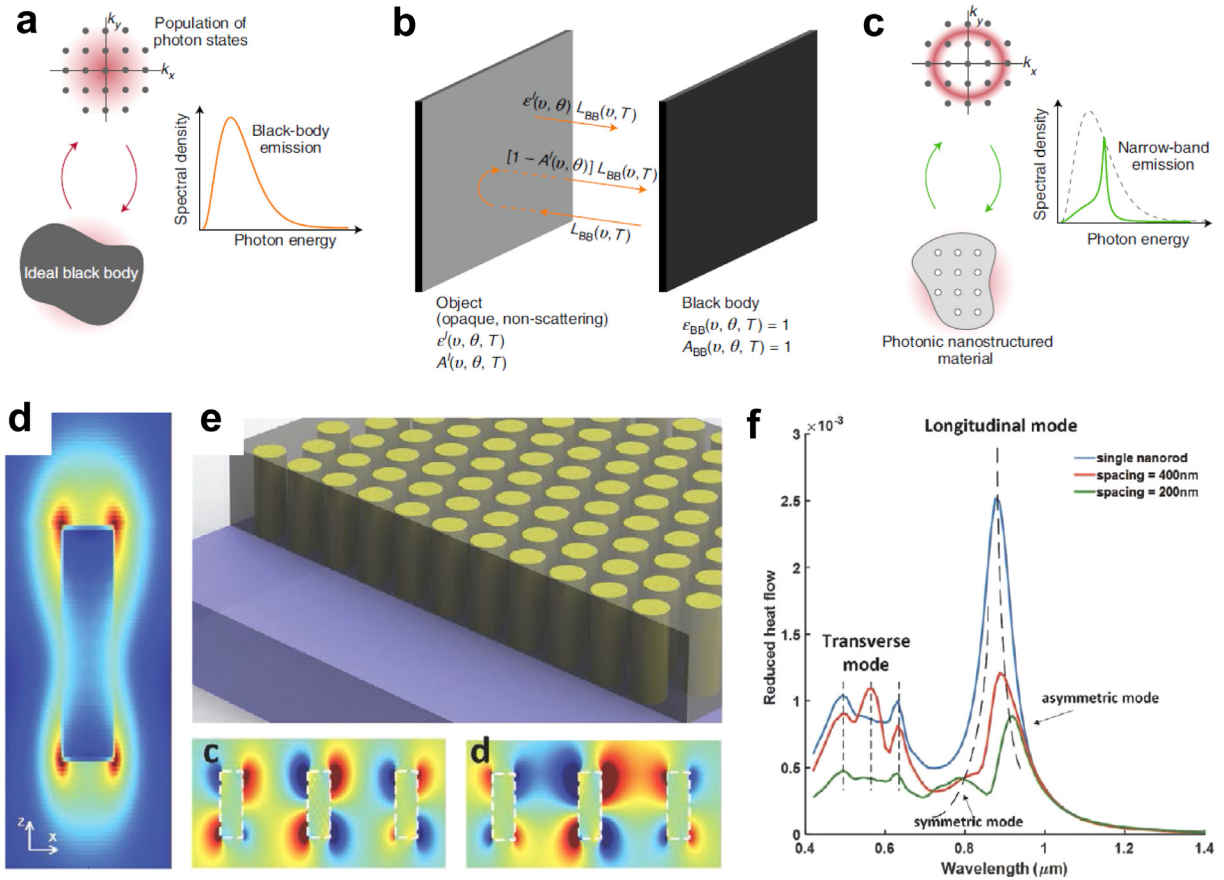
**Fig. 11.** Thermal emission physics (a) an ideal black body establishes thermal equilibrium, resulting in Planck spectrum. (b) The energy balance described by Kirchhoff's law. (c) Thermal emission from a nanostructured material has a narrowed spectrum. Reproduced with permission [161]. © 2019 Nature Publishing Group. LSPR mediated thermoplasmonic emission from gold nanorod arrays. (d) Electric field profile of the longitudinal LSPR. (e) the nanorod array embedded inside an alumina layer on a sapphire substrate with symmetric and asymmetric hybridized modes. (f) The thermal radiation spectra. Reproduced with permission [163]. © 2021 Wiley-VCH.

where $C_{geo}$ is the projected area. However, this expression may yield values of the emissivity larger than unity. A better formalism by use of the absorption cross section is expressed as [23]

$$Q_{rd} = 4\pi \int_0^\infty \frac{2hc^2 C_{abs}(\lambda)}{\lambda^5 \left[\exp(hc/\lambda k_B T) - 1\right]} d\lambda \tag{29}$$

Considerable progress has been achieved in engineering the thermal spectrum, radiation directionality, polarization and temporal response [167–169]. The emission spectrum of nanorod emitter shows narrow-band resonance peaks because the spectrum are strongly related to the LSPR properties (Fig. 11d–f) [163,166]. The thermal emission can thus be tailored by tuning the resonant modes. Fig. 11f shows the impact of hybrid mode of nanorod array on the thermal radiation. The longitudinal LSPR branches into two different modes with the total thermal emission suppressed as the distance decrease of spacing. Thermal emission often has a broad-spectrum characteristic, but the narrow-band control of emission is significant in some applications such as solar cell and radiative cooling.

## 3. Thermoplasmonic tuning strategies

Plasmonic resonance depends on the intrinsic property of constituent material, particle size and shape, as well as external couplings that includes light polarization, dipole orientation, gap distance between the coupled structures and dielectric constant of the surrounding medium [69]. Such dependences enable a static engineering of plasmon resonance [170,171]. Another effective way to control plasmon resonance is to tune the refractive index of surrounding environment. Using of reconfigurable matter provides active way for varying the plasmon resonance [172,173]. In this section, three categories of tuning strategies (Fig. 12) including self-tunable plasmon, plasmon-couplings and active plasmons are discussed for illustrating a clear picture in thermoplasmonic tuning. Most strategies have been taken to
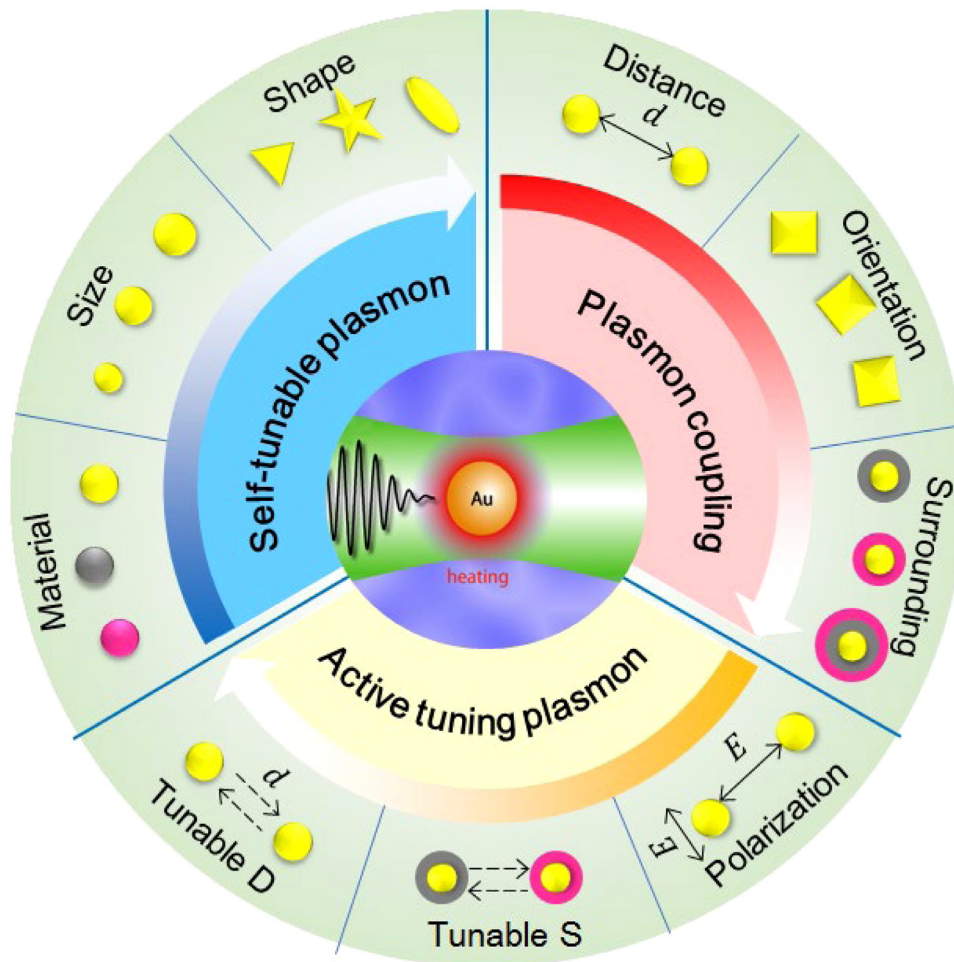
**Fig. 12.** Thermoplasmonic tuning strategies.

guide the thermoplasmonic design in solar applications. Even some strategies have not been taken in real application, they would still play an important role in the future development of solar technology.

### 3.1. Self-tunable strategies

#### 3.1.1. Constituent material

Plasmon resonance is an intrinsic characteristic of materials, mainly reflected by dielectric constant of materials. Dielectric function governs optical excitation and SPP propagation length. The peak position of SPR is decided by the real part of dielectric function. A large real part reflects an efficient screening to yield redshift of plasmon peak [172]. However, this parameter is intrinsic nature and cannot be easily modified once designed. Therefore, selecting material serves as a logical first step to design plasmon resonance [174,175]. Typically, Al and Pd particles are plasmon active in ultraviolet wavelength range, whereas Au, Ag, and Cu particles mainly function at visible wavelength of 400–650 nm. Mg, Al, and Ga mostly work in UV region due to the high plasmon frequency. There also exist other plasmonic materials, such as alloys and intermetallics, doped-semiconductors, 2D materials, metallic oxides, graphene, refractory metals, polymers, etc [23,170,176,177]. The intrinsic resonance of these materials also can be tunable to cover broad range of spectrum by adjusting the composition and structure.

Alloying or doping modification of materials can induce surprising changes of its complex optical constant, implying these approaches are feasible to tune the optical response of plasmonic systems. Nevertheless, only few successful attempts have been verified by changing the chemical composition, structure phase, or carrier density of materials. For example, alloying of Ag-Au metals has been used to arbitrarily tuning their optical behavior in UV-NIR [178,179], showing high flexibility of the permittivity over pure metals. This does not inferred that the alloy property can be tuned by a linear combination of optical constants. A refined description in terms of movement of the optical gap and Fermi
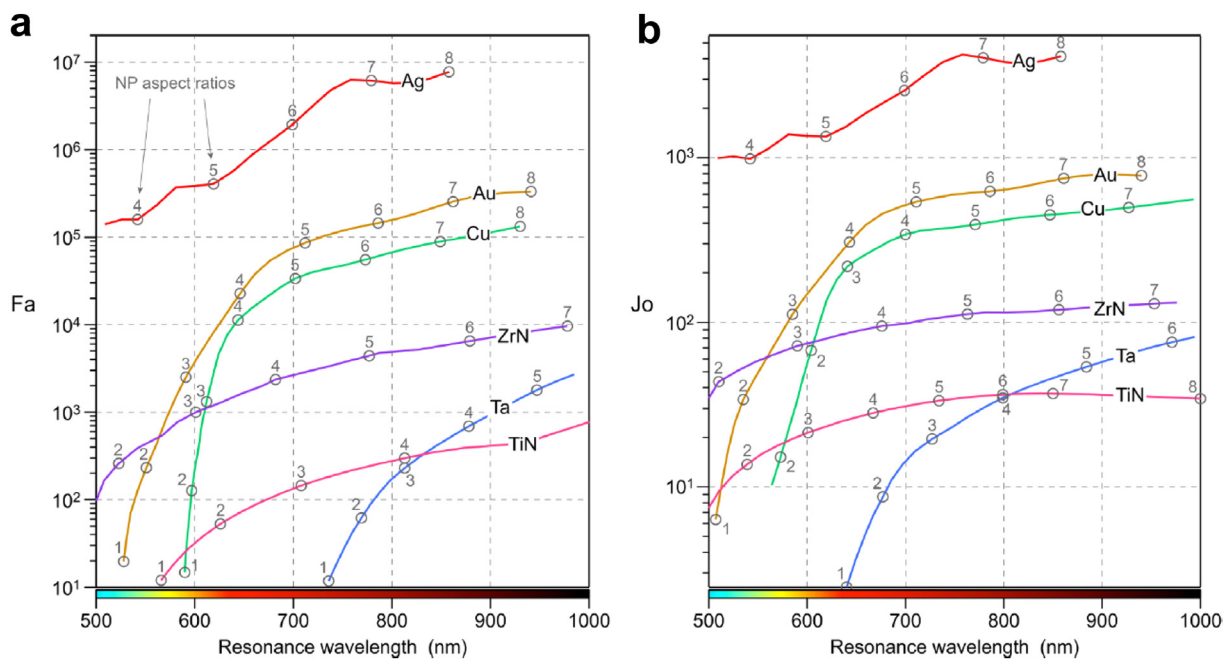
**Fig. 13.** Dimensionless numbers characterizing the ability of a plasmonic material to enhance the near-field (*Fa*) and produce heat (*Jo*) that plotted as a function of the resonance wavelength. Each wavelength corresponds to a different aspect ratio of the structure.
*Source:* Reproduced with permission [164].
© 2015 American Chemical Society.

level is required. Plasmon resonances have also been tuned in sub-stoichiometric $MoO_{3-x}$ nanobelts with high oxygen vacancy, showing flexible plasmon absorption in a range of wavelength of 200~2500 nm. This illustrates that doping or incorporating foreign atoms into semiconductor lattice can change the free carrier concentration in materials [180]. Besides, titanium, zirconium and hafnium nitrides also show plasmonic properties in longer wavelengths. These materials are good candidates to replace noble metals for high-temperature application due to the high melting-point, allowing for tailoring of plasmon resonance by controlling their composition [124,176,181].

To compare the efficiencies of materials with each other, dimensionless parameters e.g. Faraday and Joule numbers can be defined to examine the plasmonic capabilities, quantifying the capabilities of plasmonic structure to amplify the electromagnetic field and producing heat, respectively [23,164]:

$$Fa = \left| \frac{Maximum\ electric\ near-field\ over\ space}{Incoming\ electric\ field} \right|^2 = 9 \left| \frac{\varepsilon}{\varepsilon + \varepsilon_m} \right|^2 \tag{30}$$

$$Jo = \frac{e\varepsilon'}{n_m} |\boldsymbol{E_{in}}/\boldsymbol{E_0}|^2 = \frac{\lambda_{ref} C_{abs}}{2\pi V} \tag{31}$$

where $e$ is photon energy, $\varepsilon'$ is the imaginary part of permittivity, and $\lambda_{ref} = 1240$ nm. Fig. 13 presents specific values of *Fa* and *Jo* for the nanospheroids at plasmon resonance. It indicates that the deviation from sphere shape enhances the optical near field and photothermal conversion efficiency, and red-shifting the plasmon resonance. For example, Ag particles facilitate the plasmon excitation with the highest resonance intensity [182]. Semiconductors red-shift the plasmon resonance in visible-to-NIR range in contrast to that of most metals. In general, each kind of materials has their own advantages and disadvantages. Metallic materials play the dominant role in plasmonic applications, and gold remains the best metal of choice for most applications due to its good photothermal properties, and chemical stability in presence of oxygen [183–185].

### 3.1.2. Size effect

A common goal in thermoplasmonic design is to maximize the capability of photothermal conversion. Eqs. (5) and (6) indicate the cross section of absorption and scattering related to the particle size with different magnitudes. Scattering becomes more significant by increasing the particle size since it scales as $R^6$ while absorption scales as $R^3$. The cross section of scattering thus gradually becomes dominate the extinction cross section as the increase of particle size. For gold particles in water, this transition appears at diameter ~88 nm, in which the scattering and absorption cross section are equal [23]. For particles smaller than light wavelength (<25 nm), the absorption dominates over scattering. The plasmon
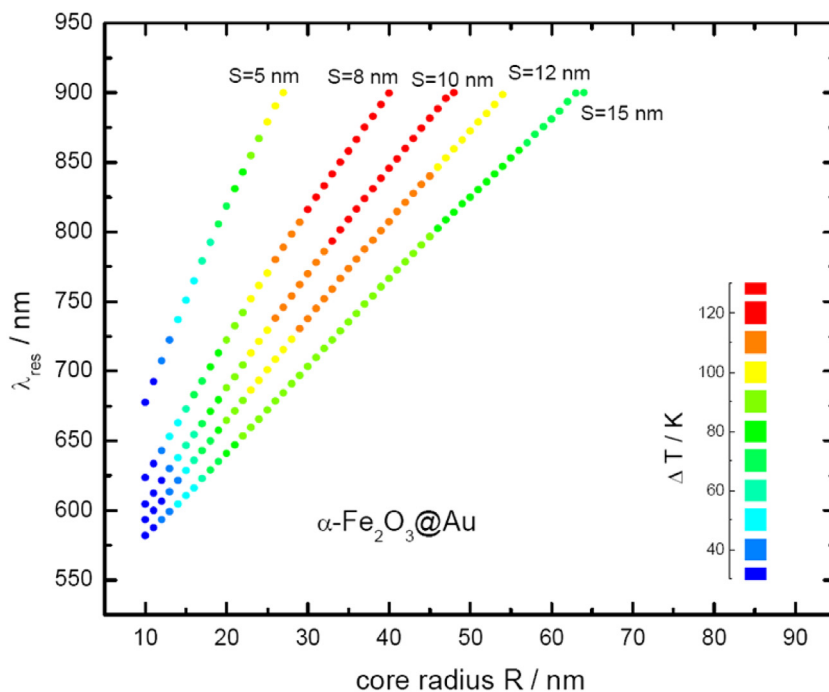
**Fig. 14.** The size effect on the resonance peak of core–shell particles, and the corresponding heating effect.
*Source:* Reproduced with permission [188]
© 2016 American Chemical Society.

band first blue-shifts as the particle size decreases from ∼20 nm but then in turns strongly red-shifts near 12 nm [186]. The plasmon bandwidth increases with the decrease of particle size, inversely proportional to the particle radius [61,187]. In general, smaller nanoparticles exhibit efficient absorption at their resonance wavelength, reflecting their advantage in converting light into heat [22,70].

For larger particles, the plasmon bandwidth is red-shifted and broadened with the increase of particle size due to the retardation effects. This comes from the fact that the particle can no longer be assumed as oscillating dipole. For gold, it is around 50 nm, and scattering becomes dominants above 90 nm [189]. If the particle is larger than this size, some retardation effects occur due to the electromagnetic interaction between distant charges within the particle [23]. Au and Ag particles are the most studied materials with the Ag cross section being greater than Au [170]. The magnitude of absorption wavelength shift is small compared to the total bandwidth of resonance. Therefore, the peak position of plasmon resonance is not discussed to the size effect [61]. However, titanium nitride and platinum efficient absorb light energy in NIR region that are good alternatives for photothermal conversion.

Experimental works on optical heating are primarily carried out on gold particles [22]. Plasmonic heating of a 100 nm gold particle in water has been studied with a NIR laser. The measured heating shows good agreement with the predicted values by dipole approximation [190]. No simple analytical expression can be found to examine the thermal response of a particle of arbitrary size. However, numerical simulations can be carried out using Mie theory. Mie theory has been extended for evaluating the extinction spectra of core–shell nanostructures (oxide@noble metal) [188]. By tuning the geometric dimension of core and shell, an adaptable plasmon band and photothermal effect are observed for the designed particles. Fig. 14 shows a dimensional size-dependent heating effect. It is found that the plasmon band red-shifts as the decrease of shell/radius ratio. The highest temperature increases to 110 K for a structure with core radius of 53 nm and a shell thickness of 8 nm when irradiated at 900 nm wavelength. This diagram supplies useful information for designing the optimized structures to maximize light-to-heat conversion.

### 3.1.3. Shape effect

Optical modulation of plasmon resonance by use of pristine materials are limited, particularly to extend the resonance band for solar absorption. Tuning the particle shape is an effective mean on plasmon absorption [191–193]. This can be understood from three aspects. The first aspect focuses on controlling the number of resonances by designing particle symmetry. For instance, small gold particles present only one plasmon resonance band at 520 nm, while two resonance bands appear as the particle symmetry is broken from spherical to cylindrical [189]. This asymmetry creates a strong redshift of the plasmon resonance, along with a strong increase of the resonance amplitude. The two resonance peaks correspond to the transverse and longitudinal oscillations with multipolar modes, which is consistent with the short and
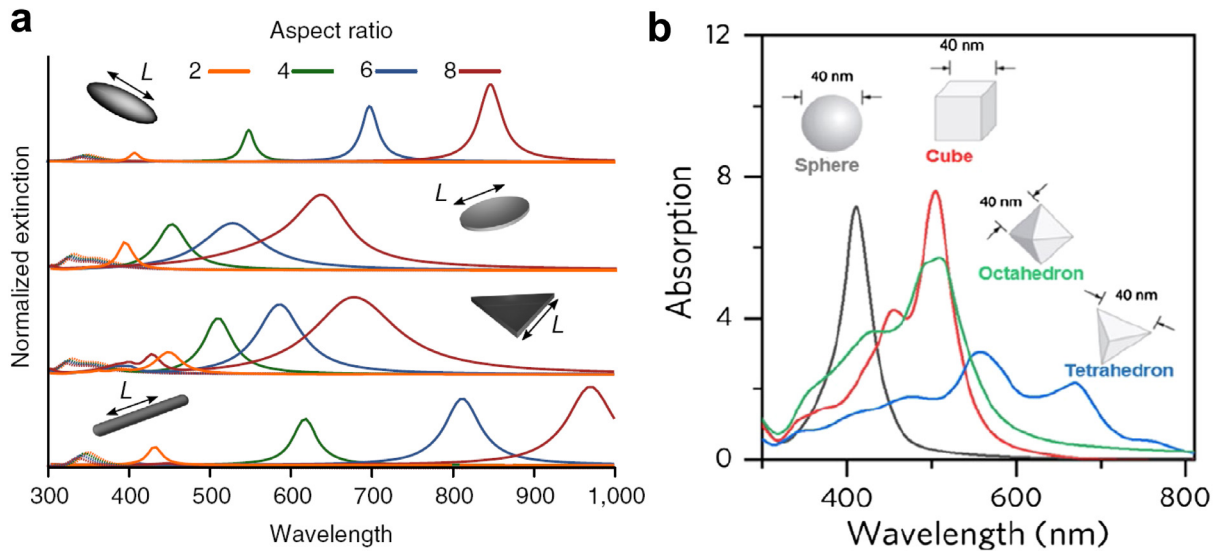
**Fig. 15.** (a) Spectra of high aspect ratio particles as ellipsoid, cylindrical disk, triangular nanoprism, nanorod. Reproduced with permission [55]. © 2014 Nature Publishing Group. (a) The dependence of absorption spectra on the shape. Adapted with permission [70,195]. © 2006 American Chemical Society.

long axes of the high aspect ratio nanorods. This difference of electron oscillation stems from the different restoring force along each axis [187,194]. The band position also can be changed by changing the aspect ratio of other geometries such as ellipsoids, cylinder, nanoprism and nanorod. Fig. 15a depicts spectra of the anisotropic particles with a 10 nm fixed short axis and varying long axis at 20–80 nm. The transverse resonance band (dashed lines) of all the shapes is weak and blue-shifts in visible-light range, while the longitudinal plasmon resonance (solid lines) is strong and red-shifts in red or NIR region as the increase of aspect ratio. Controlling the aspect ratio of these geometries allows flexible tuning the resonance peak positions from visible ∼410 nm to near-infrared ∼1000 nm [55].

The second aspect is to control the plasmon length where the carrier oscillations take place [196]. The plasmon length is an intrinsic parameter to define plasmonic structures, which determines not only the peak position but also the bandwidth of plasmon resonance. The electron-oscillation distance over a plasmon length can be tuned by both the size and shape of particle. For example, the optical spectra for gold particles of different shapes including nanocubes, icosohedra, octahedra, decahedra, and truncated bitetrahedra are measured and normalized in consideration of their edge and plasmon length. It is found that the edge-effect is insignificance for dipole modes in a size range of 50–350 nm, and no correlation can be fitted with the side length. While the different shape structures with similar plasmon length exhibit similar plasmon resonance spectra. Therefore, the oscillation distance is critical in describing the shape-dependent plasmonic properties.

The last aspect centers on the sharp tips on structure. Irregularly anisotropic structures e.g., nanocubes, nanostars or nanoprisms, enable more complex light–matter interactions that typically results in plasmon resonance over a broad range of wavelengths [192,197–200]. Fig. 15b shows the spectra difference of Ag particles with various shapes. Ag spheres and cubes with high symmetry feature strong plasmon absorption peaks. The low-symmetry polyhedron particles present a broad but weak absorption-band with multiple resonances [195]. The plasmon band of nanocube (∼500 nm) is red-shifted in contrast to the sphere particle (∼410 nm). Such transition is a result of the accumulated charges at cube corner, reducing the restoring force for carrier oscillation [70]. Moreover, the field distribution around sharp tips could be extremely strong as the largest accumulated polarization charges occurring at the tips. Nanostar is a typical case and that has been used for photochemistry and biomedical applications [22,201]. The plasmon absorption is very sensitive to its spike length. An increase of spike length from zero to 40 nm, an 80 nm sphere would cause a red-shift of plasmon band from 470 to 1050 nm, while the tip curvature or spike number has little impact on the absorption peak.

## 3.2. Plasmon coupling strategies

### 3.2.1. Inter-particle distance

Plasmon resonance is sensitive to the nearby plasmonic structures. The gap distance between the coupled structures is key parameter for the plasmon coupling [202–204]. As one plasmonic particle in close proximity with another, this near-field interaction will derive new plasmon resonances with great enhancement of electromagnetic field. The typical case of this is a particle dimer (Fig. 16a), in which the dipolar plasmon-mode is split into the bonding and antibonding modes [70,205,206]. The bonding mode has two aligned dipoles along inter-particle axis, resulting in a strong dipole-coupling to the far field. In contrast, the anti-bonding mode possesses anti-aligned dipole with a zero net dipole moment. As a result, the optical response of dimer is guided by the low-energy bonding mode.
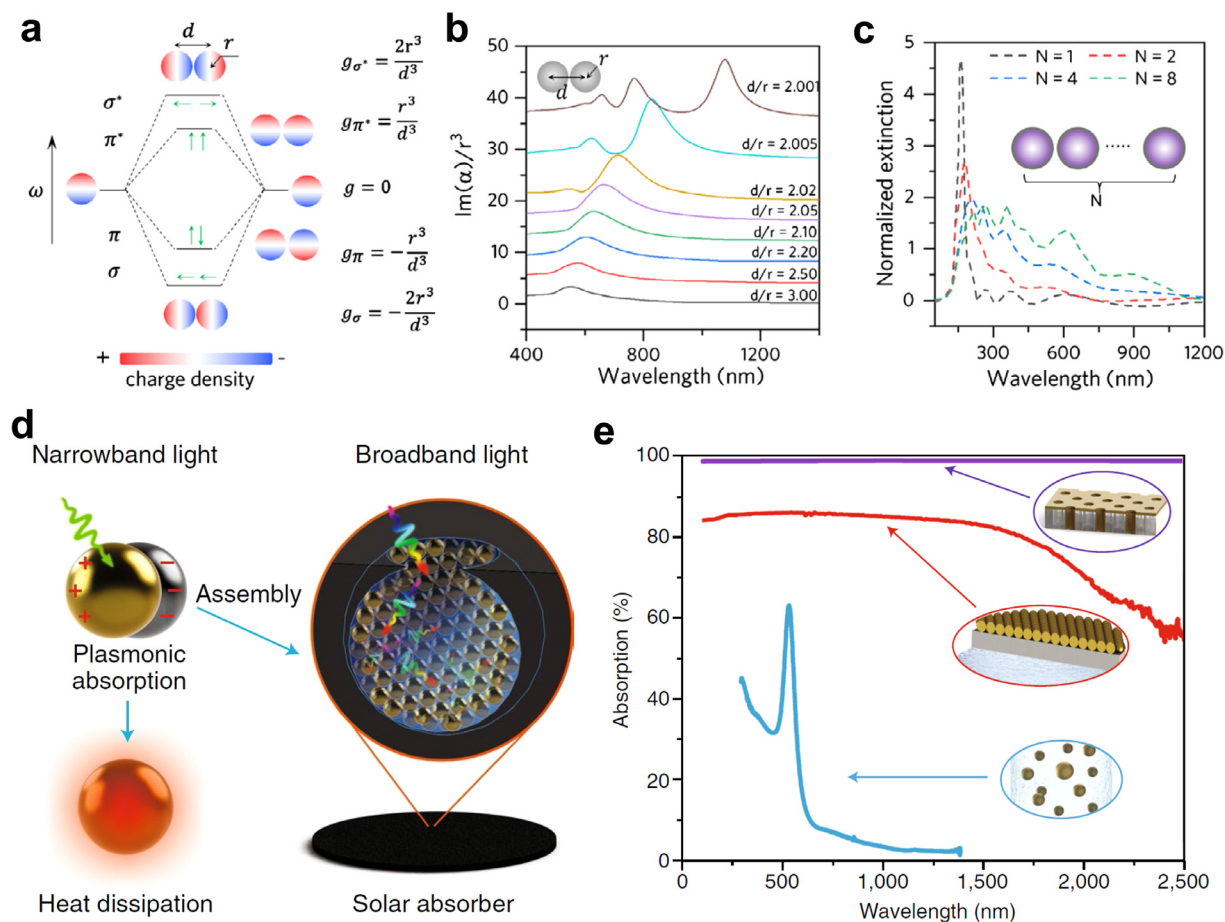
**Fig. 16.** Particle coupling effect. (a) Energy hybridization in a plasmonic dimer. (b) Absorption spectra with different interparticle distances. (c) The normalized extinction cross section ($C_{ext}/C_{geo}$) on particle number. Adapted with permission [70]. © 2021 Wiley-VCH. (d) An individual particle absorbs light at a distinct wavelength, electrons are excited and then dissipated as heat. (e) Typical absorption spectra of plasmonic particle dispersion (blue line), self-assembled film (red line) and 3D-templated film (purple line). Reproduced with permission [10]. © 2018 Nature Publishing Group.

For longitudinal excitation, the resonance band of bonding mode is red-shifted as reducing of the gap distance that induces higher-order plasmon modes with different effects on the resonance frequency, leading to band splitting and broadening. The relative shift $\Delta\lambda/\lambda_0$ is exponentially related to the gap/diameter value ($s/D$) as [69,172]

$$\frac{\Delta\lambda}{\lambda_0} = A\exp\left(-\frac{s}{\tau D}\right) \tag{32}$$

where $s$ is the interparticle edge-to-edge distance, $D$ is the particle size, $A$ is the maximal fractional plasmon shift, representing the dipolar coupling strength, and $\tau$ is the decay constant that describes the decay length of the electric field away from the particle surface. Such decay is universally independent of the constituent materials, particle size and shape. Fig. 16b shows the spectral evolution of gold dimers with 120 nm diameter and varying the interparticle distance [207]. The plasmon-coupling interaction is weak when the distance is above $3r$, demonstrating a single-dipole mode over the spectrum. As the gap distance continuously decreases to near touch, the bonding mode first exhibits a redshift, and then a higher quadrupolar resonance mode emerges in the plasmon spectrum. However, the broaden-range of plasmon resonance is limited for a dimer.

To cover a broad solar spectrum, plasmon-coupling involving many interacting particles are assembled with distributed sizes into porous films (Fig. 16c and d) [10]. Within the film, the plasmonic components are closely packed and their individual plasmon modes overlap and hybridize with each other, leading to broadband light absorption [208]. This hybrid plasmon creates a distinct red-shift of the resonant band towards visible-to-NIR regime. This approach opens up new strategies for improving photothermal conversion by engineering of nano-plasmon assemblies. Plasmonic thin films are also developed for enhanced photothermal conversion by self-assembling of the particles on paper or other substrates (Fig. 16e) [209–213]. The plasmonic particles are distributed randomly in the pores, enabling a high density of hybridized mode to broadly absorb solar energy. In addition, the porous design effectively reduces the back reflection of light. As a

consequence, the film absorbs ∼99% light energy across the full spectrum, exhibiting photothermal conversion efficiency above 90%.

It is clear that both the electric field and plasmonic heating are dependent on interparticle distance, besides the plasmon resonance [22,58,70]. The field enhancement factor can be increased to $10^6$ as decreasing the distance right down to a single-atom level [54,214,215]. This implies that the remarkable field enhancement could be derived by coupling particles with small distance. However, the ratio of temperature increase follows approximately, but not completely the ratio of light absorption power. The temperature magnitude closely follows the profile of dominant plasmon mode, showing a distinct feature at the plasmonic wavelength [24]. The local temperature of a specific particle is thus either lower or higher than that in adjacent particles by tuning the incident wavelength upon a specific distance [208].

### 3.2.2. Orientation and configuration

In case of anisotropic structures, orientation and configuration are key factors to determine the plasmon interaction and dipole moment, and thus impacting the plasmon resonances [55]. To create desired plasmonic properties, diverse anisotropic nanocrystals have been synthesized and fabricated such as nanorods, nanocubes, nanobipyramids and nanocups [216–220]. When an Au nanorod rotated around its mass center in a nanorod dimer, the coupled resonance band is blue-shifted as the increase of rotation angle due to the reduced coupling [221]. Besides, the plasmon coupling is also affected by the higher-order multipolar modes. The plasmonic enhancement at nanocube corners is of special interest, and the multipole contributions become significant depending on their orientation. This is because the high density of oscillating dipoles at corner promote more red-shift of LSPR [218,222]. In contrast to the symmetric configuration, the asymmetric coupled structure as nanosphere rotated around nanorod dipole also achieves favorable plasmon interaction as a bonding dipole–dipole mode [223].

Orientation and configuration also affect the electromagnetic field distribution around the coupled structure. For instance, Ag nanocubes have been self-assembled as one-dimensional strings with either edge–edge or face–face orientations. The strong field enhancements are observed with 800 in the gap center and 1200 at the cube corners on an edge–edge configuration [197]. This enhancement is at least two-fold stronger than that of face-to-face dimers [225]. This is because the face–face orientation has two different polarization states at the facing facets and facing corners. Whereas in the edge–edge case, the higher-order plasmon mode appears in dipolar mode with only one prominent resonance band [218]. The dipole polarization vectors and corresponding field distribution are thus more concentrated at the corners.

Design of a plasmonic absorber requires rationally analysis on both the electromagnetic field and the thermoplasmonic behavior of the structures with random orientation. This is because the experimental validation of orientation effect on thermoplasmonics is still limited. The photothermal properties of metallic nanorods, nanotriangles and nanocages have been theoretically analyzed by wave-simulation method to determine the temperature variation as the orientation change with respect to polarization (Fig. 17) [184,219]. The analysis shows that the absorption-power amplitude of nanorod decreases as the nanorod rotating away from the polarization direction (Fig. 17b). A strong absorption variation is observed following the orientation change of asymmetric nanotriangle (Fig. 17d). However, the orientation effect of nanocage is negligible as only small amplitude variation ∼2% are detected in light absorption (Fig. 17f). Hereby, the symmetry structures have more potential in photothermal conversion due to their energy absorption is largely irrelevant to spatial orientation.

### 3.2.3. Coupling with surrounding medium

The surrounding medium serves as additional factor for tuning plasmon coupling [171,224,226]. Eq. (3) indicates that the dielectric function of constituent materials and surrounding medium determine the plasmon features and corresponding dipole moments. The dielectric coupling is critical for the design of plasmon resonance. Such dielectric surrounding medium can be sorted as absorbing or non-absorbing dielectric environment [189]. In non-absorbing case, the dielectric function of medium is a real dielectric constant, and the induced polarization charges in environment increase with the dielectric constant. As a consequence, the Coulombic restoring force is weakened as going from water to glass, causing a red-shift of the plasmon peak [226].

The absorptive medium has complex dielectric function, such as polymer, $Al_2O_3$, $SiO_2$, $MoS_2$, graphene and quantum dots, or other metal oxides [172,189,227]. In such case, the plasmon resonance experiences both the spectral shift due to the change in real part of dielectric constant, and the shielding effect due to the light absorption associated to imaginary part. The plasmonic resonance can sustain from a significant enhancement to completely suppress depending on the geometry and coupling structure of materials [189]. For a surrounding medium with electronic absorption energy far from the resonance energy, the increase in real part of dielectric function would induce a red-shift of the resonance peak, while the variation of imaginary part affects the attenuation of plasmon resonance [228]. Whereas, a strong coupling regime exists for the surrounding medium with absorption energy close to the resonance energy. Such media can offset the intrinsic absorption losses in metal to enhance the plasmon resonance [61,172]. Moreover, this strong coupling may also lead to peak splitting to create hybridized resonance states [56,229].

Based on the dielectric effect, multiple metallic and dielectric materials are also designed for optimizing the plasmonic heating [224,230]. The thermodynamic problem in such case is complex since the surrounding medium consists of two media featuring different thermal conductivities. Once heat is generated, one is interested in managing such heat. The heat transport microscopically depends on the propagation of electrons and phonons [51,231], but it is also studied
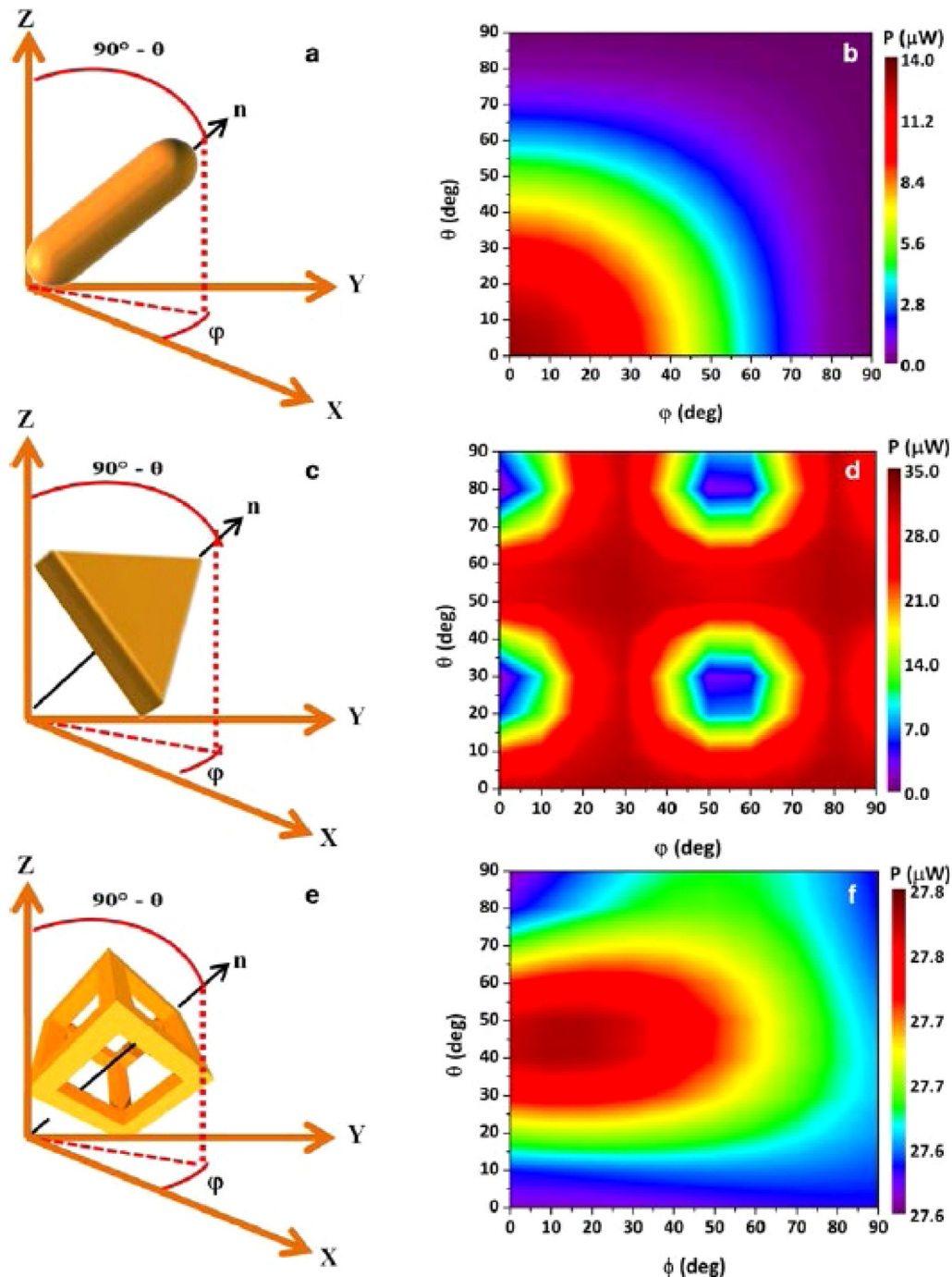
**Fig. 17.** Spatial orientation and the corresponding heating powers of (a, b) gold nanorod, (c, d) nanoplate and (e, f) nanocage.
*Source:* Reproduced with permission [219]
© 2020 Springer.

by using thermal diffusion equation. For example, the effect of optical heating of a metal nanoparticle lying on a planar substrate (e.g. glass and sapphire) and immersed in water has been investigated for understanding the thermal diffusion (Fig. 18a and b) [22,23]. The proximity of sapphire of higher thermal conductivity tends to reduce the overall temperature, especially in this medium. Another typical configuration is using multilayer core–shell structure with different permittivities to improve thermoplasmonic properties [224,230]. The dielectric multi-shell structures host the

**Fig. 18.** Thermoplasmonic coupling with surrounding medium. Temperature distribution of an irradiated gold particle on glass (a) and sapphire (b) substrates. Reproduced with permission [22]. © 2019 American Chemical Society. (c) Optical, thermal and pressure responses in plasmonic nano-oven. Reproduced with permission [224]. © 2017 American Chemical Society.
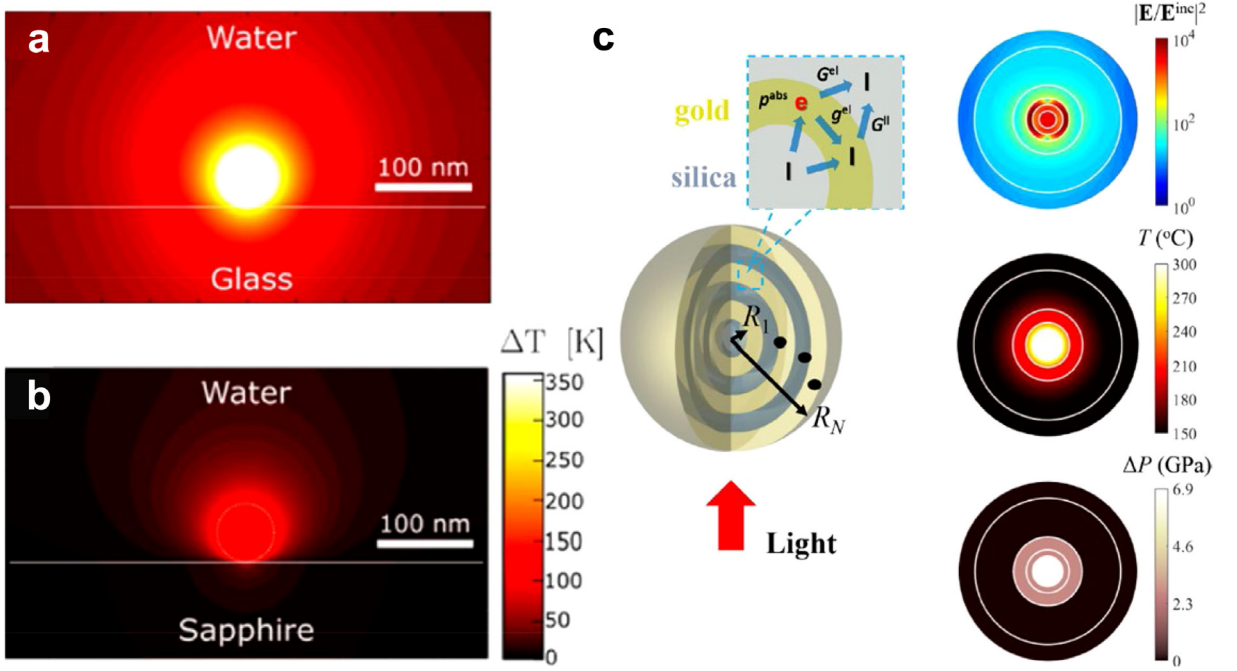
collective plasmon resonance among different metallic layers, resulting in extremely enhancement $\sim 10^4$ of near-field at core region where light absorption is maximized (Fig. 18c). This confined nanoscale space offers an unusual thermal environment upon high pressure for exploring new physical or chemical processes.

### 3.3. Active tuning strategies

#### 3.3.1. Polarization by light incident

Control of incident angle of light is a most direct route to active tuning of plasmon resonance [84,232]. A strong plasmon-coupling is established when nanoparticles get close to each other. Each particle is exposed to the near-field irradiation from $N$ neighboring particles along with the incident electric field [69,233].

$$\boldsymbol{E} = \boldsymbol{E}_0 + \sum_{i=0}^{N} \boldsymbol{E}_{i,nf} \tag{33}$$

For a particle pair, the net electric field of each dipole is expressed as

$$\boldsymbol{E} = \boldsymbol{E}_0 + \frac{\xi \boldsymbol{p}}{4\pi \varepsilon_0 r^3} \tag{34}$$

where $\boldsymbol{p}$ denotes each dipole, $\xi$ is the orientation parameter that described as [221]

$$\xi = 3 \cos \theta_1 \cos \theta_2 - \cos \theta_{12} \tag{35}$$

$\theta_1$ and $\theta_2$ are the angles between the inter-dipole axis and the direction of each dipole,respectively. $\theta_{12}$ represents the angle between these two dipoles. The temperature increase of the particle $j$ originates from a self-contribution and an additional contribution stemming for the neighboring particles [23].

$$\delta T_j = \delta T_j^{sef} + \delta T_j^{ext} \tag{36}$$

As a result, the plasmonic heating depends on not only the interparticle distance, but also the polarization or orientation of each dipole.

When light parallel polarized along the interparticle axis of a dimer, the plasmonic interaction is attractive with negative interaction energy, leading to a low plasmon frequency along with a red-shift of the plasmon band. Consistent with the optical resonant, a strong gap-field is created due to the constructive interference between dipoles. On the other
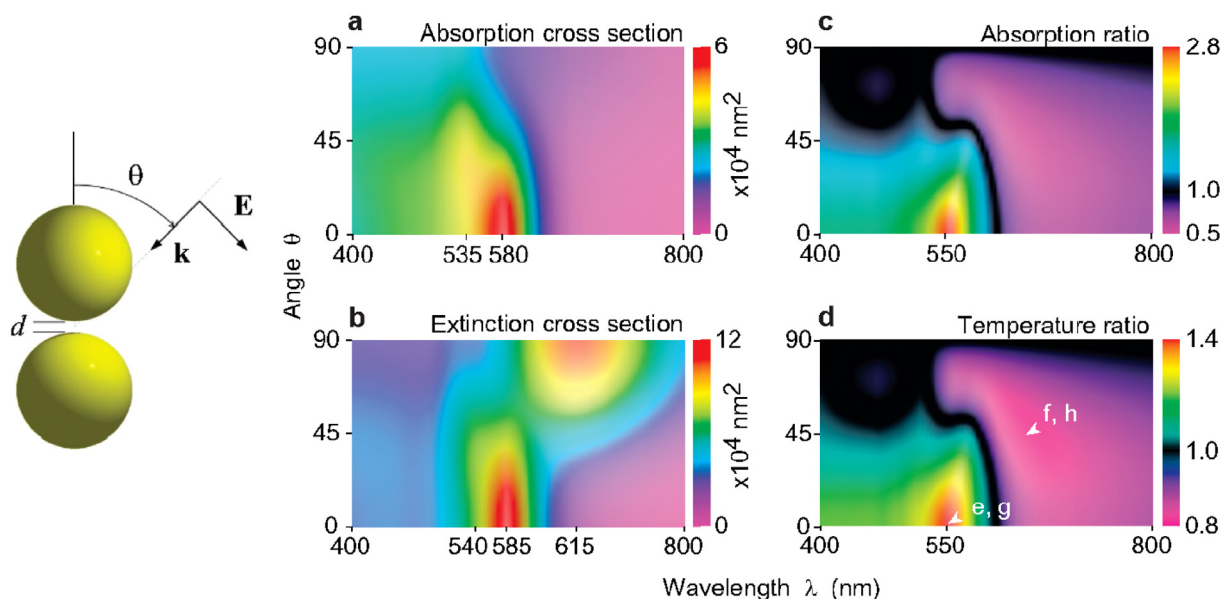
**Fig. 19.** Polarized light wave under an incidence angle. (a,b) absorption and extinction cross sections as a function of light wavelength and incidence angle, respectively. (c) Ratio of the partial absorption cross sections of the upper and lower spheres. (d) Ratio of temperature increase.
*Source:* Reproduced with permission [24]
© 2010 American Chemical Society.

hand, a slight blue-shift of plasmon band is observed along with the reduced distance as the polarization is vertical to the interparticle axis. The dipoles destructively interfere with each other, reducing the magnitude of electromagnetic field in gap [233,234]. More important, as the increase of polarization angle from 0° to 90°, the scattering spectrum of Ag dimer shifts prominently from 517 to 456 nm. The low energy spectrum at 517 nm is the longitudinal plasmon coupling ($\sigma$), whereas the high spectrum one at 456 nm originates from transverse hybrid plasmon coupling ($\pi^*$) [235]. These findings reflect that the polarization frequency, electromagnetic field and thermal distribution could be optimized by controlling the incident angle [236–238].

Fig. 19 shows a significant degree of control on the individual temperature of neighboring particles by tuning the light wavelength and incidence direction. The absorption and extinction cross-sections both present a distinct feature at 580 nm, which is most intense upon interparticle-axis incidence (Fig. 19a and b) [24]. Fig. 19 c and d show the absorption and temperature ratios, in which the below sphere has a temperature that is 1.4 times lower than that of the upper sphere at 550 nm wavelength (e, g). This supports an obvious shadowing effect from the upper sphere. However, such situation is reversed with the bottom sphere picking up more energy for oblique incidence at 650 nm (f, h). It is thus possible to control the temperature ratio by tuning the light wavelength and incidence angle. At incidence angle of zero, a temperature ratio of 0.8~1.4 can be tunable achieved in the wavelength range of 550~650 nm.

### 3.3.2. Tunable dielectric surrounding

Plasmonic materials with actively tuned properties are crucial to modulate the optical, electronic, thermal and catalytic properties. The reconfigurable plasmonic materials are usually prepared by coupling the plasmonic particles with stimuli-responsive materials [172,240]. Many active media have been used to build such active plasmonics, and that includes optically active materials such as J-aggregates, photochromic molecules and quantum dots, thermoresponsive materials such as gallium, vanadium oxide, and germanium antimony telluride, and electrically driven materials such as elastic polymers, liquid crystals and graphene, among others [59,173,241]. In response to the stimuli (e.g. light, chemicals, electricity or heat), these responsive elements switch from one state to the other to reduce the system energy. As a result, the coupling state of plasmonic particles is altered by the tunable surrounding medium, resulting in a change of plasmon resonance as well as the electromagnetic field.

The mechanism of state-transition is interesting because that involves scientific challenges in molecular dynamics, energy transport and nanoscale mechanics. Using a surrounding medium with flexible dielectric responses to light offers a facile way to control the plasmon response [242]. This can be realized since the photochemical reactions include cis–trans isomerization, pericyclic reaction, intramolecular group transfer and hydrogen transfer, and dissociation [111]. Electrochemically responsive materials allow reversible redox reactions, providing an facile ways for tuning the electronic structure to achieve variation of their dielectric functions [243]. Electric control of the electro-optic film flexible changes the refractive index, and thus varies the plasmon propagation constant and modulates light reflection [244,245]. Chemical
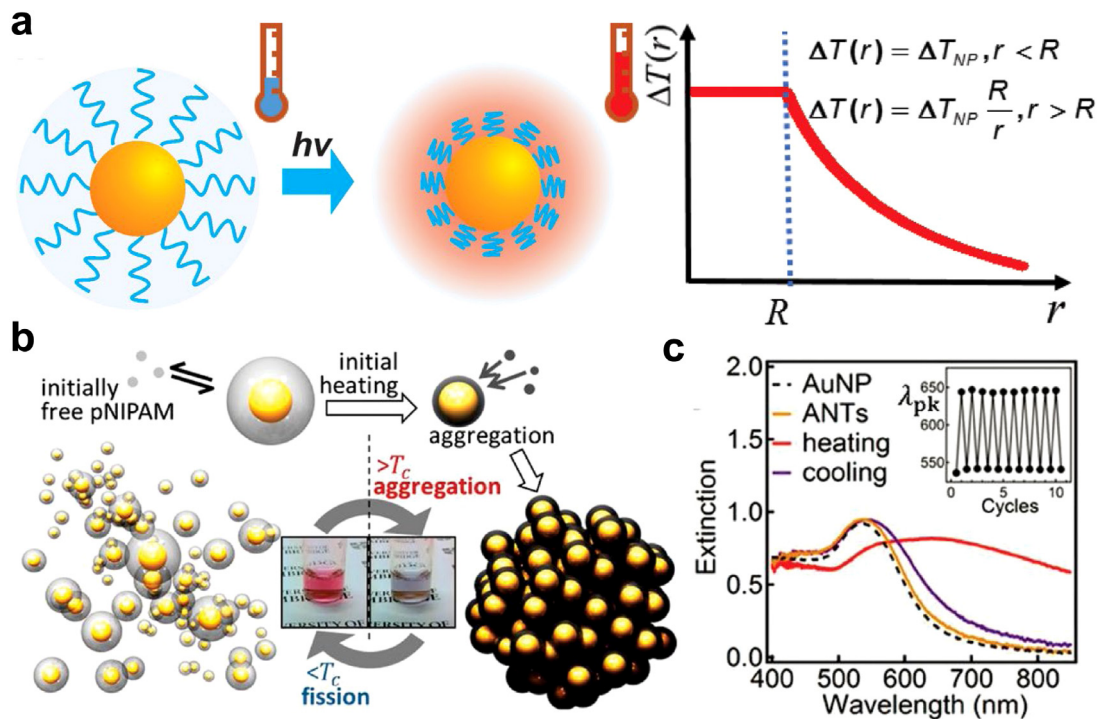
**Fig. 20.** Thermoplasmonics with tunable dielectric surroundings. (a) Temperature profile of gold particle upon irradiation. (b) Reversibly control by external irradiation. (c) Extinction spectra with cyclical heating and cooling.
*Source:* Reproduced with permission [239]
© 2016 National Academy of Sciences.

stimuli offers more abundant choices to achieve plasmon control, which possibly includes pH value and ionic strength, humidity, and DNA species [246,247]. The refractive index of thermo-controlled material continuously varies with the surrounding temperature [248,249]. Reversible tuning of the refractive index allows for active control of the plasmonic materials.

Among different thermal-response materials, thermo-optical materials stand out from all the rest because of its fast response, low threshold on transition between different states. The efficient photothermal-conversion of plasmonic structures suggests the possibility of light-controlled of their assemblies. For example, epoxy adhesives require high temperature to bond composite materials. The laser bonding of composite materials using plasmon-based photocuring can substantially decrease the curing time relative to the conventional curing process [250]. Beside, Fig. 20 shows another example based on thermo-optical response over PNIPAM-coated Au particles [239]. The surrounding temperature falls off in inversion to the distance away from particle (Fig. 20a). Compared to the conventional bulk heating, such plasmonic heating concentrates the thermal energy at nanoscale, which will be more efficient in energy conversion and potentially faster in thermal response. Optical heating of the core–shell particles above a critical temperature leads to expelling water from coatings, inducing a hydrophilic to hydrophobic state change of PNIPAM. This transition drives a controllable number of nanoparticles gathering into mesoscale clusters, which in turn reversibly switches their color from red to dark blue (Fig. 20b). Correspondingly, the plasmon peaks reversibly shift in the extinction spectra between 525 and 645 nm (Fig. 20c).

### 3.3.3. Tunable gap distance

Tuning the gap distance between plasmonic structures is an effective basis for constructing active plasmons. The successful examples have been demonstrated by integrating plasmonic crystals with some specific molecules or polymers. These specific materials support molecular conformational changes or reversible self-interaction upon external stimuli [172]. The plasmonic nanostructures in these hybrid structures can be either dispersed in solutions or embedded in/on solid matrix. The gap distance between these active components can be tuned by using the organic molecules with different lengths [251], and the shape and size of plasmonic structures largely determine the spectral response and thermoplasmonic heating.

For example, the charged Au particles in solution are self-assembled into linear structures, exhibiting significantly different optical response [240,252]. Such assembly is a result of force competition between van der Waals attraction force and electrostatic repulsion force. When the electrostatic interaction tuned by sweeping temperature over 5–40 °C, the
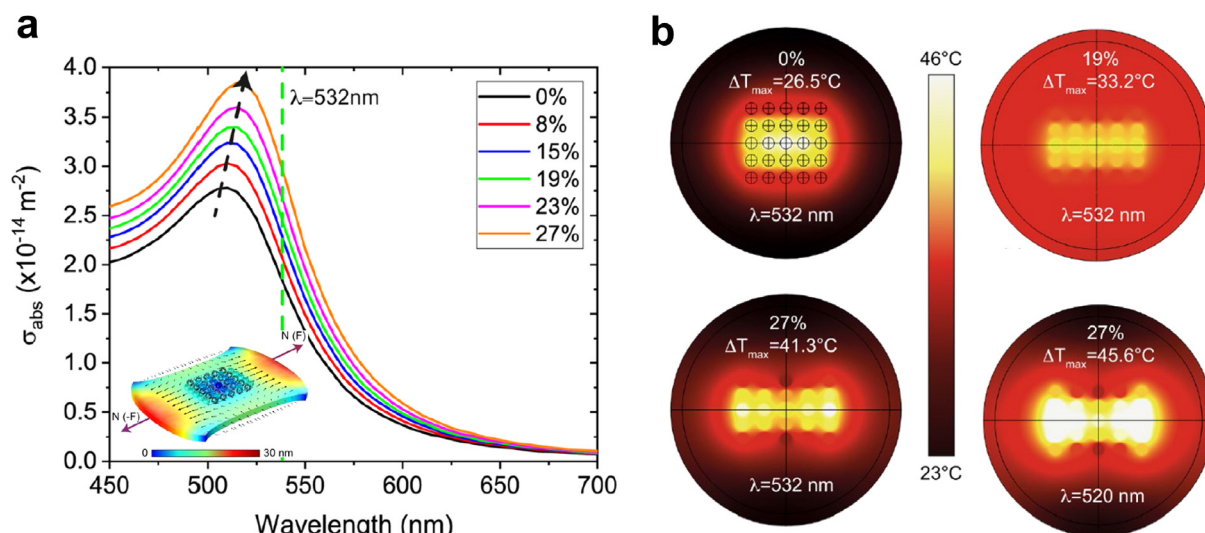
**Fig. 21.** Thermoplasmonics with tunable gap distances under stretching. (b) Absorption cross section curves and (c) temperature mapping for the different stretching.
*Source:* Reproduced with permission [257].
© 2020 AIP.

assembling process of negatively charged Au particles covered with bis(p-sulfonatophenyl)-phenylphosphine is reversibly achieved, with red color at high temperature upon disassembled state and dark blue at low temperature upon a linear chain structure [253]. However, the electrostatic force relies not only on the temperature but also on the solution pH. pH-tuned reversible assembly of gold nanorods has been verified using thiol-containing bifunctional molecules as the assembling agents [254]. The plasmon assemblies are observed with an end-to-end to a side-by-side configurations. The former configuration redshifts its plasmon band with a longitudinal peak at 220 nm, while the latter presents a 30 nm blue-shift.

Responsive polymers are often used as soft matrix to accommodate plasmonic structures. The polymer matrix acts as capping agent for preventing particle aggregation. The high density of plasmonic elements entrapped in matrix is responsible for optical spectral responses [255]. Considering external mechanical stimulus, dynamic plasmon couplings are reported by changing the elastic properties of substrate. Upon stretching, the particles separate apart in the direction of stretching and closer together in the direction perpendicular to it. This leads a drastic redshift of the plasmon band from 510 nm to 520 nm by stretching the substrate from 0% to 27%, giving rise to a polarization-dependent plasmonic feature (Fig. 21a) [256,257]. The chain formation upon stretching creates electromagnetic field and thermal hot spots that gives rise to a temperature increase (Fig. 21b). The temperature gradually increases from 26.5 °C for the substrate at rest to a much higher 41.3 °C upon 27% strain percentage [257]. These results evidence how the plasmo-mechanic system relies on light polarization, interparticle distance and spatial arrangement of the particles.

## 4. Applications in solar energy

Benefited from the tuning strategies and advanced fabrication techniques, diverse plasmonic structures and their couplings have been developed. It allows flexibly tuning their plasmon resonance, spectral spectrum, electromagnetic intensity and photothermal performance for applications in direct solar thermal conversion or indirect solar thermal chemistry. (Fig. 22). In this section, we introduce the progress of thermoplasmonic applications in solar collector, solar radiator, thermophotovoltaic, solar desalination and sterilization, solar degradation and catalysis, solar fuels and solar fertilizers. For each application, we will show how the thematics are born, the-current-state-of-the-art and remaining challenges. Particular attentions are paid on the distinct advantages of thermoplasmonic realization compared to traditional solutions.

### 4.1. Direct solar-thermal conversion

#### 4.1.1. Solar collector
Solar collector is a thermal device for converting sunlight into useful heat, which can be classified into flat and concentrating technologies. The flat technologies are used in low-temperature applications like space heating, hot water production and solar cooling applications with maximum temperature up to 90 °C with flat plate collectors and 150 °C with evacuated tube collectors. The concentrating technologies are able to operate at high temperature levels between
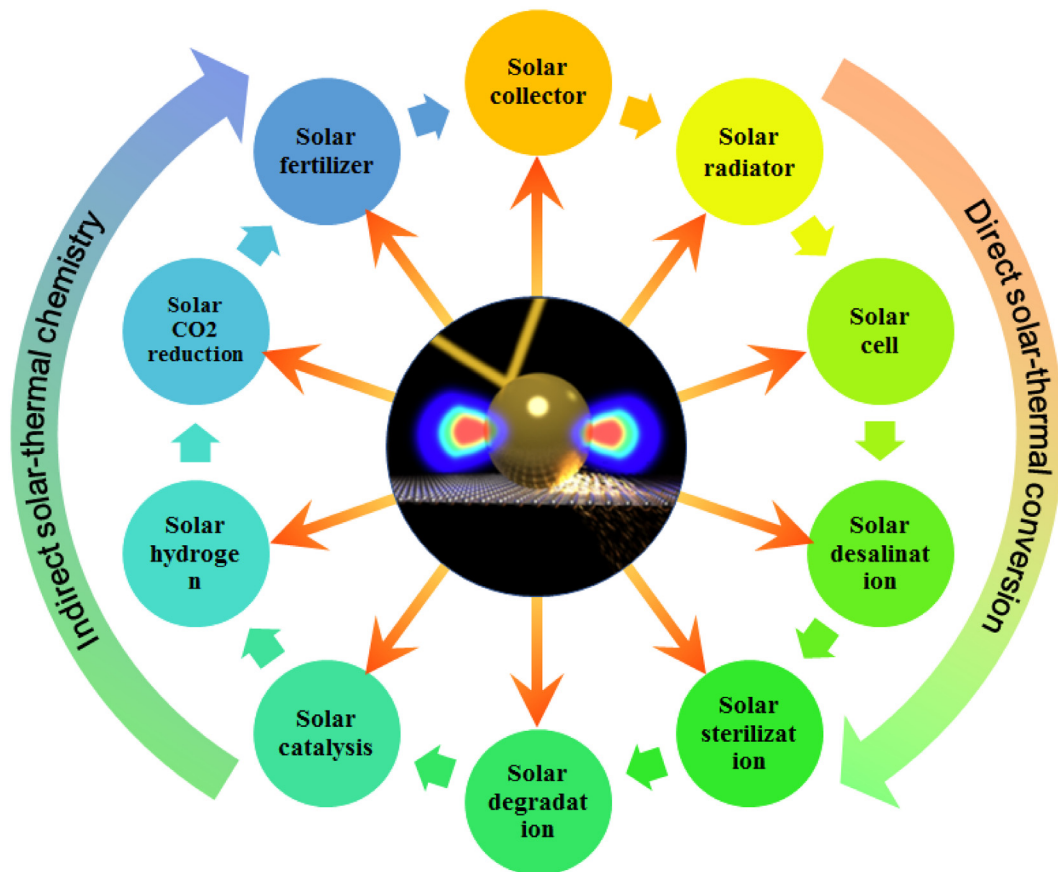
**Fig. 22.** Thermoplasmonic applications in solar energy.
*Source:* Adapted with permission [258].
© 2016 American Chemical Society.

150∼500 °C [259]. The mechanism of energy conversion is based on using a black surface to harvest solar radiation, and the absorbed energy is then transferred to the neighboring working fluid [259,260]. However, the energy efficiencies of surface collector are relatively low due to the significant thermal losses from conduction, convection radiation. This will even worse with the increase surface temperature of absorber.

In contrast to the solar-to-useful conversion process in conventional collector, the heat transfer fluid in a direct absorption solar collector harvests solar radiation by means of volumetric absorption. This significantly reduces the thermal resistance between the fluid and surface absorber [260]. Besides, the thermal trapping effect resulted from volumetric absorbers can lead to obvious reduction of convection and radiation losses [262]. Moreover, volumetric radiative absorption can be induced by either gas–particle, or liquid–particle suspensions, or porous media with distinguish advantage of high absorption ability relative to the scattering [263], which is a fascinating alternative to improve the efficiency (Fig. 23) [264–266]. The useful heat gain is calculated by

$$Q = C_p \dot{m} \left( T_{out} - T_{in} \right) \tag{37}$$

where $\dot{m}$ represents the mass flow rate, $T_{out}$ and $T_{in}$ are the outlet and inlet temperature, respectively. The thermal efficiency of collector is then derived as:

$$\eta = \frac{Q}{IA_c} \% \tag{38}$$

where $I$ is the incident radiation density, $A_c$ is the light harvesting area. For nanofluids, specific heat and density are given as [260]

$$C_{p,nf} = \frac{\rho_{bf} C_{p,bf} \left( 1 - \varphi \right) + \rho_{np} C_{p,np} \varphi}{\rho_{nf}} \tag{39}$$

$$\rho_{nf} = \rho_{bf} \left( 1 - \varphi \right) + \rho_{np} \varphi \tag{40}$$
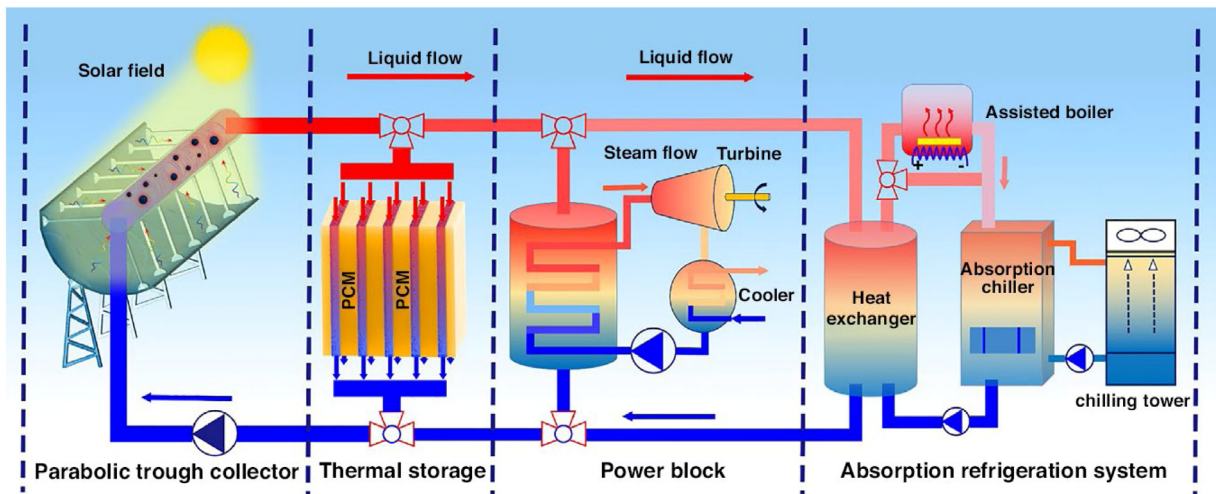
**Fig. 23.** Thermoplasmonic nanofluid used in solar collector for representative applications.
*Source:* Reproduced with permission [261].
© 2019 Elsevier.

where $C_{p,nf}$, $C_{p,np}$, and $C_{p,bf}$ are the specific heat of nanofluid, particle and base fluid, $\varphi$ is the particle volume fraction, $\rho_{nf}$, $\rho_{np}$, and $\rho_{bf}$ denote the density of nanofluid, particle and base fluid, respectively.

Physical properties of the fluid are unavoidably affected by adding nanoparticles, such as density, thermal conductivity, specific heat and viscosity. The particle absorbs heat more quickly than the base water due to its low specific heat. Owing to its large surface area with high thermal conductivity, the absorbed heat can be fast transported to the surrounding fluid [267]. As a result, the outlet temperature is increased to improve the efficiency. Diverse nanofluids have been studied by use of particles such as carbon nanotubes, graphite, noble metal, titanium and copper oxide [265]. Plasmonic nanofluids are more appealing than the metal oxide and carbon-based nanofluids because of their favorable optical properties and prominent photothermal performance. LSPR can greatly enhance solar absorption since the oscillation cross-sections are several times larger than the physical cross-section of particle [267]. Therefore, the collector can achieve high thermal efficiency even at low particle-concentrations, rendering the nanofluids ideal for sunlight harvesting.

Low-concentration nanofluids below 0.04 wt% with gold or silver have been verified for photothermal conversion. But the high absorption can only be achieved around the narrow plasmon-band, restricting their benefits for solar harvesting [262,263,268]. An improved nanofluid by blending different nanoparticles with complementary optical-properties has been developed for broad-band solar absorption [267,269]. Blended nanofluids composed of different morphologies, sizes and materials show good improvement to the photothermal efficiency. Gold nanofluid mixture including nanorods, nano-ellipsoids and nanosheets enhances the thermal efficiency by 104% compared to the nanofluid only with nanospheres [270]. Silver nanofluids with the mixture of nanosphere and nanoplate extend the extinction spectra over a wide range of wavelength 300–1200 nm at a very low concentration of 0.001 wt%, raising the thermal efficiency to more than 85% [267]. Although thermal nanofluid has not been accepted for commercial application, pioneer research showed the economic feasibility and technical advantages in energy storage, power generation, and refrigeration applications (Fig. 23) [261]. Despite the distinct optical and photothermal properties, there are some challenges to be overcome before real application of plasmonic nanofluids [264,265]. The nanofluid preparation involves ion-exchange reactions and the remaining ions in solvent bring side effects to application. Even a low-volume fraction of nanofluid is charged in solar collector, high material cost and synthesis process are the drawbacks to affect their marketing competition. Another more challenge thing is the nanofluid stability because they are prone to get agglomeration due to the change of Van der Waals bonds upon long-term solar irradiation. This will even worse when the fluid is used under concentrated solar flux at medium-to-high temperatures.

### 4.1.2. Solar radiator

Metasurfaces assembling of plasmonic structures can absorb or scatter light at nanoscale. The metasurface design with different dielectric materials offers new research horizons from radiative cooling, energy-saving window to novel routes of anti-fogging or icing [98,271,272]. LSPR of nanostructures determines their optical response and induces either light absorption or reflection. The spectral overlap of such scattering and absorption is the intrinsic drawback due to the nature properties of constituent materials [273]. To improve the performance for aforementioned uses, novel optical- and thermal-structure design is crucial step to tune the electromagnetic flux and realize full control of the absorption and scattering spectra. A concept of hybrid metal–dielectric antenna has been proposed to manipulate the absorption
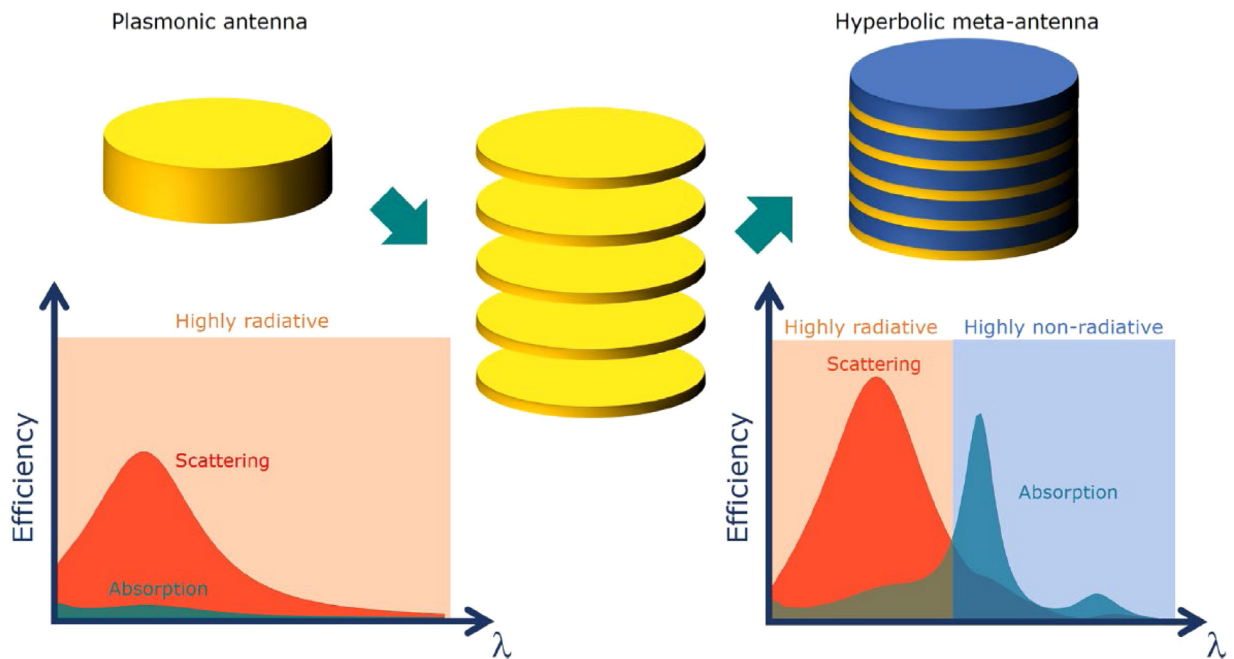
**Fig. 24.** A plasmonic antenna (left panel) displays a highly radiative spectral response, and an almost pure radiative and nonradiative region (right panel) enabled by using a dielectric spacer between antenna slices.
*Source:* Reproduced with permission [274]
© 2019 American Chemical Society.

and scattering [274]. By tuning the system geometry, the scattering and absorption ratio combined with their relative enhancement or quenching can be flexible modulated over broad spectrum. As a result, a radiative region and a non-radiation region can be designed by coupling free-space radiation with the hyperbolic-antenna, realizing the control of both channels (Fig. 24).

Radiative cooling removes heat from surfaces into far space as infrared radiation, and often functions by reflecting solar spectrum in broadband or selectively [272,275]. The radiation tuning is crucial to design radiators with unique radiative characteristics. For example, a scalable plasmonic thin film by encapsulating randomly dispersed dielectric microspheres into polymeric matrix has been designed for subambient cooling. This metamaterial film is fully transparent to visible light, while processing an infrared emissivity above 0.93 upon atmospheric window. Its radiative cooling power reaches 93 W/m$^2$ upon solar irradiation after back coating it with silver [276]. A Janus emitter composed of Ag-polydimethylsiloxane on quartz substrate was also proposed to reduce the emissivity loss [277]. The spatial separation of selective and broadband emission has been achieved on the two sides of structure, resulting in not only an obvious surface cooling but also a passive mitigation of greenhouse effect in the enclosures.

Plasmonic surfaces can produce heat from NIR absorption while simultaneously sustain transparent in visible region. Such surfaces typically consist of a collection of basic optical elements to support specified plasmon resonance, collective display spectrum and tunable light absorption with spectral and directional selectivity [273]. These functional surfaces provide novel strategies to design the energy-saving windows of building with optimized energy transport. The energy-saving window composed of nanoarrays of multi-element gold and nickel plasmonic antennas on glass substrate increases the glazing temperature to 8 °C upon solar radiation, while permits light transmission without any change of color [98]. Gold particle-chain solar radiator increases the glazing temperature of window by up to 9 °C, while maintaining high visible transmittance [278]. These findings open up new ways to build smart window with transparent heating elements powered by sunlight.

Surface icing or fogging has detrimental effects in wind turbines, airplanes and power lines. Current method relies on mechanical or chemical removal. On-site electrical heating for anti-icing or frogging involves drawbacks ranging from energy-intensive, high costs to technical interventions [279,280]. Recent efforts are dedicated to solar anti-icing/frosting surfaces, which harvests sunlight and converts light energy into heat, thereby preventing ice formation [271,281,282]. Plasmonic surfaces concentrate sunlight into small volume, yielding significant temperature increase at the air/material interface, where the condensate or icing is most likely to occur, preventing freezing or weakening ice adhesion. The effectiveness of such surfaces is determined by the maximum temperature increase and the thermal response on surface upon solar radiation [280]. These factors can be rationally balanced by engineering plasmonic structures to fast spread the heat laterally over the interface while maintain the transparency of window. Even upon super-cooled conditions, this
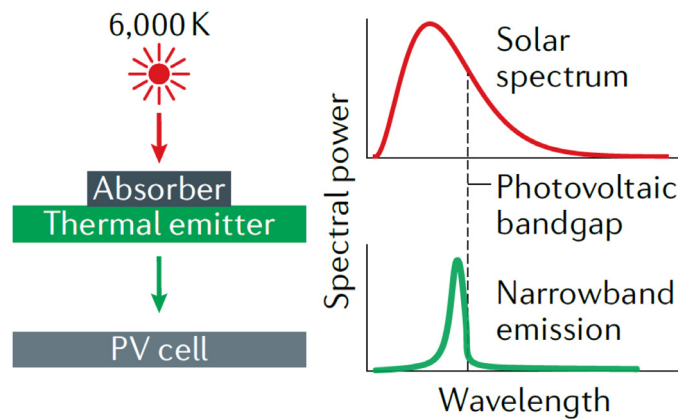
**Fig. 25.** Solar thermophotovoltaics. An intermediate plasmonic absorber harvests the incoming sunlight to heat up, and then generates thermal emission tailored for the bandgap of solar cell.
*Source:* Reproduced with permission [18].
© 2021 Nature Publishing Group.

transparent metasurface combined with hierarchical micro/nano textures can also effectively avoid frosting and water nucleation [283].

### 4.1.3. Solar thermophotovoltaic

Solar cells allow direct conversion of solar energy into electricity, serving a crucial role in energy field. The cell performance rely on their light-absorption ability, the effectiveness of charge-carrier accumulation and exciton dissociation [284]. Traditional solar cells have an intrinsic Shockley–Queisser efficiency limit, which arises from thermal relaxation and sub-bandgap photon losses [13,58]. Plasmonic materials can improve the cell performance via effective light trapping, energetic carrier generation and resonance energy transfer [32,33,258,285,286]. Such enhancement often realizes through cooperative interaction of plasmonic active components with semiconductor layers. Light scattering extends light traveling-pathway to enhance the absorption. Hot energetic carriers surmount the Schottky barrier at metal–semiconductor interface and create more free electrons over the conduction band of semiconductor, leading to high absorbance across broad wavelengths [286]. The third enhancement comes from the resonance energy transfer between semiconductor and plasmonic component by dipole or multipolar coupling. The more detailed description of these mechanisms can be referred to the literatures [32–34].

A different way to reduce thermal loss is turning all electromagnetic energy into heat. Solar thermophotovoltaics (STPVs) are such devices to utilize locally radiated heat, in which an intermediate element absorbs the incident light, heating up and then creates thermal emission tailored for the bandgap of solar cell (Fig. 25) to improve its efficiency [18,287,288]. The overall efficiency $\eta_{stpv}$ is expressed as a product of the optical efficiency of concentrating sunlight $\eta_0$, the thermal efficiency of converting sunlight as heat to the emitter $\eta_t$, and the efficiency of generating electrical power from the thermal emission $\eta_{tpv}$ [289,290]:

$$\eta_{stpv} = \eta_0 \eta_t \eta_{tpv} \tag{41}$$

To reach high efficiencies, STPV must overcome several challenges. First, plasmonic materials and structures must have good thermal stability to support their functions upon high temperature. In this regard, refractory metals are good candidates. Photonic crystals of titanium nitride are proposed to build an emitter structure that has shown to be stable up to 1400 °C [124,287,291]. Second, an infrared thermal emitter must be complementary interfaced to an efficient absorber in shorter wavelength range. This spectral selectivity with high or low absorption has to be rationally designed for a specific system to maximize the cell efficiency. For instance, tungsten thermal emitters and metasurface absorbers have been used as the intermediate structures. The absorber exhibits high absorption capability at visible-to-NIR range, while the emitter greatly quenches upon long wavelengths to decrease the radiative loss, leading to an overall efficiency as high as 18.5% [287].

An even more promising approach is to use near-field STPVs, in which the drastic enhancement of thermal radiation between the emitter and cell can be achieved when the objects are brought to very close to each other [12,13]. This is because the tiny gap is at an order of wavelength, the optical tunneling effect across the gap would give rise to an evanescent near-field of thermal excitation that strongly improves the electromagnetic energy transfer. This resonant energy tunneling overcomes the Stefan–Boltzmann law of several orders and thus can convert more heat to electricity through the solar cells. There are growing numbers of theoretical analyses to the near-field STPVs with plasmon structures, while the experimental validations are relative less [292–295].

Overall, thermoplasmonic effect is valuable strategy to enhance the performance of solar cell. But several issues need to be addressed before application [32,34]. First, noble metals are expensive and also require tailoring the material morphology to achieve optimal plasmonic effect, limiting their practical application. Besides, the structure stability has not been fully examined by careful investigation upon harsh environments or annealing processes. There are also limitations in consideration of their stability on optical absorption, charge transport and photothermal properties. The last but not the least, it is challenge to develop a universal mean to anchor plasmonic structures into solar cell for gaining a robust performance improvement.

### 4.1.4. Solar desalination

Seawater occupies above 90% water on earth, and freshwater shortage is one of global challenges [296,297]. Desalination is an important way for producing freshwater, and various techniques including multistage flash and reverse osmosis are developed to translate seawater into freshwater [298,299]. However, the current technologies need significant energy input and economic investment. Fortunately, many countries have access to rich solar radiation that spurs substantial interest in developing solar desalination technologies. Tremendous interests in developing desalination systems have emerged in recent years, especially in solar-driven interfacial evaporation and solar membrane distillation systems [10,93,300,301]. These solar-enabled systems normally require three key steps for production of freshwater: (i) solar absorber efficiently absorbs and converts solar radiation into thermal energy, (ii) use of the generated heat for steam generation, and (iii) condensation of the releasing vapor to freshwater. The evaporation efficiency is a key metric to judge the ratio of stored thermal energy in vapor to solar flux

$$\eta = \frac{\dot{m}h_{fg}}{q_{solar}A} \tag{42}$$

here $\dot{m}$ denotes the evaporation rate, $h_{fg}$ is the latent heat of vaporization, $A$ is the absorber area. Improving the evaporation rate and efficiency is the goal of desalination research. The current-state-of-the-art efficiency has been approaching to 94%.

Solar desalination requires the absorbers with high efficiency in converting solar photons into thermal energy. Plasmonic materials gained significant attention as the plasmon resonance can concentrate solar energy within small volumes. The confined electric energy is then dissipated as heat loss, driving the adjacent water to evaporate [302]. Vapor generation was firstly studied in consideration of bubbles generation from single nanostructure [28,132,133]. Subsequent researches focus on the synergistic effect of multi-particles with many built-in hotspots in attempt to realizing broadband solar absorption [212,303]. However, the random-distributed individual structures in solutions have poor stability and low photothermal efficiency since the collective synergy effect cannot sustain over such long distances between nanoparticles.

Another effective approach to improve the absorption is by particle coupling. This requires plasmonic structures coupling close to each other and a size distribution with complex geometries, e.g. particle aggregates or assemblies in porous structures. A bio-inspired surface has been fabricated as floating gold particle films at air/water interface [304,305]. The plasmonic heating locally concentrates at the water surface where the phase-change evaporation. This in-situ energy utilization thus reduces the heat losses. Besides, the absorptivity above 90% were also achieved with the film-supported gold, silver or aluminum nanomaterials in solar desalination [185,209,210,213,306–308]. Al particles randomly distributed on the pores create a hybridized plasmon resonance to fully cover solar spectrum (Fig. 26), resulting in high evaporation efficiency of 90% [209]. Plasmon-decorated natural woods are also reported for steam generation with high conversion efficiencies [211]. These film absorbers are less expensive than the other counterparts or nanofluids. They also have synergistic effect in collective heating and can float spontaneously on water surface [309].

Solar interfacial desalination requires further research and development at both the material and system levels. Although plasmonic materials have distinct advantages but it is not always cheap. Easily accessible, efficient solar-thermal materials must be developed for large-scale application [93,308]. Besides, previous efforts are mostly accomplished under laboratory conditions with brine as water source. Rarely attention focuses on the materials and devices against corrosion in real sea condition, which contains contaminants, such as oil and organic compounds, metal ions, and bacteria. Therefore, more effort should be paid to address the corrosion and fouling issue. The active plasmonic elements thus require surface engineering to reserve their stability in harsh environments [297]. From the system level, it is valuable to combine desalination system with other industrial processes to synergistically drive the thermal cycles for more benefit application [299].

### 4.1.5. Solar sterilization

Sterilization not only prevents airborne epidemics, but also plays an important role in control of water pathogens. It is thus important for medical industries, food production, public and environmental health [310,311]. The viability of bacteria will be reduced when experiencing a temperature above 45 °C, and thus the steam exposing is widely accepted for sterilization. The performance of steam sterilization depends on both the steam temperature and the exposing duration. In consideration of the heating temperature, the sterilization mechanism can be sorted as mechanical damage and thermal denaturation [31]. Thermal denaturation works before approaching the critical temperature. In this situation, several ways leading to protein denaturation that includes directly affecting ribosomes, or destroying the structure of enzymes, and
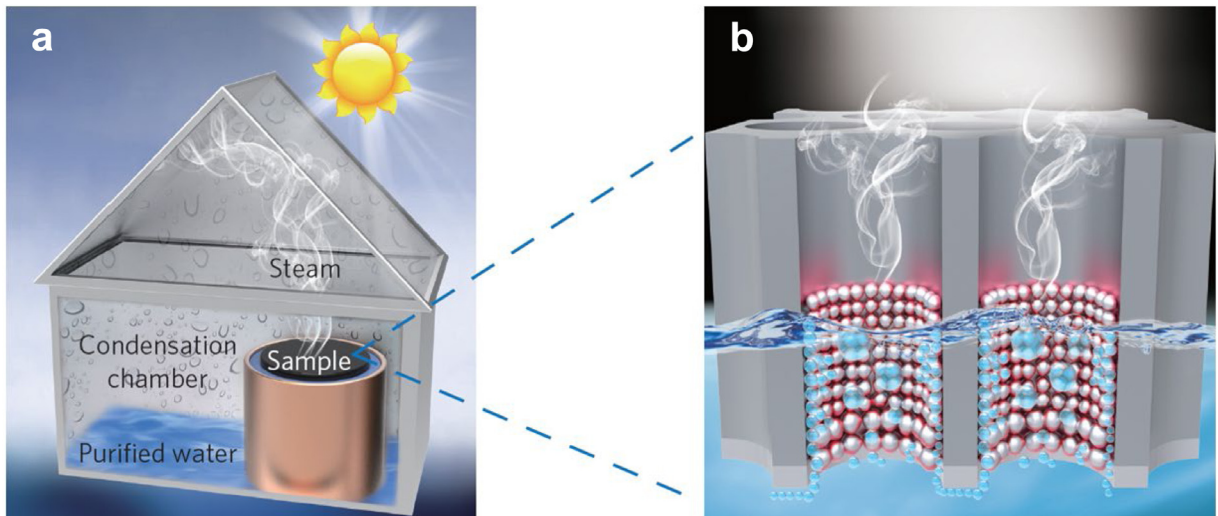
**Fig. 26.** Solar interfacial desalination. (a) Experimental setup and (b) the plasmon-enhanced process.
*Source:* Reproduced with permission [209].
© 2016 Nature Publishing Group.

making cells inactive. This thermal damage functions as the temperature is above a denaturation temperature $T_D$. The thermal denaturation duration $\tau_D$ upon a working temperature $T$ is expressed as [31]

$$\tau_D = \frac{\bar{h}}{k_B} \exp(\frac{\Delta H - T\Delta S}{R_g T}) \tag{43}$$

Whereas the thermo-mechanical damage is driven by shock wave or pressure wave from bubble emission or explosive boiling process, destroying the cell structure and functional components, leading to bacteria damage.

Au nanoshells have been used as solar heater to produce water steam for efficient sterilization [29], which is particularly interest to disinfect of surgical implants. To achieve broadband absorption, the nanofluid mixtures with Au nanorods and/or carbon blacks are developed for inactivation of bacteria and viruses, achieving a 5-, 1.3- and 1.6-log inactivation of E. coli, MS2 and PR772, respectively [312]. Recent research focuses on using plasmonic films for solar sterilization as the film is more efficient than nanofluid since it can confine solar energy at fluid/structure interface [313–315]. By dispersing light harvesting nanoparticles into transparent curable polymer, film-based reactors have been designed to show the scalability of solar water disinfection (Fig. 27) [316]. Moreover, a near-field radiative reactor using heat concentrated strategy has been proposed to improve the thermal flux [317]. Such device features the spatial separation of sterilization surface from absorption surface, thus solving the pore blockage issues or the dirty over active surface. In future, plasmonic sterilization combined with bubble technologies including nucleation or cavitation, may potentially further enhance the treatment [31]. This is due to that the small bubbles can enhance biological water treatment, while spontaneously inactivate pathogens and mitigate biofouling. The induced mechanical, thermal and chemical effects along cavitation are also beneficial to inactivate microorganisms.

COVID-19 pandemic is now threatening the world because the fast spreading of respiration droplets with viruses. Superhydrophobic and thermoplasmonic coating on the respirators demonstrated better protection to people than the current protection equipment in use [318–320]. The effective plasmonic heating improves the mask surface temperature to 80 °C within one minute upon solar irradiation. The hydrophobic nature prohibits respiration droplets staying on the mask surface. The deposited silver particles offer additional protection with ion disinfection to microbes [321]. These synergistic effects derived from the masks enable better personal protection and inspire people to build better protection equipment for combating COVID-19 [31].

### 4.2. Indirect solar-thermal chemistry

#### 4.2.1. Solar degradation

As growing industrialization and urbanization, organic pollutants pose a severe threat to our ecosystem. Photocatalytic degradation is an environmentally friendly approach in environmental purification [322–324]. Numerous photocatalysts have been developed to promote solar photocatalytic degradation. Among which, metal/semiconductor plasmonic catalysts stand out of the others as the most promising candidate [148,151]. In contrast to pristine semiconductors, the most advantage of plasmonic catalyst lies in its high visible-light absorption ability due to the SPR effect. Besides, the
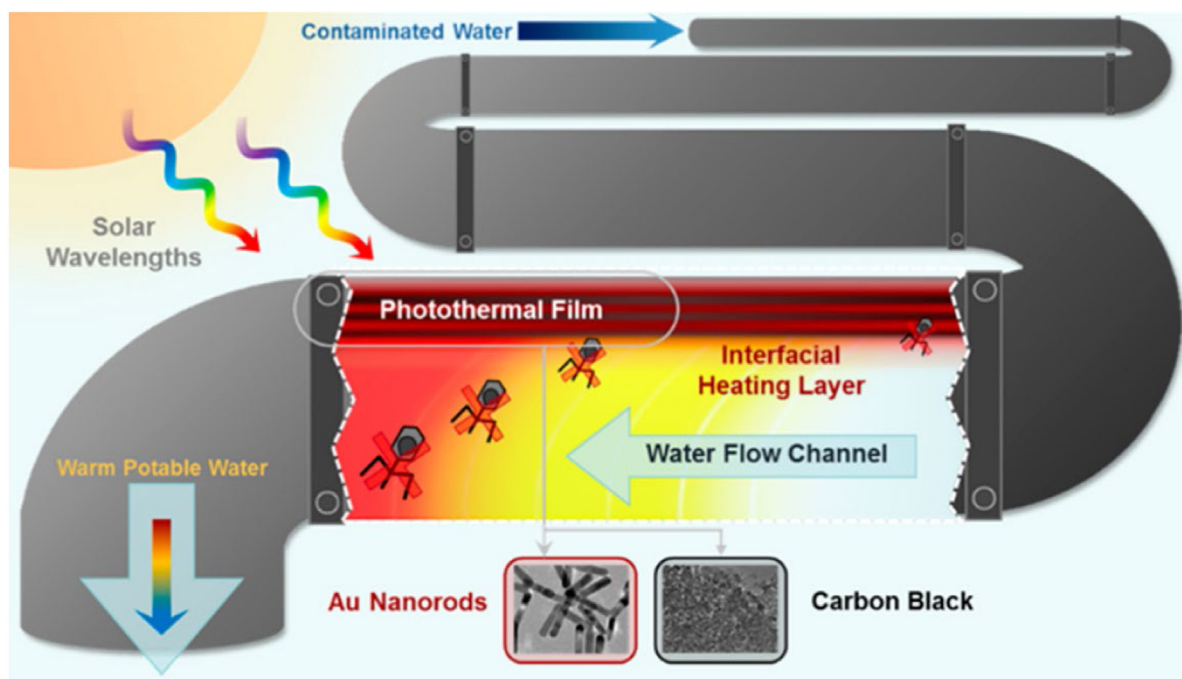
**Fig. 27.** Solar water sterilization.
*Source:* Reproduced with permission [316].
© 2019 American Chemical Society.

plasmon-excited electrons injected into the conduction band of semiconductor can efficiently separate the photo-excited carriers to enhance the photocatalytic activity [325]. This direct charge injection and plasmon-induced field enhancement are considered as the key contributions to enhance activity.

Plasmon-hybrid catalysts are extensively studied for pollution remediation [326]. Au-embedded TiO$_2$ nanofiber catalysts are used for photodegradation of Rhodamine B and methylene blue. The effective charge separation across the interface and the visible-light absorption at the resonance band are key factors for the improved performance [327]. Ghaly et al. developed a stable plasmonic Ag/AgCl-polyaniline catalyst to degrade methylene blue upon sunlight. The catalyst exhibited high degradation activity owing to the high surface areas, strong visible-light harvesting ability, and the synergistic effect from hetero-structure [328]. Moreover, Au particles with different sizes and morphologies loaded onto Bi$_2$O$_3$/Bi$_2$O$_2$CO$_3$ structures give rise to 4–11 times increase in catalytic activities for dye degradation. The size effect on activity follows that of Au NRs (30 nm)>Au NRs (35 nm)>Au nanorods (20 nm)>Au nanospheres (30 nm). The boosting activity is a result of the effective charge separation with more production of ●OH radicals from the plasmonic structures [329]. Therefore, the plasmon-catalytic effect is strongly defined by the plasmon structure size and morphology, substrate material, morphology and crystallinity, as well as the interaction between plasmonic components and substrate.

Plasmonic particles have good photocatalytic activities, but their hot-electrons only can be excited in limited wavelengths. If these energetic carriers not working for charge transfer, this would yield a temperature increase of the particles. Such effect can directly channel the heating to the active sites for exactly enhancing the catalytic reaction [330,331]. Plasmonic photocatalysis has been conducted under controlled illumination to distinguish the thermal or nonthermal effect. Gold nanorods partially coated with silica show high activity in oxidative degradation of actual organic micropollutants that including bisphenol A, and amoxicillin in water under either dark or light conditions (Fig. 28). It is found that the direct electron transfer under dark (1), photothermal heating (2) and hot-electron transfer (3) all contributed to the enhanced oxidation [332]. Furthermore, Pt/$\gamma$-Al$_2$O$_3$ has been tested for toluene decomposition upon solar radiation due to the thermoplasmonic effect of Pt particles, which functions as both solar absorber and active reaction sites [333]. These works provide ideal platform for studying thermoplasmonic degradation, opening the door for solar remediation of recalcitrant pollutants.

### 4.2.2. Solar chemical synthesis

Chemical reaction plays critical roles in our life. Thermoplasmonics confine heat closing to the thermodynamic provides new opportunities in chemical synthesis [14,334]. The enhanced magnetic field, excited hot-electrons and concentrated
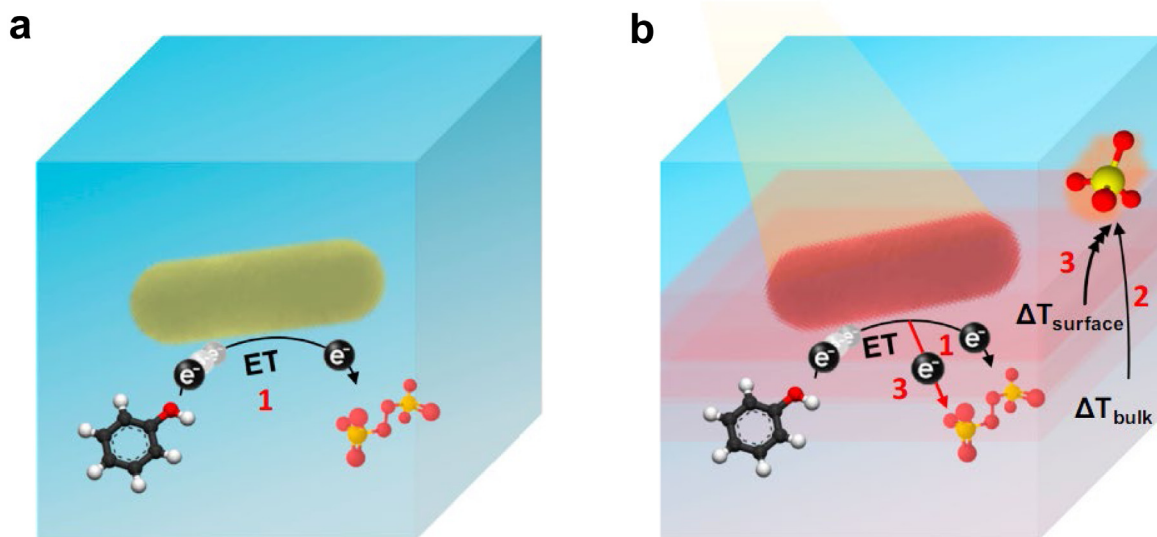
**Fig. 28.** Solar degradation of phenol in water, and the mechanisms involved under (a) dark and (b) solar irradiation.
*Source:* Reproduced with permission [332].
© 2020 National Academy of Sciences.

local heating significantly promote chemical reactions near the structure surface [78,335,336]. The efficient energy transfer between metal and surface adsorbates further triggers chemical transformations according to Arrhenius law [336,337]. Synergistic optimization of photo-electron-thermo-chemical contributions in plasmonic catalysis has great potential to tune their selectivity and improve reaction rate, even under ambient conditions [7,338,339]. Therefore, thermoplasmonic catalysis is an important complement to traditional catalysis for solar energy utilization [340,341].

Several works use plasmonic heating to enhance chemical reactions. The catalytic ethanol reforming is tested in a microfluidic reactor embedded with Au NPs [342]. Upon laser radiation over an ethanol–water mixture at the plasmon frequency, gas products of CO, $CO_2$ and hydrogen are observed from the endothermic reactions driven by plasmonic heating. The plasmonic Au-Pd and $Cu_7S_4$@Pd nanostructures are subsequently reported for Suzuki reactions [343,344]. The reaction yield upon solar radiation is two times higher than that of the thermal reaction at same temperature [343]. In addition, the thermoplasmonic catalysis over Au and Ag nanocrystals, Pd nanostructures and TiN cylindrical nanocavities have also been found to accelerate CO oxidation, hydrogenation of olefins and ethylene epoxidation, etc [345–348].

Improving the reaction selectivity and efficiency are main goals in solar chemistry [349,350]. But these two objects are reciprocal competition. Recent attempts try to address this challenge by using SPR to control selectivity [38,141,350,351]. Tian et al. showed that the SPR excitation satisfies the both targets for achieving simultaneous high yields and selectivity of acrolein or propylene oxide. Fig. 29 shows the mechanisms of selective propylene oxidation. Hot electrons enhance the oxygen activation and thus adapt the selective reaction pathway towards acrolein. While the nanoconfined SPR effect isolates the active region that effectively avoids overoxidation, and thus improving the selectivity of oxidation products [141]. However, our understanding of the duel effects on selectivity and efficiency is still limited, particularly in the nanoconfined reaction that involved with both hot carriers and plasmon heating [143,352]. Such situations featured with inhomogeneous fields with enhanced magnetic field, thermal and/or chemical gradient that may have total different effects on the reactions.

*4.2.3. Solar hydrogen*

Using solar energy for sustainable hydrogen production is a promising technology in energy sector [353–355]. The synergistic design of photo-thermo-chemical catalytic process is critical important to improve the water splitting reaction. By effective light absorption and energy confinement, plasmonic catalysts show great potential to improve the reaction via photocatalytic and/or photoelectrochemical catalysis [41,356–358]. Such enhancement mainly functions in three pathways, i.e., hot carrier, electromagnetic field enhancement, and plasmon heating effect [337,359–361]. As redox reaction is the dominant reaction, the charge transfer inevitably involved in photocatalysis, and thus the charge separation and transportation of energetic carriers is critical important in driving the reaction [362,363]. Moreover, the redox reaction is also influenced by the operation temperature following Nernst equation. The plasmonic heating effect must be carefully considered in solar water splitting even it is not assumed as key role.

Solar water oxidation has been studied by use of Au/TiO$_2$ catalysts [39,364–366]. It is found that the hot holes concentrated near the hetero-junction interface play the key role for water oxidation. Density functional theory discloses the promotion role of interfacial Ti–O–Au structure for oxygen evolution, further supporting the findings [364]. Au-TiO$_2$
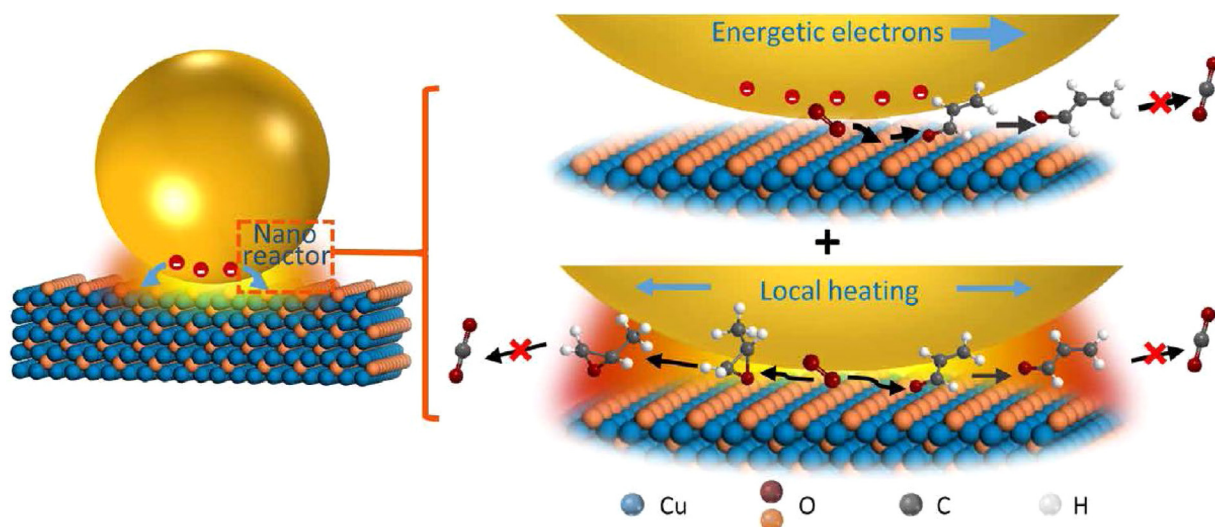
**Fig. 29.** Solar chemical synthesis. Both energetic electrons and local heating effects influence the chemical reaction of propylene over Au-Cu$_2$O catalysts.
*Source:* Reproduced with permission [141].
© 2021 AAAS.

Janus catalysts have the confined plasmon near-fields near the hetero-interface that is beneficial for visible-light-driven hydrogen generation [367]. The optical transitions of localized electronic states in TiO$_2$ are strongly coupled to the near-fields at interface, which enhances light absorption and promotes the electron–hole generation for the improved reaction. In contrast to isolated plasmonic nanostructures, the collective excitations of embedded metallic particles and composite materials demonstrate as a more effective strategy to enhance solar water splitting [8,368,369]. The hydrogen evolution from Au-nanochain increases 3.5 times in comparison with that of conventional isolated particles owing to the highly intense electromagnetic field enabled by the coupled plasmonic structure [370]. Enhanced water splitting was further verified by using gold nanoparticles/TiO$_2$/Au-film structure as the photo-electrode because that enables strong modal couplings between the F–P modes of hybrid film and the LSPR of gold particles [8].

Thermoplasmonic water splitting is similar to that of thermal catalysis by external heating [337]. However, thermo-photocatalytic water splitting is still lack of consensus in evaluating the thermal contribution to the reaction [40,371–373]. Li et al. firstly reported the hydrogen generation on TiSi$_2$ and Pt/TiO$_2$ catalysts under visible light, and found that the pressure increase is essential to produce hydrogen effectively at 190 °C [374]. The core–shell nanostructures SiO$_2$/Ag@TiO$_2$ are also designed for seawater catalysis reactions due to their excellent photothermal properties. This solar-thermal reactor is made from a quartz tube coupled with a parabolic trough concentrator for achieving high energy flux, as illustrated in Fig. 30 [303]. The plasmonic heating arising from Ag particles creates a high-temperature thermal boundary around the interfaces to trigger seawater catalysis as well as steam generation process. A field test proves the enhanced performance in dehydrogenation of oxygenates. The hydrogen generation rate reaches 13.3 mmol/h · gcat in seawater–glycerol solution at 100 °C temperatures. This result offers the direct evidence of thermoplasmonic hydrogen generation upon natural sunlight, which is promising for real seawater catalysis to produce both hydrogen and freshwater.

*4.2.4. Solar CO$_2$ reduction*

Converting carbon dioxide into high-value chemicals plays a key role in green transformation of chemical industry to fight climate change [36,377,378]. Solar transformation of CO$_2$ seems to be the most promising route to tackle this issue, since the process not only stores renewable energy in hydrocarbon form but it also leads to reduced CO$_2$ concentrations [322,377]. Since Halmann discovered the CO$_2$ reduction into organic compounds [379], growing interest has evolved worldwide in solar-to-fuel conversion, but advances on this field are still in proof-of-concept stage [380–383]. The key challenges of such process lie in the light adsorption, CO$_2$ molecule activation and the charge generation and transport towards reduction of CO$_2$ into an hydrocarbon fuel. This requires the collaborative work between electrons and active reaction sites on substrates to promote the final C-H bond formation, while simultaneously avoiding diverse side products. Recent advances brought metallic nanostructures that supporting LSPR to the forefront for enhancing the catalytic performance [37,384,385].

CO$_2$ reductions have been probed over plasmonic silver catalyst at single-particle spatial resolution [386]. The photo-generated intermediate HOCO* resulted from the interactions between surface/adsorbate and photo-excited states plays the key role for efficient production of solar fuels. Ultrafine Pt particles coated TiO$_2$ crystals exhibit extremely high photoreduction efficiency of CO$_2$ with selective formation of methane [387]. Such improvements are mainly attributed to
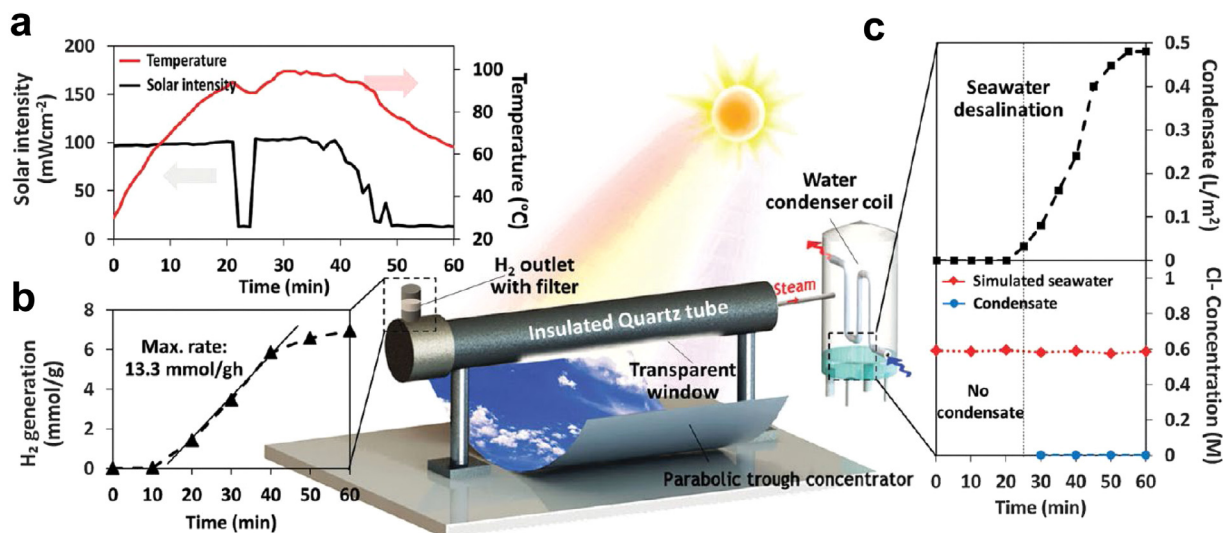
**Fig. 30.** Solar hydrogen generation (a) solar intensity and temperature, (b) hydrogen production rate, and (c) the condensate (top) and chlorine concentration (bottom).
*Source:* Reproduced with permission [303].
© 2016 Royal Society of Chemistry.

the fast carrier transport in crystals and effective charge-separation enabled by Pt particles. Thermoplasmonic catalysis has also been conducted over plasmonic catalysts with Au and Rh promoter on SAB-15 [388]. The enhanced electromagnetic near-fields offer a strong capability to activate $CH_4$ and $CO_2$, leading to selective methane conversion. Besides, several alloy particles including Au-Cu [383,389], and Cu-Ru have also been verified as catalysts for $CO_2$ reduction. The Au and/or Cu plasmonic elements are assumed for strong light absorption and efficient carrier generation, whereas the single-atom Ru offers highly active sites for the reaction [38]. Moreover, the highly selective $CO_2$ reduction also can be realized by rational design of plasmonic hetero-structure photocatalysts e.g. metal/insulator/semiconductor configuration or polar facet etc [390,391].

Compared with plasmonic catalysis, thermoplasmonic catalysis makes full spectrum use of sunlight by translating photons into heat [392–394]. Great efforts have been paid on the heating effect to boost the conversion performance [375,382,395,396]. The thermoplasmonic hydrogenation of $CO_2$ has been studied over $Pd@Nb_2O_5$ nanorod catalysts. The local temperature induced by high concentration of Pd nanoheaters reaches 470 °C, which is high enough to drive the endothermic reaction. Small Pd nanocrystals result in 99.5% selectivity towards CO with a remarkable conversion rate of 18.8 mol $h^{-1}g_{Pd}^{-1}$ [396]. Inspired by the greenhouse effect, supra-photothermal catalysts consisting of nanoporous-silica-encapsulated nickel nanocrystal ($Ni@p-SiO_2$) are recently proposed to boost $CO_2$ hydrogenation (Fig. 31) [375]. The local temperature achieved by the core/shell structure far exceeds than that of nickel catalysts (Fig. 31b). The enhanced performance mainly comes from the supra-photothermal effect at nickel core, which functions of infrared shell shielding and thermal insulation to confine the energy [375]. It should be noticed that such high temperatures might influence the optical response of nanostructure by affecting its absorption efficiency [397]. By rational design of catalyst structures, it is possible to increase or decrease the light-to-heat conversion rate depending on the system temperature.

Photothermal conversion $CO_2$ in plasmonic catalytic systems represents the convolution of multi-physical processes at a variety of timescales [15,388]. The simultaneously presence of photochemical and thermochemical processes renders thermoplasmonic conversion of solar energy a robust strategy for heterogeneous catalysis [393,398]. Initial efforts showed the potential for converting $CO_2$ and water into fuels using abundant solar energy [389,396]. Nevertheless, the understanding of behind mechanistic is still limited, the selective control of product is poor and the efficiencies are low [36,380,399].

### 4.2.5. Solar fertilizer

Fertilizer is critical to agriculture for increasing crop yield. Ammonia bringing nitrogen from air to soils and plants is an essential precursor of fertilizers [400]. Ammonia is often industrial produced by thermochemical Haber-Bosch process [401,402]. However, this process is not particularly efficient, consuming 1%–3% of the world's energy annually [403]. The N–N bond activation often needs to be operated at high temperature and pressure. This operation decreases equilibrium conversion and increases the capital costs, which stimulates researcher to consider alternative approaches for $N_2$ fixation. Solar thermo-catalytic conversion of atmospheric dinitrogen towards nitrogen products offers a sustainable approach [400,404,405]. This technology mitigates the energy and carbon footprint for ammonia synthesis, reducing
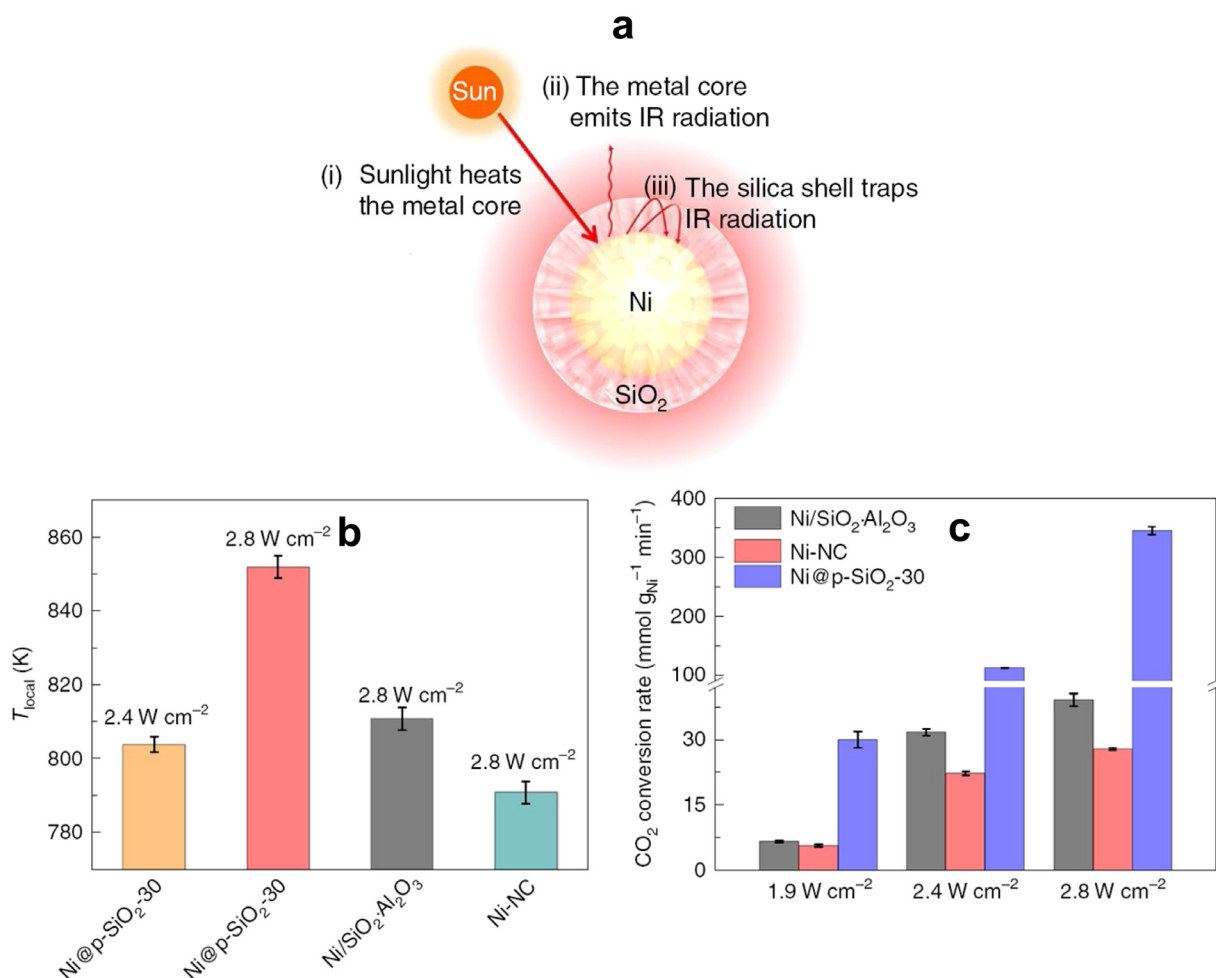
**Fig. 31.** Solar $CO_2$ reduction (a) the nanoscale greenhouse effect. (b) Estimated local temperature and (c) $CO_2$ conversion rate.
*Source:* Reproduced with permission [375].
© 2021 Nature Publishing Group.

transportation costs and integrating with existing infrastructure. But some challenges require to be overcome before real application, which includes selecting effective photocatalysts and integrating the material system for solar fertilizer within agricultural framework.

Owing to LSPR, metallic structures show great potential for enhancing the catalytic properties [153,406]. A sandwich-like nanostructured ($TiO_2$/Au/a-$TiO_2$) electrode has been fabricated to promote nitrogen fixation. Surface oxygen vacancies in outer amorphous layer (a-$TiO_2$) enhance the nitrogen adsorption and activation, promoting nitrogen transformation into ammonia by hot-electron transfer from plasmonic gold particles to semiconductor $TiO_2$ [407]. To achieve efficient light harvesting, Au and Ru particles are separately loaded on the two sides of Nb-doped $SrTiO_3$ film as co-catalyst. Such electrodes co-loaded with Au and Ru exhibited to be active for ammonia synthesis upon solar radiation [44]. The action spectrum is consistent with the plasmon band of gold particles. The same parent electrode co-loaded with gold and Zr/ZrO$_x$ has further been proposed for ammonia synthesis by plasmon-mediated charge separation [46]. In the both cases, the plasmon resonance effect is considered as major contribution to the improved performance. In addition, integrating system with photovoltaic cell is a feasible strategy to enhance the efficiency. A photoelectrochemical cell based on plasmon-enhanced black silicon has been demonstrated for nitrogen transformation to ammonia with a high yield of 13.3 mg m$^{-2}$ h$^{-1}$ under two suns [45]. This high performance is ascribed to the strong light absorption and carrier generation, the effective charge separation as well as the additional cocatalyst effect.

Ammonia synthesis reaction has a yield limit according to the equilibrium law. This is a result of the reaction balance between nitrogen dissociation and ammonia decomposition upon high operation temperature [145,408]. To surmount the thermal limit, a solar thermal avenue on K/Ru/TiO$_{2-x}$H$_x$ catalysts has been designed for ammonia synthesis (Fig. 32) [376]. The photothermal catalyst shows high absorbing ability to sunlight, resulting in a temperature increase to 360 °C due
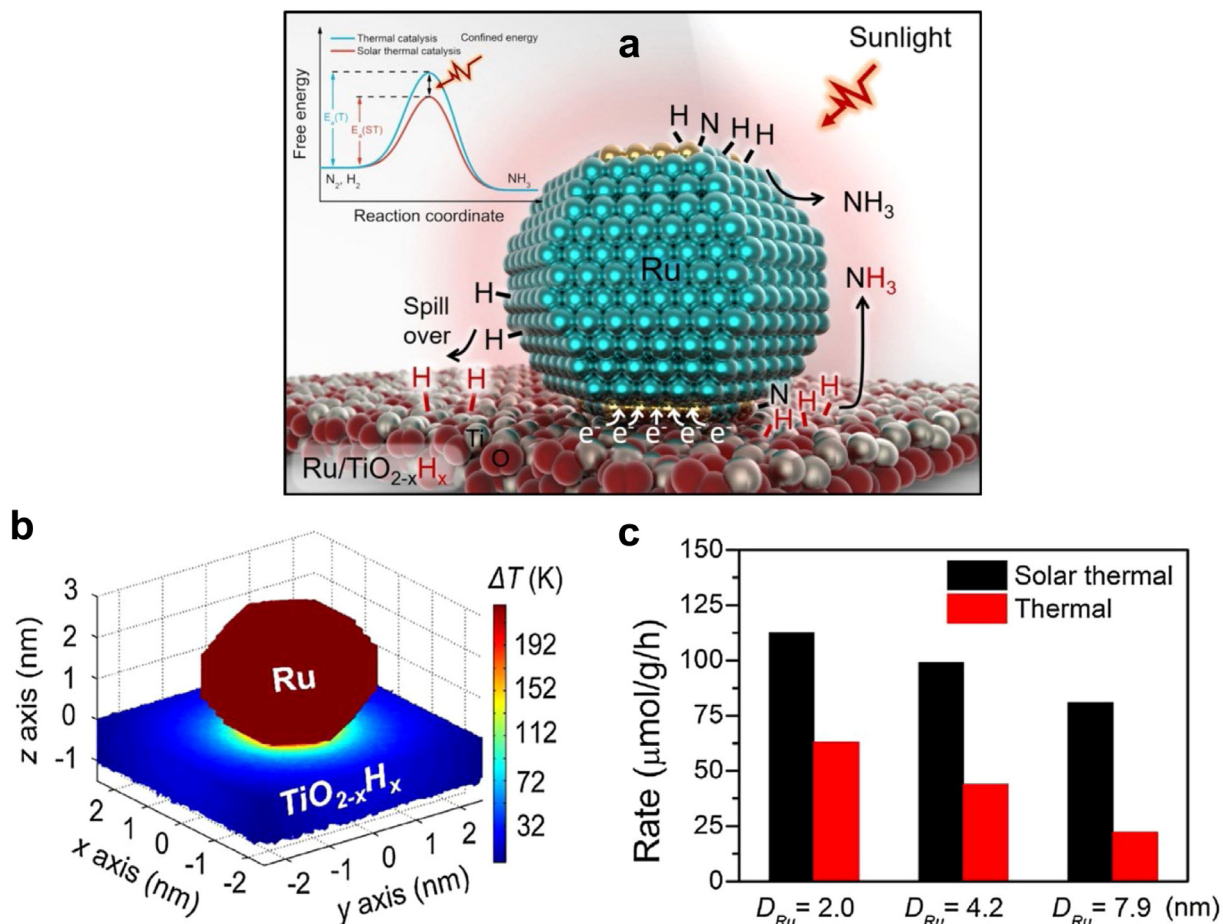
**Fig. 32.** (a) Solar ammonia synthesis. (b) Temperature profile around Ru cluster. (c) Ammonia generation rates with the catalysts of different size.
*Source:* Reproduced with permission [376].
© 2018 Elsevier.

to its effective heating effect. The decorated Ru catalyst activates nitrogen even at room temperature due to the hot-electron donation from $TiO_{2-x}H_x$. Compared to thermal catalysis, this hetero-structure confines electromagnetic field and heat flux around Ru cluster, which prominently reduces activation energy and enhances activity (Fig. 32 b and c). Recently, thermoplasmonic catalysis built on Fe-nanonecklace hydrogenated titanium hybrid has been tested to improve the performance with a dual-temperature-zone feature [145]. The apparent temperature of catalyst reaches 495 °C with a temperature difference 137 °C across the hot (Fe) and cold zone ($TiO_{2-x}H_y$). The hot zone supports hot electrons to dissociates nitrogen efficiently, while the cold zone is responsible for successive hydrogenation of the spilled-over $N$ from Fe, which thus greatly reduces the reverse shift reaction to achieve high yields beyond the theoretical equilibrium limits. These approaches pave promising scenarios for solar ammonia synthesis.

## 5. Summary and prospects

Metallic nanostructures can induce surface plasmon resonances that played as efficient nanosources of light, hot electrons and heat. They offer many advantages and unique playground for solar-to-thermal and solar-to-chemical conversions. This paper reviews recent advance in thermoplasmonics for solar energy applications. Light–matter reaction is briefly revisited for exploring the band structures versus their optical responses. Plasmon resonance is discussed with focus on basic modes of LSPR and SPP, as well as the coupling modes. Fundamentals of the plasmonic heating are distinguished as the local and collective heating effects. Heat transfer schemes including conduction, convection and radiation have been considered to detail how the dissipation energy leads to a local increase of temperature. The thermal-induced processes are elaborated on the aspects of mass transport, phase transition and stress wave, chemical reactions, refractive index variation and thermal emission. Plasmonic tuning strategies are then fully discussed in consideration of self-tunable plasmon, plasmon-coupling and active plasmons. Self-tunable plasmons are realized by tuning the constituent

material, size and shape of the component. The principles and structures of plasmon-couplings are additionally presented by control over the interparticle distance, orientation of individual components, configurations and surrounding media. Active plasmons by controlling the incident angle or use of reconfigurable matter as the surrounding medium are also considered to dynamic regulate the plasmon responses. Furthermore, various plasmonic structures and their couplings are demonstrated to collect solar energy for diverse applications. Plasmon thin film structures including nanoporous arrays, aggregated nanowire bundles, densely packed particles with random sizes and distributions are particularly highlighted for use in solar collector and radiator, thermophotovoltaic, solar desalination and sterilization, degradation and catalysis, solar fuels and fertilizers. Despite these exciting advances in thermoplasmonic science and engineering, many important points concerning the solar thermoplasmonics still need to be clear. Some suggestions are outlined below for further development of this field:

● Current works in thermoplasmonic design focus on thermal response of single structure e.g. nanosphere, nanostar, core–shell particle and nanowire. A fully understanding on the more complex geometries and structure assemblies is required for tuning the heating magnitude in the plasmonic nanostructures

● Macroscale thermal-induced processes such as mass transport, phase transition, chemical reactions or stress wave are undoubtedly evidenced in some experiments, but the real temperature of the structure is still unknown. In this sense, thermal imaging techniques relying on near-field and far-field methods may contribute to further insight.

● We should explore the influence of non-homogeneous effect of electronic structure and optical response over anisotropy geometrics on the generation of energetic carriers, and to disclose the propagation of energy stored in charge carriers over the multicomponent systems. These basic physics will tell us how the energy is created and transported over the spatial and temporal domain.

● Plasmon resonance is closely correlated with the interparticle spacing that defines the local electromagnetic field and the coupled plasmon frequencies. Precise control of the plasmon coupling offers delicate improvement on their optical and thermal responses. However, challenges still exist in precise fabrication of the coupling structures, especially in accurate controlling the distance between different components with respect to their specific orientation and positions.

● The flexible choice of stimuli and diverse structural ingredients endow the active plasmonics with high design flexibility in the field-dependent assembly or disassembly of nanoparticles. Future research should focus more on the development of novel functional materials, facile and advanced stimuli approach for constructing more efficient active structures.

● Plasmonic structures are promising for solar energy application by the confinement and manipulation of light. Plasmon component is responsible for photon absorption and confining the energy near the surface. While the supplement part serves for charge manipulation to control plasmon resonance and/or heat propagation. An appropriate modeling of complex interplays between photons, charge carriers and phonons is highly beneficial to specific applications.

● Plasmonic absorbers are beneficial to improve solar energy harvesting, and thus reducing the covering area of solar power system. For high-temperature application, solar absorbers need to run upon high-temperature condition with long-term duration. This requires use of refractory materials such as molybdenum, nickel and titanium to construct the plasmonic element and/or supporting substrate working at high temperatures. More opportunities may also exist to improve the thermal performance by use of novel materials such as composite metals, polymers, aerogels and phase change materials.

● Thermoplasmonic catalysis is an attractive supplement to photocatalysis for solar energy conversion. SPR effectively transforms low-energy photons into energetic carriers and heat to drive the desired chemical reactions. The process potentially realizes controlled reaction ways. But this design must find equilibrium between plasmonic and catalytic properties. Theoretical study of molecular behavior upon the excited plasmon states will be helpful to understand how to reduce the energy barrier and break the rate-limiting step towards the selective catalytic reaction.

In sum, thermoplasmonics turn thermal losses into an asset, which not only creates a unique set of conditions with great significance from the viewpoint of fundamental research, but also provides a promising route to facilitate light-to-thermal or chemical transformations for effective utilization of solar energy. Solar thermoplasmonic concepts involve many science fields including optics, solid physics, energy, material science, thermodynamics, and fluid dynamics, chemistry, which offers a forum for different scientific disciplines to come together and learn about the different facets of this sector. With the deepening of our understanding on thermoplasmonics, we believe that more and more unique features and new applications will be discovered in near future.

## Declaration of competing interest

The authors declare that they have no known competing financial interests or personal relationships that could have appeared to influence the work reported in this paper.

## Acknowledgments

# References

[1] A.A. Lacis, G.A. Schmidt, D. Rind, R.A. Ruedy, Atmospheric $CO_2$: Principal control knob governing earth's temperature, Science 330 (2010) 356–359.

[2] H. Ritchie, M. Roser, $CO_2$ and greenhouse gas emissions, our world in data $CO_2$ and greenhouse gas, 2020, https://ourworldindata.org/co2-and-other-greenhouse-gas-emissions.

[3] N.S. Lewis, Research opportunities to advance solar energy utilization, Science 351 (2016) aad1920.

[4] Renewable Energy Market Update, Outlook for 2020 and 2021, http://www.iea.org/.

[5] L.A. Weinstein, J. Loomis, B. Bhatia, D.M. Bierman, E.N. Wang, G. Chen, Concentrating solar power, Chem. Rev. 115 (2015) 12797–12838.

[6] D. Erickson, D. Sinton, D. Psaltis, Optofluidics for energy applications, Nat. Photonics 5 (2011) 583–590.

[7] P. Christopher, H. Xin, S. Linic, Visible-light-enhanced catalytic oxidation reactions on plasmonic silver nanostructures, Nature Chem. 3 (2011) 467–472.

[8] X. Shi, K. Ueno, T. Oshikiri, Q. Sun, K. Sasaki, H. Misawa, Enhanced water splitting under modal strong coupling conditions, Nature Nanotechnol. 13 (2018) 953–958.

[9] C.F. William C. Chueh, Mandy Abbott, Danien Scipio, Philipp Furler, Sossina M. Haile, Aldo Steinfeld, High-flux solar-driven thermochemical dissociation of $CO_2$ and $H_2O$ using nonstoichiometric ceria, Science 330 (2010) 1787–1797.

[10] P. Tao, G. Ni, C. Song, W. Shang, J. Wu, J. Zhu, G. Chen, T. Deng, Solar-driven interfacial evaporation, Nat. Energy 3 (2018) 1031–1041.

[11] E. Kazuma, J. Jung, H. Ueba, M. Trenary, Y. Kim, Real-space and real-time observation of a plasmon-induced chemical reaction of a single molecule, Science 360 (2018) 521–526.

[12] G. Baffou, F. Cichos, R. Quidant, Applications and challenges of thermoplasmonics, Nature Mater. 19 (2020) 946–958.

[13] D. Shin, G. Kang, P. Gupta, S. Behera, H. Lee, A.M. Urbas, W. Park, K. Kim, Thermoplasmonic and photothermal metamaterials for solar energy applications, Adv. Opt. Mater. 6 (2018) 1800317.

[14] S. Linic, P. Christopher, D.B. Ingram, Plasmonic-metal nanostructures for efficient conversion of solar to chemical energy, Nature Mater. 10 (2011) 911–921.

[15] M.L. Brongersma, N.J. Halas, P. Nordlander, Plasmon-induced hot carrier science and technology, Nature Nanotechnol. 10 (2015) 25–34.

[16] S. Linic, S. Chavez, R. Elias, Flow and extraction of energy and charge carriers in hybrid plasmonic nanostructures, Nature Mater. 20 (2021) 916–924.

[17] P.V. Kamat, G.V. Hartland, Plasmons for energy conversion, ACS Energy Lett. 3 (2018) 1467–1469.

[18] Y. Li, W. Li, T. Han, X. Zheng, J. Li, B. Li, S. Fan, C.W. Qiu, Transforming heat transfer with thermal metamaterials and devices, Nat. Rev. Mater. 6 (2021) 488–507.

[19] J. Lin, J.P. Mueller, Q. Wang, G. Yuan, N. Antoniou, X.C. Yuan, F. Capasso, Polarization-controlled tunable directional coupling of surface plasmon polaritons, Science 340 (2013) 331–334.

[20] J.A. Schuller, E.S. Barnard, W. Cai, Y.C. Jun, J.S. White, M.L. Brongersma, Plasmonics for extreme light concentration and manipulation, Nature Mater. 9 (2010) 193–204.

[21] P. Dombi, Z. Pápa, J. Vogelsang, S.V. Yalunin, M. Sivis, G. Herink, S. Schäfer, P. Groß, C. Ropers, C. Lienau, Strong-field nano-optics, Rev. Modern Phys. 92 (2020).

[22] L. Jauffred, A. Samadi, H. Klingberg, P.M. Bendix, L.B. Oddershede, Plasmonic heating of nanostructures, Chem. Rev. 119 (2019) 8087–8130.

[23] G. Baffou, Thermoplasmonics Heating Metal Nanoparticles using Light, Cambridge University Press, 2017.

[24] G. Baffou, R. Quidant, F.J. Garcia de Abajo, Nanoscale control of optical heating in complex plasmonic systems, ACS Nano 4 (2010) 709–716.

[25] E.C. Garnett, W. Cai, J.J. Cha, F. Mahmood, S.T. Connor, M. Greyson Christoforo, Y. Cui, M.D. McGehee, M.L. Brongersma, Self-limited plasmonic welding of silver nanowire junctions, Nature Mater. 11 (2012) 241–249.

[26] G. Baffou, R. Quidant, Thermo-plasmonics: Using metallic nanostructures as nano-sources of heat, Laser Photonics Rev. 7 (2013) 171–187.

[27] J.G. Smith, J.A. Faucheaux, P.K. Jain, Plasmon resonances for solar energy harvesting: A mechanistic outlook, Nano Today 10 (2015) 67–80.

[28] M.S. Zielinski, J.W. Choi, T. La Grange, M. Modestino, S.M. Hashemi, Y. Pu, S. Birkhold, J.A. Hubbell, D. Psaltis, Hollow mesoporous plasmonic nanoshells for enhanced solar vapor generation, Nano Lett. 16 (2016) 2159–2167.

[29] O. Neumann, C. Feronti, A.D. Neumann, A. Dong, K. Schell, B. Lu, E. Kim, M. Quinn, S. Thompson, N. Grady, P. Nordlander, M. Oden, N.J. Halas, Compact solar autoclave based on steam generation using broadband light-harvesting nanoparticles, Proc. Natl. Acad. Sci. USA 110 (2013) 11677–11681.

[30] G. Ni, N. Miljkovic, H. Ghasemi, X. Huang, S.V. Boriskina, C.T. Lin, J. Wang, Y. Xu, M.M. Rahman, T. Zhang, G. Chen, Volumetric solar heating of nanofluids for direct vapor generation, Nano Energy 17 (2015) 290–301.

[31] L. Wang, Y. Feng, K. Wang, G. Liu, Solar water sterilization enabled by photothermal nanomaterials, Nano Energy 87 (2021) 106158.

[32] Y.H. Jang, Y.J. Jang, S. Kim, L.N. Quan, K. Chung, D.H. Kim, Plasmonic solar cells: From rational design to mechanism overview, Chem. Rev. 116 (2016) 14982–15034.

[33] W.R. Erwin, H.F. Zarick, E.M. Talbert, R. Bardhan, Light trapping in mesoporous solar cells with plasmonic nanostructures, Energy Environ. Sci. 9 (2016) 1577–1601.

[34] K. Ueno, T. Oshikiri, Q. Sun, X. Shi, H. Misawa, Solid-state plasmonic solar cells, Chem. Rev. 118 (2018) 2955–2993.

[35] T. Burger, C. Sempere, B. Roy-Layinde, A. Lenert, Present efficiencies and future opportunities in thermophotovoltaics, Joule 4 (2020) 1660–1680.

[36] Z.J. Wang, H. Song, H. Liu, J. Ye, Coupling of solar energy and thermal energy for carbon dioxide reduction: Status and prospects, Angew. Chem. 59 (2020) 8016–8035.

[37] X. Zhang, X. Li, D. Zhang, N.Q. Su, W. Yang, H.O. Everitt, J. Liu, Product selectivity in plasmonic photocatalysis for carbon dioxide hydrogenation, Nature Commun. 8 (2017) 14542.

[38] L. Zhou, J.M.P. Martirez, J. Finzel, C. Zhang, D.F. Swearer, S. Tian, H. Robatjazi, M. Lou, L. Dong, L. Henderson, P. Christopher, E.A. Carter, P. Nordlander, N.J. Halas, Light-driven methane dry reforming with single atomic site antenna-reactor plasmonic photocatalysts, Nat. Energy 5 (2020) 61–70.

[39] S. Mubeen, J. Lee, N. Singh, S. Kramer, G.D. Stucky, M. Moskovits, An autonomous photosynthetic device in which all charge carriers derive from surface plasmons, Nature Nanotechnol. 8 (2013) 247–251.

[40] K. Czelej, J.C. Colmenares, K. Jabłczyńska, K. Ćwieka, Ł. Werner, L. Gradoń, Sustainable hydrogen production by plasmonic thermophotocatalysis, Catal. Today (2021).

[41] P. Zhang, T. Wang, J. Gong, Mechanistic understanding of the plasmonic enhancement for solar water splitting, Adv. Mater. 27 (2015) 5328–5342.

[42] J. He, C. Janáky, Recent advances in solar-driven carbon dioxide conversion: Expectations versus reality, ACS Energy Lett. 5 (2020) 1996–2014.

[43] Y. Kim, J.G. Smith, P.K. Jain, Harvesting multiple electron–hole pairs generated through plasmonic excitation of Au nanoparticles, Nature Chem. 10 (2018) 763–769.

[44] T. Oshikiri, K. Ueno, H. Misawa, Plasmon-induced ammonia synthesis through nitrogen photofixation with visible light irradiation, Angew. Chem. 53 (2014) 9802–9805.

[45] M. Ali, F. Zhou, K. Chen, C. Kotzur, C. Xiao, L. Bourgeois, X. Zhang, D.R. MacFarlane, Nanostructured photoelectrochemical solar cell for nitrogen reduction using plasmon-enhanced black silicon, Nature Commun. 7 (2016) 11335.

[46] T. Oshikiri, K. Ueno, H. Misawa, Selective dinitrogen conversion to ammonia using water and visible light through plasmon-induced charge separation, Angew. Chem. 55 (2016) 3942–3946.

[47] S. Jones, Mass Transport Via Thermoplasmonics (Thesis for the Degree of Doctor of Philosophy), Department of Physics, Chalmers University of Technology, 2021.

[48] J. Guan, J.E. Park, S. Deng, M.J.H. Tan, J. Hu, T.W. Odom, Light-matter interactions in hybrid material metasurfaces, Chem. Rev. (2022) http://dx.doi.org/10.1021/acs.chemrev.2c00011.

[49] J. Lee, D.J. Jeon, J.S. Yeo, Quantum plasmonics: Energy transport through plasmonic gap, Adv. Mater. (2021) e2006606.

[50] K. Yang, X. Yao, B. Liu, B. Ren, Metallic plasmonic array structures: Principles, fabrications, properties, and applications, Adv. Mater. (2021) e2007988.

[51] J. Cunha, T.L. Guo, G. Della Valle, A.N. Koya, R. Proietti Zaccaria, A. Alabastri, Controlling light, heat, and vibrations in plasmonics and phononics, Adv. Opt. Mater. 8 (2020) 2001225.

[52] J. Pettine, S.M. Meyer, F. Medeghini, C.J. Murphy, D.J. Nesbitt, Controlling the spatial and momentum distributions of plasmonic carriers: Volume vs surface effects, ACS Nano 15 (2021) 1566–1578.

[53] Z. Gao, S. Shao, W. Gao, D. Tang, D. Tang, S. Zou, M.J. Kim, X. Xia, Morphology-invariant metallic nanoparticles with tunable plasmonic properties, ACS Nano 15 (2021) 2428–2438.

[54] D. Yoo, F. de León-Pérez, M. Pelton, I.H. Lee, D.A. Mohr, M.B. Raschke, J.D. Caldwell, L. Martín-Moreno, S.H. Oh, Ultrastrong plasmon–phonon coupling via epsilon-near-zero nanocavities, Nat. Photonics 15 (2020) 125–130.

[55] M.B. Ross, M.G. Blaber, G.C. Schatz, Using nanoscale and mesoscale anisotropy to engineer the optical response of three-dimensional plasmonic metamaterials, Nature Commun. 5 (2014) 4090.

[56] E. Prodan, A hybridization model for the plasmon response of complex nanostructures, Science 302 (2003) 419–422.

[57] M.S. Tame, K.R. McEnery, Ş.K. Özdemir, J. Lee, S.A. Maier, M.S. Kim, Quantum plasmonics, Nat. Phys. 9 (2013) 329–340.

[58] C. Kuppe, K.R. Rusimova, L. Ohnoutek, D. Slavov, V.K. Valev, Hot in plasmonics: Temperature-related concepts and applications of metal nanostructures, Adv. Opt. Mater. 8 (2019) 1901166.

[59] Luciano De Sio, Active Plasmonic Nanomaterials, CRC Press © 2016 by Taylor & Francis Group, LLC.

[60] N.J. Halas, S. Lal, W.S. Chang, S. Link, P. Nordlander, Plasmons in strongly coupled metallic nanostructures, Chem. Rev. 111 (2011) 3913–3961.

[61] O. Hess, J.B. Pendry, S.A. Maier, R.F. Oulton, J.M. Hamm, K.L. Tsakmakidis, Active nanoplasmonic meta materials, Nature Mater. 11 (2012) 573–584.

[62] B. Wang, P. Yu, W. Wang, X. Zhang, H.C. Kuo, H. Xu, Z.M. Wang, High-q plasmonic resonances: Fundamentals and applications, Adv. Opt. Mater. 9 (2021) 2001520.

[63] L. Feng, P. Huo, Y. Liang, T. Xu, Photonic metamaterial absorbers: Morphology engineering and interdisciplinary applications, Adv. Mater. 32 (2020) e1903787.

[64] M. Hertzog, B. Munkhbat, D. Baranov, T. Shegai, K. Borjesson, Enhancing vibrational light-matter coupling strength beyond the molecular concentration limit using plasmonic arrays, Nano Lett. 21 (2021) 1320–1326.

[65] J. Huang, H. Wang, Z. Qi, P. Lu, D. Zhang, B. Zhang, Z. He, H. Wang, Multifunctional metal-oxide nanocomposite thin film with plasmonic Au nanopillars embedded in magnetic $La_{0.67}Sr_{0.33}MnO_3$ matrix, Nano Lett. 21 (2021) 1032–1039.

[66] A. Teulle, M. Bosman, C. Girard, K.L. Gurunatha, M. Li, S. Mann, E. Dujardin, Multimodal plasmonics in fused colloidal networks, Nature Mater. 14 (2015) 87–94.

[67] B. Luk'yanchuk, N.I. Zheludev, S.A. Maier, N.J. Halas, P. Nordlander, H. Giessen, C.T. Chong, The Fano resonance in plasmonic nanostructures and metamaterials, Nature Mater. 9 (2010) 707–715.

[68] C. Cherqui, M.R. Bourgeois, D. Wang, G.C. Schatz, Plasmonic surface lattice resonances: Theory and computation, Acc. Chem. Res. 52 (2019) 2548–2558.

[69] D. Liu, C. Xue, Plasmonic coupling architectures for enhanced photocatalysis, Adv. Mater. (2021) e2005738.

[70] J. Chen, Z. Ye, F. Yang, Y. Yin, Plasmonic nanostructures for photothermal conversion, Small Sci. 1 (2021) 2000055.

[71] Z. Fang, X. Zhu, Plasmonics in nanostructures, Adv. Mater. 25 (2013) 3840–3856.

[72] T.X. Wenqi Zhu, Haozhu Wang, Cheng Zhang, Parag B. Deotare, Amit Agrawal, Henri J. Lezec, Surface plasmon polariton laser based on a metallic trench Fabry–Perot resonator, Sci. Adv. 3 (2017) e1700909.

[73] Y.H. Fu, J.B. Zhang, Y.F. Yu, B. Luk'yanchuk, Generating and manipulating higher order Fano resonances in dual-disk ring plasmonic nanostructures, ACS Nano 6 (2012) 5130–5137.

[74] R.B. Claire Deeb, Jérôme Plain, Anne-Laure Baudrion, Safi Jradi, Alexandre Bouhelier, Olivier Soppera, Prashant K. Jain, Libai Huang, Carole Ecoffet, Lavinia Balan, Pascal Royer, Quantitative analysis of localized surface plasmons based on molecular probing, ACS Nano 4 (2010) 4579–4586.

[75] O. Nicoletti, F. de la Pena, R.K. Leary, D.J. Holland, C. Ducati, P.A. Midgley, Three-dimensional imaging of localized surface plasmon resonances of metal nanoparticles, Nature 502 (2013) 80–84.

[76] H.H. Shin, J.J. Koo, K.S. Lee, Z.H. Kim, Chemical reactions driven by plasmon-induced hot carriers, Appl. Mater. Today 16 (2019) 112–119.

[77] P. Narang, R. Sundararaman, H.A. Atwater, Plasmonic hot carrier dynamics in solid-state and chemical systems for energy conversion, Nanophotonics 5 (2016) 96–111.

[78] Z. Zhang, C. Zhang, H. Zheng, H. Xu, Plasmon-driven catalysis on molecules and nanomaterials, Acc. Chem. Res. 52 (2019) 2506–2515.

[79] J. Cunha, T.L. Guo, A.N. Koya, A. Toma, M. Prato, G. Della Valle, A. Alabastri, R. Proietti Zaccaria, Photoinduced temperature gradients in sub-wavelength plasmonic structures: The thermoplasmonics of nanocones, Adv. Opt. Mater. 8 (2020) 2000568.

[80] A. Schirato, M. Maiuri, A. Toma, S. Fugattini, R. Proietti Zaccaria, P. Laporta, P. Nordlander, G. Cerullo, A. Alabastri, G. Della Valle, Transient optical symmetry breaking for ultrafast broadband dichroism in plasmonic metasurfaces, Nat. Photonics 14 (2020) 723–727.

[81] P.B. Guillaume Baffou, Esteban Bermúdez Ureña, Romain Quidan, Serge Monneret, Julien Polleux, Hervé Rigneault, Photoinduced heating of nanoparticle arrays, ACS Nano 7 (2013) 6478–6488.

[82] A.S.L. Theodore L. Bergman, Frank P. Incropera, David P. DeWitt, Fundamentals of Heat and Mass Transfer, eighth ed., John Wiley and Sons Inc, 2017.

[83] V.K. Pustovalov, Light-to-heat conversion and heating of single nanoparticles, their assemblies, and the surrounding medium under laser pulses, RSC Adv. 6 (2016) 81266–81289.

[84] S. Manrique-Bedoya, M. Abdul-Moqueet, P. Lopez, T. Gray, M. Disiena, A. Locker, S. Kwee, L. Tang, R.L. Hood, Y. Feng, N. Large, K.M. Mayer, Multiphysics modeling of plasmonic photothermal heating effects in gold nanoparticles and nanoparticle arrays, J. Phys. Chem. C 124 (2020) 17172–17182.

[85] M.T.C. Hugh H. Richardson, Peter J. Tandler, Pedro Hernandez, Alexander O. Govorov, Experimental and theoretical studies of light-to-heat conversion and collective heating effects in metal nanoparticle solutions, Nano Lett. 9 (2009) 1139–1146.

[86] M. Mutlu, J.H. Kang, S. Raza, D. Schoen, X. Zheng, P.G. Kik, M.L. Brongersma, Thermoplasmonic ignition of metal nanoparticles, Nano Lett. 18 (2018) 1699–1706.

[87] K.R. Berry, J.R. Dunklin, P.A. Blake, D.K. Roper, Thermal dynamics of plasmonic nanoparticle composites, J. Phys. Chem. C 119 (2015) 10550–10557.

[88] A. Yuksel, E.T. Yu, M. Cullinan, J. Murthy, Investigation of heat transfer modes in plasmonic nanoparticles, Int. J. Heat Mass Transfer 156 (2020) 119869.

[89] X. Chen, Y. Chen, M. Yan, M. Qiu, Nanosecond photothermal effects in plasmonic nanostructures, ACS Nano 6 (2012) 2550–2557.

[90] Z. Chen, X. Shan, Y. Guan, S. Wang, J.J. Zhu, N. Tao, Imaging local heating and thermal diffusion of nanomaterials with plasmonic thermal microscopy, ACS Nano 9 (2015) 11574–11581.

[91] M.N.Ö. David W. Hahn, Heat Conduction, third ed., John Wiley & Sons, Inc., 2012.

[92] M.I. Tribelsky, A.E. Miroshnichenko, Y.S. Kivshar, B.S. Luk'yanchuk, A.R. Khokhlov, Laser pulse heating of spherical metal particles, Phys. Rev. X 1 (2011).

[93] Z. Xu, Z. Li, Y. Jiang, G. Xu, M. Zhu, W.C. Law, K.T. Yong, Y. Wang, C. Yang, B. Dong, F. Xing, Recent advances in solar-driven evaporation systems, J. Mater. Chem. A 8 (2020) 25571–25600.

[94] L. Zhu, M. Gao, C.K.N. Peh, G.W. Ho, Solar-driven photothermal nanostructured materials designs and prerequisites for evaporation and catalysis applications, Mater. Horiz. 5 (2018) 323–343.

[95] J.S. Donner, G. Baffou, D. McCloskey, R. Quidant, Plasmon-assisted optofluidics, ACS Nano 5 (2011) 5457–5462.

[96] John R. Howell, M.P.M., Kyle Daun, Robert Siegel, Thermal Radiation Heat Transfer, seventh ed., CRC Press, 2021.

[97] S. Sanders, L. Zundel, W.J.M. Kort-Kamp, D.A.R. Dalvit, A. Manjavacas, Near-field radiative heat transfer eigenmodes, Phys. Rev. Lett. 126 (2021).

[98] G. Jonsson, D. Tordera, T. Pakizeh, M. Jaysankar, V. Miljkovic, L. Tong, M.P. Jonsson, A. Dmitriev, Solar transparent radiators by optical nanoantennas, Nano Lett. 17 (2017) 6766–6772.

[99] H. Sipova-Jungova, D. Andren, S. Jones, M. Kall, Nanoscale inorganic motors driven by light: Principles, realizations, and opportunities, Chem. Rev. 120 (2020) 269–287.

[100] I. Buttinoni, G. Volpe, F. Kümmel, G. Volpe, C. Bechinger, Active Brownian motion tunable by light, J. Phys.: Condens. Matter 24 (2012) 284129.

[101] B. ten Hagen, S. van Teeffelen, H. Löwen, Brownian motion of a self-propelled particle, J. Phys.: Condens. Matter 23 (2011) 194119.

[102] J. Gargiulo, T. Brick, I.L. Violi, F.C. Herrera, T. Shibanuma, P. Albella, F.G. Requejo, E. Cortés, S.A. Maier, F.D. Stefani, Understanding and reducing photothermal forces for the fabrication of Au nanoparticle dimers by optical printing, Nano Lett. 17 (2017) 5747–5755.

[103] B.J. Roxworthy, A.M. Bhuiya, S.P. Vanka, K.C. Toussaint. Jr., Understanding and controlling plasmon-induced convection, Nature Commun. 5 (2014) 3173.

[104] S. Jones, D. Andren, T.J. Antosiewicz, A. Stilgoe, H. Rubinsztein-Dunlop, M. Kall, Strong transient flows generated by thermoplasmonic bubble nucleation, ACS Nano (2020).

[105] A.N. Volkov, C. Sevilla, L.V. Zhigilei, Numerical modeling of short pulse laser interaction with Au nanoparticle surrounded by water, Appl. Surf. Sci. 253 (2007) 6394–6399.

[106] J. Lombard, J. Lam, F. Detcheverry, T. Biben, S. Merabia, Strong and fast rising pressure waves emitted by plasmonic vapor nanobubbles, Phys. Rev. Res. 3 (2021).

[107] E. Cortés, Activating plasmonic chemistry, Science 362 (2018) 28–29.

[108] U. Aslam, V.G. Rao, S. Chavez, S. Linic, Catalytic conversion of solar to chemical energy on plasmonic metal nanostructures, Nat. Catal. 1 (2018) 656–665.

[109] Y. Zhang, S. He, W. Guo, Y. Hu, J. Huang, J.R. Mulcahy, W.D. Wei, Surface-plasmon-driven hot electron photochemistry, Chem. Rev. 118 (2018) 2927–2954.

[110] B. Ciraulo, J. Garcia-Guirado, I. de Miguel, J. Ortega Arroyo, R. Quidant, Long-range optofluidic control with plasmon heating, Nature Commun. 12 (2021).

[111] L. Lin, X. Peng, M. Wang, L. Scarabelli, Z. Mao, L.M. Liz-Marzan, M.F. Becker, Y. Zheng, Light-directed reversible assembly of plasmonic nanoparticles using plasmon-enhanced thermophoresis, ACS Nano 10 (2016) 9659–9668.

[112] Z. Chen, P.S. Kollipara, H. Ding, A. Pughazhendi, Y. Zheng, Liquid optothermoelectrics: Fundamentals and applications, Langmuir : ACS J. Surfaces Colloids 37 (2021) 1315–1336.

[113] S. Liu, L. Lin, H.-B. Sun, Opto-thermophoretic manipulation, ACS Nano 15 (2021) 5925–5943.

[114] L. Lin, M. Wang, X. Peng, E.N. Lissek, Z. Mao, L. Scarabelli, E. Adkins, S. Coskun, H.E. Unalan, B.A. Korgel, L.M. Liz-Marzan, E.L. Florin, Y. Zheng, Opto-thermoelectric nanotweezers, Nat. Photonics 12 (2018) 195–201.

[115] M. Mittasch, P. Gross, M. Nestler, A.W. Fritsch, C. Iserman, M. Kar, M. Munder, A. Voigt, S. Alberti, S.W. Grill, M. Kreysing, Non-invasive perturbations of intracellular flow reveal physical principles of cell organization, Nature Cell Biol. 20 (2018) 344–351.

[116] F.C. Martin Fränzl, Hydrodynamic Manipulation of Nano-Objects By Thermo-Osmotic Flows, Cornell University, 2021.

[117] Y. Zhang, C. Min, X. Dou, X. Wang, H.P. Urbach, M.G. Somekh, X. Yuan, Plasmonic tweezers: For nanoscale optical trapping and beyond, Light, Sci. Appl. 10 (2021) 59.

[118] A.P. Bregulla, A. Würger, K. Günther, M. Mertig, F. Cichos, Thermo-osmotic flow in thin films, Phys. Rev. Lett. 116 (2016).

[119] E.J. Avital, T. Miloh, Light-induced heat-conducting micro/nano spheroidal particles and their thermoosmotic velocity fields, Int. J. Heat Mass Transfer 143 (2019) 118541.

[120] A.O. Govorov, H.H. Richardson, Generating heat with metal nanoparticles, Nano Today 2 (2007) 30–38.

[121] A.B. Taylor, A.M. Siddiquee, J.W.M. Chon, Below melting point photothermal reshaping of single gold nanorods driven by surface diffusion, ACS Nano 8 (2014) 12071–12079.

[122] G. Gonzalez-Rubio, A. Guerrero-Martinez, L.M. Liz-Marzan, Reshaping, fragmentation, and assembly of gold nanoparticles assisted by pulse lasers, Acc. Chem. Res. 49 (2016) 678–686.

[123] D. Dalacu, L. Martinu, Temperature dependence of the surface plasmon resonance of Au/SiO$_2$ nanocomposite films, Appl. Phys. Lett. 77 (2000) 4283–4285.

[124] T. Krekeler, S.S. Rout, G.V. Krishnamurthy, M. Störmer, M. Arya, A. Ganguly, D.S. Sutherland, S.I. Bozhevolnyi, M. Ritter, K. Pedersen, A.Y. Petrov, M. Eich, M. Chirumamilla, Unprecedented thermal stability of plasmonic titanium nitride films up to 1400 °C, Adv. Opt. Mater. (2021) 2100323.

[125] Y. Li, C. Lin, Z. Wu, Z. Chen, C. Chi, F. Cao, D. Mei, H. Yan, C.Y. Tso, C.Y.H. Chao, B. Huang, Solution-processed all-ceramic plasmonic metamaterials for efficient solar-thermal conversion over 100-727 degrees C, Adv. Mater. 33 (2021) e2005074.

[126] H.H. Richardson, Z.N. Hickman, A.O. Govorov, A.C. Thomas, W. Zhang, M.E. Kordesch, Thermooptical properties of gold nanoparticles embedded in ice: Characterization of heat generation and melting, Nano Letters 6 (2006) 783–788.

[127] F. Meder, G.A. Naselli, A. Sadeghi, B. Mazzolai, Remotely light-powered soft fluidic actuators based on plasmonic-driven phase transitions in elastic constraint, Adv. Mater. 31 (2019) 1905671.

[128] S. Jones, D. Andren, T.J. Antosiewicz, M. Kall, Ultrafast modulation of thermoplasmonic nanobubbles in water, Nano Lett. 19 (2019) 8294–8302.

[129] K. Metwally, S. Mensah, G. Baffou, Fluence threshold for photothermal bubble generation using plasmonic nanoparticles, J. Phys. Chem. C 119 (2015) 28586–28596.

[130] J. Lombard, T. Biben, S. Merabia, Kinetics of nanobubble generation around overheated nanoparticles, Phys. Rev. Lett. 112 (2014) 105701.

[131] Y. Wang, M.E. Zaytsev, G. Lajoinie, H.L. The, J.C.T. Eijkel, A. van den Berg, M. Versluis, B.M. Weckhuysen, X. Zhang, H.J.W. Zandvliet, D. Lohse, Giant and explosive plasmonic bubbles by delayed nucleation, Proc. Natl. Acad. Sci. 115 (2018) 7676–7681.

[132] Z. Fang, Y.R. Zhen, O. Neumann, A. Polman, F.J. Garcia de Abajo, P. Nordlander, N.J. Halas, Evolution of light-induced vapor generation at a liquid-immersed metallic nanoparticle, Nano Lett. 13 (2013) 1736–1742.

[133] O. Neumann, A.S. Urban, J. Day, S. Lal, P. Nordlander, N.J. Halas, Solar vapor generation enabled by nanoparticles, ACS Nano 7 (2013) 42–49.

[134] Y. Wang, M.E. Zaytsev, H.L. The, J.C. Eijkel, H.J. Zandvliet, X. Zhang, D. Lohse, Vapor and gas-bubble growth dynamics around laser-irradiated, water-immersed plasmonic nanoparticles, ACS Nano 11 (2017) 2045–2051.

[135] Y. Zhang, A. Prosperetti, Dynamics, heat and mass transfer of a plasmonic bubble on a solid surface, Int. J. Heat Mass Transfer 167 (2021) 120814.

[136] L. Hou, M. Yorulmaz, N.R. Verhart, M. Orrit, Explosive formation and dynamics of vapor nanobubbles around a continuously heated gold nanosphere, New J. Phys. 17 (2015) 013050.

[137] S.A. Lindley, Q. An, W.A. Goddard, 3rd, J.K. Cooper, Spatiotemporal temperature and pressure in thermoplasmonic gold nanosphere-water systems, ACS Nano 15 (2021) 6276–6288.

[138] F. Magaletti, L. Marino, C.M. Casciola, Shock wave formation in the collapse of a vapor nanobubble, Phys. Rev. Lett. 114 (2015).

[139] A. Dagallier, E. Boulais, C. Boutopoulos, R. Lachaine, M. Meunier, Multiscale modeling of plasmonic enhanced energy transfer and cavitation around laser-excited nanoparticles, Nanoscale 9 (2017) 3023–3032.

[140] G. Baffou, I. Bordacchini, A. Baldi, R. Quidant, Simple experimental procedures to distinguish photothermal from hot-carrier processes in plasmonics, Light: Sci. Appl. 9 (2020).

[141] C. Zhan, Q.X. Wang, J. Yi, L. Chen, D.Y. Wu, Y. Wang, Z.X. Xie, M. Moskovits, Z.Q. Tian, Plasmonic nanoreactors regulating selective oxidation by energetic electrons and nanoconfined thermal fields, Sci. Adv. 7 (2021) eabf0962.

[142] J. Li, S.K. Cushing, F. Meng, T.R. Senty, A.D. Bristow, N. Wu, Plasmon-induced resonance energy transfer for solar energy conversion, Nat. Photonics 9 (2015) 601–607.

[143] L. Zhou, D.F. Swearer, C. Zhang, H. Robatjazi, H. Zhao, L. Henderson, L. Dong, P. Christopher, E.A. Carter, P. Nordlander, N.J. Halas, Quantifying hot carrier and thermal contributions in plasmonic photocatalysis, Science 362 (2018) 69–72.

[144] C. Zhan, M. Moskovits, Z.-Q. Tian, Recent progress and prospects in plasmon-mediated chemical reaction, Matter 3 (2020) 42–56.

[145] C. Mao, H. Li, H. Gu, J. Wang, Y. Zou, G. Qi, J. Xu, F. Deng, W. Shen, J. Li, S. Liu, J. Zhao, L. Zhang, Beyond the thermal equilibrium limit of ammonia synthesis with dual temperature zone catalyst powered by solar light, Chem 5 (2019) 2702–2717.

[146] S. Linic, U. Aslam, C. Boerigter, M. Morabito, Photochemical transformations on plasmonic metal nanoparticles, Nature Mater. 14 (2015) 567–576.

[147] J.M.P. Martirez, J.L. Bao, E.A. Carter, First-principles insights into plasmon-induced catalysis, Annu. Rev. Phys. Chem. 72 (2021) 99–119.

[148] J.W. Hong, D.H. Wi, S.U. Lee, S.W. Han, Metal-semiconductor heteronanocrystals with desired configurations for plasmonic photocatalysis, J. Am. Chem. Soc. 138 (2016) 15766–15773.

[149] J.A. Tomko, E.L. Runnerstrom, Y.S. Wang, W. Chu, J.R. Nolen, D.H. Olson, K.P. Kelley, A. Cleri, J. Nordlander, J.D. Caldwell, O.V. Prezhdo, J.P. Maria, P.E. Hopkins, Long-lived modulation of plasmonic absorption by ballistic thermal injection, Nature Nanotechnol. 16 (2021) 47–51.

[150] K. Wu, J. Chen, J.R. McBride, T. Lian, Efficient hot-electron transfer by a plasmon-induced interfacial charge-transfer transition, Science 349 (2015) 632–635.

[151] M. Wang, M. Ye, J. Iocozzia, C. Lin, Z. Lin, Plasmon-mediated solar energy conversion via photocatalysis in noble metal/semiconductor composites, Adv. Sci. 3 (2016) 1600024.

[152] P.C.a.M. Moskovits, Hot charge carrier transmission from plasmonic nanostructures, Annu. Rev. Phys. Chem. 68 (2017) 379–398.

[153] E. Cortes, L.V. Besteiro, A. Alabastri, A. Baldi, G. Tagliabue, A. Demetriadou, P. Narang, Challenges in plasmonic catalysis, ACS Nano 14 (2020) 16202–16219.

[154] C. Zhao, Y. Liu, Y. Zhao, N. Fang, T.J. Huang, A reconfigurable plasmofluidic lens, Nature Commun. 4 (2013) 2305.

[155] E. Haque, M. Anwar Hossain, Y. Namihira, F. Ahmed, Microchannel-based plasmonic refractive index sensor for low refractive index detection, Appl. Opt. 58 (2019) 1547.

[156] D. Madaan, A. Kapoor, V.K. Sharma, Ultrahigh sensitivity plasmonic refractive-index sensor for aqueous environment, IEEE Photonics Technol. Lett. 30 (2018) 149–152.

[157] J.S. Donner, J. Morales-Dalmau, I. Alda, R. Marty, R. Quidant, Fast and transparent adaptive lens based on plasmonic heating, ACS Photonics 2 (2015) 355–360.

[158] Y. Shen, J. Zhou, T. Liu, Y. Tao, R. Jiang, M. Liu, G. Xiao, J. Zhu, Z.K. Zhou, X. Wang, C. Jin, J. Wang, Plasmonic gold mushroom arrays with refractive index sensing figures of merit approaching the theoretical limit, Nature Commun. 4 (2013) 2381.

[159] M.J. Horton, O.S. Ojambati, R. Chikkaraddy, W.M. Deacon, N. Kongsuwan, A. Demetriadou, O. Hess, J.J. Baumberg, Nanoscopy through a plasmonic nanolens, Proc. Natl. Acad. Sci. 117 (2020) 2275–2281.

[160] P.T. David Boyer, Abdelhamid Maali, Brahim Lounis, Michel Orrit, Photothermal imaging of nanometer-sized metal particles among scatterers, Science 297 (2002) 1160–1163.

[161] D.G. Baranov, Y. Xiao, I.A. Nechepurenko, A. Krasnok, A. Alù, M.A. Kats, Nanophotonic engineering of far-field thermal emitters, Nature Mater. 18 (2019) 920–930.

[162] S. Fan, Thermal photonics and energy applications, Joule 1 (2017) 264–273.

[163] J. Li, J. Wuenschell, Z. Li, S. Bera, K. Liu, R. Tang, H. Du, P.R. Ohodnicki, S. Shen, Fiber coupled near-field thermoplasmonic emission from gold nanorods at 1100 K, Small 17 (2021) 2007214.

[164] A. Lalisse, G. Tessier, J. Plain, G. Baffou, Quantifying the efficiency of plasmonic materials for near-field enhancement and photothermal conversion, J. Phys. Chem. C 119 (2015) 25518–25528.

[165] H. Kallel, R. Carminati, K. Joulain, Temperature of a nanoparticle above a substrate under radiative heating and cooling, Phys. Rev. B 95 (2017).

[166] B. Liu, W. Gong, B. Yu, P. Li, S. Shen, Perfect thermal emission by nanoscale transmission line resonators, Nano Lett. 17 (2017) 666–672.

[167] J.W. Cho, S.J. Park, S.J. Park, Y.B. Kim, Y.J. Moon, S.K. Kim, Cooling metals via gap plasmon resonance, Nano Lett. 21 (2021) 3974–3980.

[168] J. Li, B. Yu, S. Shen, Scale law of far-field thermal radiation from plasmonic metasurfaces, Phys. Rev. Lett. 124 (2020).

[169] A.C. Overvig, S.A. Mann, A. Alù, Thermal metasurfaces: Complete emission control by combining local and nonlocal light-matter interactions, Phys. Rev. X 11 (2021).

[170] N.E. Motl, A.F. Smith, C.J. DeSantis, S.E. Skrabalak, Engineering plasmonic metal colloids through composition and structural design, Chem. Soc. Rev. 43 (2014) 3823–3834.

[171] L. Wang, M. Hasanzadeh Kafshgari, M. Meunier, Optical properties and applications of plasmonic-metal nanoparticles, Adv. Funct. Mater. 30 (2020) 2005400.

[172] N. Jiang, X. Zhuo, J. Wang, Active plasmonics: Principles, structures, and applications, Chem. Rev. 118 (2018) 3054–3099.

[173] S. Lee, K. Sim, S.Y. Moon, J. Choi, Y. Jeon, J.M. Nam, S.J. Park, Controlled assembly of plasmonic nanoparticles: From static to dynamic nanostructures, Adv. Mater. (2021) e2007668.
[174] P.R. West, S. Ishii, G.V. Naik, N.K. Emani, V.M. Shalaev, A. Boltasseva, Searching for better plasmonic materials, Laser Photonics Rev. 4 (2010) 795–808.
[175] G.V. Naik, V.M. Shalaev, A. Boltasseva, Alternative plasmonic materials: Beyond gold and silver, Adv. Mater. 25 (2013) 3264–3294.
[176] U. Guler, A. Boltasseva, V.M. Shalaev, Refractory plasmonics, Science 344 (2014) 263–264.
[177] C. Ma, J. Yan, Y. Huang, C. Wang, G. Yang, The optical duality of tellurium nanoparticles for broadband solar energy harvesting and efficient photothermal conversion, Sci. Adv. 4 (2018) eaas9894.
[178] M. Rebello Sousa Dias, M.S. Leite, Alloying: A platform for metallic materials with on-demand optical response, Acc. Chem. Res. 52 (2019) 2881–2891.
[179] M. Cao, Q. Liu, M. Chen, L. Chen, D. Yang, H. Hu, L. He, G. Zhang, Q. Zhang, Fully alloying AuAg nanorods in a photothermal nano-oven: Superior plasmonic property and enhanced chemical stability, ACS Omega 3 (2018) 18623–18629.
[180] X. Li, D. Wang, Y. Zhang, L. Liu, W. Wang, Surface-ligand protected reduction on plasmonic tuning of one-dimensional $MoO_{3-x}$ nanobelts for solar steam generation, Nano Res. 13 (2020) 3025–3032.
[181] S. Ishii, R.P. Sugavaneshwar, T. Nagao, Titanium nitride nanoparticles as plasmonic solar heat transducers, J. Phys. Chem. C 120 (2016) 2343–2348.
[182] A. Manjavacas, J.G. Liu, V. Kulkarni, P. Nordlander, Plasmon-induced hot carriers in metallic nanoparticles, ACS Nano 8 (2014) 7630–7638.
[183] G.S. Javier González-Colsa, José María Saiz, Dolores Ortiz, Francisco González, Fernando Bresme, Fernando Moreno, Pablo Albella, Gold nanodoughnut as an outstanding nanoheater for photothermal applications, Opt. Express 30 (2022) 125–137.
[184] J. Qiu, M. Xie, T. Wu, D. Qin, Y. Xia, Gold nanocages for effective photothermal conversion and related applications, Chem. Sci. 11 (2020) 12955–12973.
[185] K. Bae, G. Kang, S.K. Cho, W. Park, K. Kim, W.J. Padilla, Flexible thin-film black gold membranes with ultrabroadband plasmonic nanofocusing for efficient solar vapour generation, Nature Commun. 6 (2015) 10103.
[186] S. Peng, J.M. McMahon, G.C. Schatz, S.K. Gray, Y. Sun, Reversing the size-dependence of surface plasmon resonances, Proc. Natl. Acad. Sci. 107 (2010) 14530–14534.
[187] S. Link, M.A. El-Sayed, Spectral properties and relaxation dynamics of surface plasmon electronic oscillations in gold and silver nanodots and nanorods, J. Phys. Chem. B 103 (1999) 8410–8426.
[188] E.R. Encina, E.A. Coronado, Size optimization of iron oxide@noble metal core–shell nanohybrids for photothermal applications, J. Phys. Chem. C 120 (2016) 5630–5639.
[189] V. Amendola, R. Pilot, M. Frasconi, O.M. Maragò, M.A. Iatì, Surface plasmon resonance in gold nanoparticles: A review, J. Phys.: Condens. Matter 29 (2017) 203002.
[190] Y. Seol, A.E. Carpenter, T.T. Perkins, Gold nanoparticles: Enhanced optical trapping and sensitivity coupled with significant heating, Opt. Lett. 31 (2006) 2429.
[191] E.Y. Santiago, L.V. Besteiro, X.T. Kong, M.A. Correa-Duarte, Z. Wang, A.O. Govorov, Efficiency of hot-electron generation in plasmonic nanocrystals with complex shapes: Surface-induced scattering, hot spots, and interband transitions, ACS Photonics 7 (2020) 2807–2824.
[192] G.A. Vinnacombe-Willson, N. Chiang, L. Scarabelli, Y. Hu, L.K. Heidenreich, X. Li, Y. Gong, D.T. Inouye, T.S. Fisher, P.S. Weiss, S.J. Jonas, In situ shape control of thermoplasmonic gold nanostars on oxide substrates for hyperthermia-mediated cell detachment, ACS Central Sci. 6 (2020) 2105–2116.
[193] H. Yuan, A.M. Fales, T. Vo-Dinh, Tat peptide-functionalized gold nanostars: Enhanced intracellular delivery and efficient NIR photothermal therapy using ultralow laser irradiance, J. Am. Chem. Soc. 134 (2012) 11358–11361.
[194] H. Liu, T.E. Gage, P. Singh, A. Jaiswal, R.D. Schaller, J. Tang, S.T. Park, S.K. Gray, I. Arslan, Visualization of plasmonic couplings using ultrafast electron microscopy, Nano Lett. 21 (2021) 5842–5849.
[195] B.J. Wiley, S.H. Im, Z.Y. Li, J. McLellan, A. Siekkinen, Y. Xia, Maneuvering the surface plasmon resonance of silver nanostructures through shape-controlled synthesis, J. Phys. Chem. B 110 (2006) 15666–15675.
[196] E. Ringe, M.R. Langille, K. Sohn, J. Zhang, J. Huang, C.A. Mirkin, R.P. Van Duyne, L.D. Marks, Plasmon length: A universal parameter to describe size effects in gold nanoparticles, J. Phys. Chem. Lett. 3 (2012) 1479–1483.
[197] B. Gao, G. Arya, A.R. Tao, Self-orienting nanocubes for the assembly of plasmonic nanojunctions, Nature Nanotechnol. 7 (2012) 433–437.
[198] M. Ha, S.H. Nam, K. Sim, S.E. Chong, J. Kim, Y. Kim, Y. Lee, J.M. Nam, Highly efficient photothermal therapy with cell-penetrating peptide-modified bumpy Au triangular nanoprisms using low laser power and low probe dose, Nano Lett. 21 (2021) 731–739.
[199] G. Baffou, C. Girard, R. Quidant, Mapping heat origin in plasmonic structures, Phys. Rev. Lett. 104 (2010) 136805.
[200] J. Reguera, J. Langer, D. Jimenez de Aberasturi, L.M. Liz-Marzan, Anisotropic metal nanoparticles for surface enhanced Raman scattering, Chem. Soc. Rev. 46 (2017) 3866–3885.
[201] J. Pettine, P. Choo, F. Medeghini, T.W. Odom, D.J. Nesbitt, Plasmonic nanostar photocathodes for optically-controlled directional currents, Nature Commun. 11 (2020).
[202] C. Rossner, T.A.F. König, A. Fery, Plasmonic properties of colloidal assemblies, Adv. Opt. Mater. 9 (2021) 2001869.
[203] L. Lermusiaux, V. Many, P. Barois, V. Ponsinet, S. Ravaine, E. Duguet, M. Treguer-Delapierre, A. Baron, Toward huygens' sources with dodecahedral plasmonic clusters, Nano Lett. 21 (2021) 2046–2052.
[204] L.O. Herrmann, V.K. Valev, C. Tserkezis, J.S. Barnard, S. Kasera, O.A. Scherman, J. Aizpurua, J.J. Baumberg, Threading plasmonic nanoparticle strings with light, Nature Commun. 5 (2014) 4568.
[205] V. Myroshnychenko, J. Rodríguez-Fernández, I. Pastoriza-Santos, A.M. Funston, C. Novo, P. Mulvaney, L.M. Liz-Marzán, F.J. García de Abajo, Modelling the optical response of gold nanoparticles, Chem. Soc. Rev. 37 (2008) 1792.
[206] K.H. Su, Q.H. Wei, X. Zhang, J.J. Mock, D.R. Smith, S. Schultz, Interparticle coupling effects on plasmon resonances of nanogold particles, Nano Lett. 3 (2003) 1087–1090.
[207] I. Romero, J. Aizpurua, G.W. Bryant, F.J. García De Abajo, Plasmons in nearly touching metallic nanoparticles: singular response in the limit of touching dimers, Opt. Express 14 (2006) 9988.
[208] A. Sanchot, G. Baffou, R. Marty, A. Arbouet, R. Quidant, C. Girard, E. Dujardin, Plasmonic nanoparticle networks for light and heat concentration, ACS Nano 6 (2012) 3434–3440.
[209] L. Zhou, Y. Tan, J. Wang, W. Xu, Y. Yuan, W. Cai, S. Zhu, J. Zhu, 3D self-assembly of aluminium nanoparticles for plasmon-enhanced solar desalination, Nat. Photonics 10 (2016) 393–398.
[210] Y. Liu, S. Yu, R. Feng, A. Bernard, Y. Liu, Y. Zhang, H. Duan, W. Shang, P. Tao, C. Song, T. Deng, A bioinspired, reusable, paper-based system for high-performance large-scale evaporation, Adv. Mater. 27 (2015) 2768–2774.
[211] M. Zhu, Y. Li, F. Chen, X. Zhu, J. Dai, Y. Li, Z. Yang, X. Yan, J. Song, Y. Wang, E. Hitz, W. Luo, M. Lu, B. Yang, L. Hu, Plasmonic wood for high-efficiency solar steam generation, Adv. Energy Mater. 8 (2018) 1701028.
[212] L. Tian, J. Luan, K.K. Liu, Q. Jiang, S. Tadepalli, M.K. Gupta, R.R. Naik, S. Singamaneni, Plasmonic biofoam: A versatile optically active material, Nano Lett. 16 (2016) 609–616.

[213] L. Zhou, Y. Tan, D. Ji, B. Zhu, P. Zhang, J. Xu, Q. Gan, Z. Yu, J. Zhu, Self-assembly of highly efficient, broadband plasmonic absorbers for solar steam generation, Sci. Adv. 2 (2016) e1501227.

[214] J.A. Bordley, N. Hooshmand, M.A. El-Sayed, The coupling between gold or silver nanocubes in their homo-dimers: A new coupling mechanism at short separation distances, Nano Lett. 15 (2015) 3391–3397.

[215] J.J. Baumberg, J. Aizpurua, M.H. Mikkelsen, D.R. Smith, Extreme nanophotonics from ultrathin metallic gaps, Nature Mater. 18 (2019) 668–678.

[216] R. Jiang, F. Qin, Y. Liu, X.Y. Ling, J. Guo, M. Tang, S. Cheng, J. Wang, Colloidal gold nanocups with orientation-dependent plasmonic properties, Adv. Mater. 28 (2016) 6322–6331.

[217] V.A. Tamma, Y. Cui, J. Zhou, W. Park, Nanorod orientation dependence of tunable Fano resonance in plasmonic nanorod heptamers, Nanoscale 5 (2013) 1592.

[218] N. Hooshmand, M.A. El-Sayed, Collective multipole oscillations direct the plasmonic coupling at the nanojunction interfaces, Proc. Natl. Acad. Sci. 116 (2019) 19299–19304.

[219] S. Farooq, D. Rativa, R.E. de Araujo, Orientation effects on plasmonic heating of near-infrared colloidal gold nanostructures, Plasmonics 15 (2020) 1507–1515.

[220] R. Pardehkhorram, S. Bonaccorsi, H. Zhu, V.R. Goncales, Y. Wu, J. Liu, N.A. Lee, R.D. Tilley, J.J. Gooding, Intrinsic and well-defined second generation hot spots in gold nanobipyramids versus gold nanorods, Chem. Commun. 55 (2019) 7707–7710.

[221] C. Tabor, D. Van Haute, M.A. El-Sayed, Effect of orientation on plasmonic coupling between gold nanorods, ACS Nano 3 (2009) 3670–3678.

[222] A.H. El-Saeed, N.K. Allam, Refractory plasmonics: Orientation-dependent plasmonic coupling in TiN and ZrN nanocubes, Phys. Chem. Chem. Phys. 20 (2018) 1881–1888.

[223] L. Shao, C. Fang, H. Chen, Y.C. Man, J. Wang, H.Q. Lin, Distinct plasmonic manifestation on gold nanorods induced by the spatial perturbation of small gold nanospheres, Nano Lett. 12 (2012) 1424–1430.

[224] L. Meng, R. Yu, M. Qiu, F.J. Garcia de Abajo, Plasmonic nano-oven by concatenation of multishell photothermal enhancement, ACS Nano 11 (2017) 7915–7924.

[225] N. Hooshmand, J.A. Bordley, M.A. El-Sayed, The sensitivity of the distance dependent plasmonic coupling between two nanocubes to their orientation: Edge-to-edge versus face-to-face, J. Phys. Chem. C 120 (2016) 4564–4570.

[226] M.A. Mahmoud, M. Chamanzar, A. Adibi, M.A. El-Sayed, Effect of the dielectric constant of the surrounding medium and the substrate on the surface plasmon resonance spectrum and sensitivity factors of highly symmetric systems: Silver nanocubes, J. Am. Chem. Soc. 134 (2012) 6434–6442.

[227] M. ElKabbash, A. Sousa-Castillo, Q. Nguyen, R. Mariño-Fernández, N. Hoffman, M.A. Correa-Duarte, G. Strangi, Tunable black gold: Controlling the near-field coupling of immobilized au nanoparticles embedded in mesoporous silica capsules, Adv. Opt. Mater. 5 (2017) 1700617.

[228] Z. Wang, X. Quan, Z. Zhang, P. Cheng, Optical absorption of carbon-gold core–shell nanoparticles, J. Quant. Spectrosc. Radiat. Transfer 205 (2018) 291–298.

[229] M. Ha, J.H. Kim, M. You, Q. Li, C. Fan, J.M. Nam, Multicomponent plasmonic nanoparticles: From heterostructured nanoparticles to colloidal composite nanostructures, Chem. Rev. 119 (2019) 12208–12278.

[230] X. Huang, S. Tang, B. Liu, B. Ren, N. Zheng, Enhancing the photothermal stability of plasmonic metal nanoplates by a core–shell architecture, Adv. Mater. 23 (2011) 3420–3425.

[231] A. Alkurdi, J. Lombard, F. Detcheverry, S. Merabia, Enhanced heat transfer with metal-dielectric core–shell nanoparticles, Phys. Rev. A 13 (2020).

[232] T. Shegai, Z. Li, T. Dadosh, Z. Zhang, H. Xu, G. Haran, Managing light polarization via plasmon-molecule interactions within an asymmetric metal nanoparticle trimer, Proc. Natl. Acad. Sci. 105 (2008) 16448–16453.

[233] M.B. Ross, C.A. Mirkin, G.C. Schatz, Optical properties of one-, two-, and three-dimensional arrays of plasmonic nanostructures, J. Phys. Chem. C 120 (2016) 816–830.

[234] P.K. Jain, W. Huang, M.A. El-Sayed, On the universal scaling behavior of the distance decay of plasmon coupling in metal nanoparticle pairs: A plasmon ruler equation, Nano Lett. 7 (2007) 2080–2088.

[235] S. Sheikholeslami, Y.W. Jun, P.K. Jain, A.P. Alivisatos, Coupling of optical resonances in a compositionally asymmetric plasmonic nanoparticle dimer, Nano Lett. 10 (2010) 2655–2660.

[236] P.R. Wiecha, M.M. Mennemanteuil, D. Khlopin, J. Martin, A. Arbouet, A. Gérard, A. Bouhelier, J. Plain, A. Cuche, Local field enhancement and thermoplasmonics in multimodal aluminum structures, Phys. Rev. B 96 (2017).

[237] Z.J. Coppens, W. Li, D.G. Walker, J.G. Valentine, Probing and controlling photothermal heat generation in plasmonic nanostructures, Nano Lett. 13 (2013) 1023–1028.

[238] K. Metwally, S. Mensah, G. Baffou, Isosbestic thermoplasmonic nanostructures, ACS Photonics 4 (2017) 1544–1551.

[239] T. Ding, V.K. Valev, A.R. Salmon, C.J. Forman, S.K. Smoukov, O.A. Scherman, D. Frenkel, J.J. Baumberg, Light-induced actuating nanotransducers, Proc. Natl. Acad. Sci. 113 (2016) 5503–5507.

[240] Z. Qian, D.S. Ginger, Reversibly reconfigurable colloidal plasmonic nanomaterials, J. Am. Chem. Soc. 139 (2017) 5266–5276.

[241] X. Duan, N. Liu, Magnesium for dynamic nanoplasmonics, Acc. Chem. Res. 52 (2019) 1979–1989.

[242] Z. Li, Y. Yin, Stimuli-responsive optical nanomaterials, Adv. Mater. 31 (2019) 1807061.

[243] Y. Montelongo, D. Sikdar, Y. Ma, A.J.S. McIntosh, L. Velleman, Anthony R. Kucernak, J.B. Edel, A.A. Kornyshev, Electrotunable nanoplasmonic liquid mirror, Nature Mater. 16 (2017) 1127–1135.

[244] S. Khatua, W.S. Chang, P. Swanglap, J. Olson, S. Link, Active modulation of nanorod plasmons, Nano Lett. 11 (2011) 3797–3802.

[245] M.S. Ergoktas, G. Bakan, E. Kovalska, L.W. Le Fevre, R.P. Fields, P. Steiner, X. Yu, O. Salihoglu, S. Balci, V.I. Fal'ko, K.S. Novoselov, R.A.W. Dryfe, C. Kocabas, Multispectral graphene-based electro-optical surfaces with reversible tunability from visible to microwave wavelengths, Nat. Photonics 15 (2021) 493–498.

[246] A. Kuzyk, R. Schreiber, H. Zhang, A.O. Govorov, T. Liedl, N. Liu, Reconfigurable 3D plasmonic metamolecules, Nature Mater. 13 (2014) 862–866.

[247] L. Liu, R. Aleisa, Y. Zhang, J. Feng, Y. Zheng, Y. Yin, W. Wang, Dynamic color-switching of plasmonic nanoparticle films, Angew. Chem. Int. Edition 58 (2019) 16307–16313.

[248] T. Ding, J.J. Baumberg, Thermo-responsive plasmonic systems: Old materials with new applications, Nanoscale Adv. 2 (2020) 1410–1416.

[249] W. Lewandowski, M. Fruhnert, J. Mieczkowski, C. Rockstuhl, E. Górecka, Dynamically self-assembled silver nanoparticles as a thermally tunable metamaterial, Nature Commun. 6 (2015).

[250] A.T. Roberts, J. Yang, M.E. Reish, A. Alabastri, N.J. Halas, P. Nordlander, H.O. Everitt, Plasmonic nanoparticle-based epoxy photocuring: A deeper look, Mater. Today 27 (2019) 14–20.

[251] L. Liu, Z. Gao, B. Jiang, Y. Bai, W. Wang, Y. Yin, Reversible assembly and dynamic plasmonic tuning of ag nanoparticles enabled by limited ligand protection, Nano Lett. 18 (2018) 5312–5318.

[252] Z. Li, W. Wang, Y. Yin, Colloidal assembly and active tuning of coupled plasmonic nanospheres, Trends Chem. 2 (2020) 593–608.

[253] Z. Sun, W. Ni, Z. Yang, X. Kou, L. Li, J. Wang, PH-controlled reversible assembly and disassembly of gold nanorods, Small 4 (2008) 1287–1292.

[254] Y. Liu, X. Han, L. He, Y. Yin, Thermoresponsive assembly of charged gold nanoparticles and their reversible tuning of plasmon coupling, Angew. Chem. Int. Ed. 51 (2012) 6373–6377.

[255] G.E. Lio, G. Palermo, A. De Luca, R. Caputo, Tensile control of the thermal flow in plasmonic heaters realized on flexible substrates, J. Chem. Phys. 151 (2019) 244707.
[256] G.E. Lio, G. Palermo, R. Caputo, A. De Luca, Opto-mechanical control of flexible plasmonic materials, J. Appl. Phys. 125 (2019) 082533.
[257] G. Emanuele Lio, A. De Luca, C.P. Umeton, R. Caputo, Opto-mechanically induced thermoplasmonic response of unclonable flexible tags with hotspot fingerprint, J. Appl. Phys. 128 (2020) 093107.
[258] S.K. Cushing, N. Wu, Progress and perspectives of plasmon-enhanced solar energy conversion, J. Phys. Chem. Lett. 7 (2016) 666–675.
[259] E. Bellos, C. Tzivanidis, Alternative designs of parabolic trough solar collectors, Prog. Energy Combust. Sci. 71 (2019) 81–117.
[260] A.H. Elsheikh, S.W. Sharshir, M.E. Mostafa, F.A. Essa, M.K. Ahmed Ali, Applications of nanofluids in solar energy: A review of recent advances, Renew. Sustain. Energy Rev. 82 (2018) 3483–3502.
[261] B. Fu, J. Zhang, H. Chen, H. Guo, C. Song, W. Shang, P. Tao, T. Deng, Optical nanofluids for direct absorption-based solar-thermal energy harvesting at medium-to-high temperatures, Curr. Opin. Chem. Eng. 25 (2019) 51–56.
[262] O.Z. Sharaf, D.C. Kyritsis, E. Abu-Nada, Impact of nanofluids, radiation spectrum, and hydrodynamics on the performance of direct absorption solar collectors, Energy Convers. Manage. 156 (2018) 706–722.
[263] B.J. Lee, K. Park, T. Walsh, L. Xu, Radiative heat transfer analysis in plasmonic nanofluids for direct solar thermal absorption, J. Solar Energy Eng. 134 (2012).
[264] A.R. Mallah, M.N. Mohd Zubir, O.A. Alawi, K.M. Salim Newaz, A.B. Mohamad Badry, Plasmonic nanofluids for high photothermal conversion efficiency in direct absorption solar collectors: Fundamentals and applications, Sol. Energy Mater. Sol. Cells 201 (2019) 110084.
[265] O.Z. Sharaf, R.A. Taylor, E. Abu-Nada, On the colloidal and chemical stability of solar nanofluids: From nanoscale interactions to recent advances, Phys. Rep. 867 (2020) 1–84.
[266] C. Qin, K. Kang, I. Lee, B.J. Lee, Optimization of the spectral absorption coefficient of a plasmonic nanofluid for a direct absorption solar collector, Sol. Energy 169 (2018) 231–236.
[267] A.R. Mallah, S.N. Kazi, M.N.M. Zubir, A. Badarudin, Blended morphologies of plasmonic nanofluids for direct absorption applications, Appl. Energy 229 (2018) 505–521.
[268] C. Qin, J.B. Kim, B.J. Lee, Performance analysis of a direct-absorption parabolic-trough solar collector using plasmonic nanofluids, Renew. Energy 143 (2019) 24–33.
[269] J. Jeon, S. Park, B.J. Lee, Analysis on the performance of a flat-plate volumetric solar collector using blended plasmonic nanofluid, Sol. Energy 132 (2016) 247–256.
[270] M. Du, G.H. Tang, Plasmonic nanofluids based on gold nanorods/nanoellipsoids/nanosheets for solar energy harvesting, Sol. Energy 137 (2016) 393–400.
[271] C. Walker, E. Mitridis, T. Kreiner, H. Eghlidi, T.M. Schutzius, D. Poulikakos, Transparent metasurfaces counteracting fogging by harnessing sunlight, Nano Lett. 19 (2019) 1595–1604.
[272] X. Yin, R. Yang, G. Tan, S. Fan, Terrestrial radiative cooling: Using the cold universe as a renewable and sustainable energy source, Science 370 (2020) 786–791.
[273] J.C. Ndukaife, V.M. Shalaev, A. Boltasseva, Plasmonics-turning loss into gain, Science 351 (2016) 334–335.
[274] N. Maccaferri, Y. Zhao, T. Isoniemi, M. Iarossi, A. Parracino, G. Strangi, F. De Angelis, Hyperbolic meta-antennas enable full control of scattering and absorption of light, Nano Lett. 19 (2019) 1851–1859.
[275] J. Xu, J. Mandal, A.P. Raman, Broadband directional control of thermal emission, Science 372 (2021) 393–397.
[276] Y. Zhai, Y. Ma, S.N. David, D. Zhao, R. Lou, G. Tan, R. Yang, X. Yin, Scalable-manufactured randomized glass-polymer hybrid metamaterial for daytime radiative cooling, Science 355 (2017) 1062–1066.
[277] S.Y. Heo, G.J. Lee, D.H. Kim, Y.J. Kim, S. Ishii, M.S. Kim, T.J. Seok, B.J. Lee, H. Lee, Y.M. Song, A Janus emitter for passive heat release from enclosures, Sci. Adv. 6 (2020) eabb1906.
[278] M. Guo, L. Gao, Y. Wei, Y. Ma, Y. Jianyong, B. Ding, Solar transparent radiators based on in-plane worm-like assemblies of metal nanoparticles, Sol. Energy Mater. Sol. Cells 219 (2021) 110796.
[279] E. Mitridis, T.M. Schutzius, A. Sicher, C.U. Hail, H. Eghlidi, D. Poulikakos, Metasurfaces leveraging solar energy for icephobicity, ACS Nano 12 (2018) 7009–7017.
[280] S. Dash, J. de Ruiter, K.K. Varanasi, Photothermal trap utilizing solar illumination for ice mitigation, Sci. Adv. 4 (2018) eaat0127.
[281] H. Zhang, G. Zhao, S. Wu, Y. Alsaid, W. Zhao, X. Yan, L. Liu, G. Zou, J. Lv, X. He, Z. He, J. Wang, Solar anti-icing surface with enhanced condensate self-removing at extreme environmental conditions, Proc. Natl. Acad. Sci. 118 (2021) e2100978118.
[282] W. Li, C. Lin, W. Ma, Y. Li, F. Chu, B. Huang, S. Yao, Transparent selective photothermal coatings for antifogging applications, Cell Rep. Phys. Sci. 2 (2021) 100435.
[283] E. Mitridis, H. Lambley, S. Tröber, T.M. Schutzius, D. Poulikakos, Transparent photothermal metasurfaces amplifying superhydrophobicity by absorbing sunlight, ACS Nano 14 (2020) 11712–11721.
[284] A.A.A. Muheeb Ahmad Alkhalayfeh, Mohd Zamir Pakhuruddin, An overview of enhanced polymer solar cells with embedded plasmonic nanoparticles, Renew. Sustain. Energy Rev. 141 (2021) 110726.
[285] H.A. Atwater, A. Polman, Plasmonics for improved photovoltaic devices, Nature Mater. 9 (2010) 205–213.
[286] F. Enrichi, A. Quandt, G.C. Righini, Plasmonic enhanced solar cells: Summary of possible strategies and recent results, Renew. Sustain. Energy Rev. 82 (2018) 2433–2439.
[287] C.C. Chang, W.J.M. Kort-Kamp, J. Nogan, T.S. Luk, A.K. Azad, A.J. Taylor, D.A.R. Dalvit, M. Sykora, H.T. Chen, High-temperature refractory metasurfaces for solar thermophotovoltaic energy harvesting, Nano Lett. 18 (2018) 7665–7673.
[288] D. Fan, T. Burger, S. McSherry, B. Lee, A. Lenert, S.R. Forrest, Near-perfect photon utilization in an air-bridge thermophotovoltaic cell, Nature 586 (2020) 237–241.
[289] A. Lenert, D.M. Bierman, Y. Nam, W.R. Chan, I. Celanovic, M. Soljacic, E.N. Wang, A nanophotonic solar thermophotovoltaic device, Nature Nanotechnol. 9 (2014) 126–130.
[290] B. Yang, C. Li, Z. Wang, Q. Dai, Thermoplasmonics in solar energy conversion: Materials, nanostructured designs, and applications, Adv. Mater. 34 (2022) e2107351.
[291] V. Rinnerbauer, A. Lenert, D.M. Bierman, Y.X. Yeng, W.R. Chan, R.D. Geil, J.J. Senkevich, J.D. Joannopoulos, E.N. Wang, M. Soljačić, I. Celanovic, Metallic photonic crystal absorber-emitter for efficient spectral control in high-temperature solar thermophotovoltaics, Adv. Energy Mater. 4 (2014) 1400334.
[292] G.T. Papadakis, S. Buddhiraju, Z. Zhao, B. Zhao, S. Fan, Broadening near-field emission for performance enhancement in thermophotovoltaics, Nano Lett. 20 (2020) 1654–1661.
[293] R. St-Gelais, G.R. Bhatt, L. Zhu, S. Fan, M. Lipson, Hot carrier-based near-field thermophotovoltaic energy conversion, ACS Nano 11 (2017) 3001–3009.
[294] X. Liu, R.Z. Zhang, Z. Zhang, Near-perfect photon tunneling by hybridizing graphene plasmons and hyperbolic modes, ACS Photonics 1 (2014) 785–789.

[295] E.J. Tervo, W.A. Callahan, E.S. Toberer, M.A. Steiner, A.J. Ferguson, Solar thermoradiative-photovoltaic energy conversion, Cell Rep. Phys. Sci. 1 (2020) 100258.

[296] M. Gao, L. Zhu, C.K. Peh, G.W. Ho, Solar absorber material and system designs for photothermal water vaporization towards clean water and energy production, Energy Environ. Sci. 12 (2019) 841–864.

[297] G. Liu, T. Chen, J. Xu, G. Yao, J. Xie, Y. Cheng, Z. Miao, K. Wang, Salt-rejecting solar interfacial evaporation, Cell Rep. Phys. Sci. 2 (2021) 100310.

[298] Z. Wang, T. Horseman, A.P. Straub, N.Y. Yip, D. Li, M. Elimelech, S. Lin, Pathways and challenges for efficient solar-thermal desalination, Sci. Adv. 5 (2019) eaax0763.

[299] L. Zhang, Z. Xu, L. Zhao, B. Bhatia, Y. Zhong, S. Gong, E.N. Wang, Passive, High-efficiency thermally-localized solar desalination, Energy Environ. Sci. 14 (2021) 1771–1793.

[300] G. Liu, J. Xu, K. Wang, Solar water evaporation by black photothermal sheets, Nano Energy 41 (2017) 269–284.

[301] P.D. Dongare, A. Alabastri, S. Pedersen, K.R. Zodrow, N.J. Hogan, O. Neumann, J. Wu, T. Wang, A. Deshmukh, M. Elimelech, Q. Li, P. Nordlander, N.J. Halas, Nanophotonics-enabled solar membrane distillation for off-grid water purification, Proc. Natl. Acad. Sci. 114 (2017) 6936–6941.

[302] A. Politano, P. Argurio, G. Di Profio, V. Sanna, A. Cupolillo, S. Chakraborty, H.A. Arafat, E. Curcio, Photothermal membrane distillation for seawater desalination, Adv. Mater. 29 (2017).

[303] M. Gao, P.K.N. Connor, G.W. Ho, Plasmonic photothermic directed broadband sunlight harnessing for seawater catalysis and desalination, Energy Environ. Sci. 9 (2016) 3151–3160.

[304] Z. Wang, Y. Liu, P. Tao, Q. Shen, N. Yi, F. Zhang, Q. Liu, C. Song, D. Zhang, W. Shang, T. Deng, Bio-inspired evaporation through plasmonic film of nanoparticles at the air–water interface, Small 10 (2014) 3234–3239.

[305] X. Wang, X. He, X. Liu, G. Cheng, J. Zhu, Solar steam generation through bio-inspired interface heating of broadband-absorbing plasmonic membranes, Appl. Energy 195 (2017) 414–425.

[306] H. Liu, X. Zhang, Z. Hong, Z. Pu, Q. Yao, J. Shi, G. Yang, B. Mi, B. Yang, X. Liu, H. Jiang, X. Hu, A bioinspired capillary-driven pump for solar vapor generation, Nano Energy 42 (2017) 115–121.

[307] L. Mascaretti, A. Schirato, R. Zbořil, Š. Kment, P. Schmuki, A. Alabastri, A. Naldoni, Solar steam generation on scalable ultrathin thermoplasmonic TiN nanocavity arrays, Nano Energy 83 (2021) 105828.

[308] J. Chen, J. Feng, Z. Li, P. Xu, X. Wang, W. Yin, M. Wang, X. Ge, Y. Yin, Space-confined seeded growth of black silver nanostructures for solar steam generation, Nano Lett. 19 (2019) 400–407.

[309] Y. Yang, X. Yang, L. Fu, M. Zou, A. Cao, Y. Du, Q. Yuan, C.-H. Yan, Two-dimensional flexible bilayer Janus membrane for advanced photothermal water desalination, ACS Energy Lett. 3 (2018) 1165–1171.

[310] P.J.J. Alvarez, C.K. Chan, M. Elimelech, N.J. Halas, D. Villagran, Emerging opportunities for nanotechnology to enhance water security, Nature Nanotechnol. 13 (2018) 634–641.

[311] J. Gamage McEvoy, Z. Zhang, Antimicrobial and photocatalytic disinfection mechanisms in silver-modified photocatalysts under dark and light conditions, J. Photochem. Photobiol. C: Photochem. Rev. 19 (2014) 62–75.

[312] S. Loeb, C. Li, J.H. Kim, Solar photothermal disinfection using broadband-light absorbing gold nanoparticles and carbon black, Environ. Sci. Technol. 52 (2018) 205–213.

[313] A. Kulkarni, A. Kapley, R.S. Dhodapkar, P. Nagababu, S. Rayalu, Plasmonics driven engineered pasteurizers for solar water disinfection (SWADIS), J. Hard Mater. 369 (2019) 474–482.

[314] F. Brasili, A. Capocefalo, D. Palmieri, F. Capitani, E. Chiessi, G. Paradossi, F. Bordi, F. Domenici, Assembling patchy plasmonic nanoparticles with aggregation-dependent antibacterial activity, J. Colloid Interface Sci. 580 (2020) 419–428.

[315] J. Li, M. Du, G. Lv, L. Zhou, X. Li, L. Bertoluzzi, C. Liu, S. Zhu, J. Zhu, Interfacial solar steam generation enables fast-responsive, energy-efficient, and low-cost off-grid sterilization, Adv. Mater. 30 (2018) e1805159.

[316] S.K. Loeb, J. Kim, C. Jiang, L.S. Early, H. Wei, Q. Li, J.H. Kim, Nanoparticle enhanced interfacial solar photothermal water disinfection demonstrated in 3-D printed flow-through reactors, Environ. Sci. Technol. 53 (2019) 7621–7631.

[317] L. Zhao, B. Bhatia, L. Zhang, E. Strobach, A. Leroy, M.K. Yadav, S. Yang, T.A. Cooper, L.A. Weinstein, A. Modi, S.B. Kedare, G. Chen, E.N. Wang, A passive high-temperature high-pressure solar steam generator for medical sterilization, Joule 4 (2020) 2733–2745.

[318] H. Zhong, Z. Zhu, P. You, J. Lin, C.F. Cheung, V.L. Lu, F. Yan, C.Y. Chan, G. Li, Plasmonic and superhydrophobic self-decontaminating N95 respirators, ACS Nano 14 (2020) 8846–8854.

[319] H. Zhong, Z. Zhu, J. Lin, C.F. Cheung, V.L. Lu, F. Yan, C.Y. Chan, G. Li, Reusable and recyclable graphene masks with outstanding superhydrophobic and photothermal performances, ACS Nano 14 (2020) 6213–6221.

[320] S. Kumar, M. Karmacharya, S.R. Joshi, O. Gulenko, J. Park, G.H. Kim, Y.K. Cho, Photoactive antiviral face mask with self-sterilization and reusability, Nano Lett. 21 (2021) 337–343.

[321] A.K. Bhardwaj, A. Shukla, S. Maurya, S.C. Singh, K.N. Uttam, S. Sundaram, M.P. Singh, R. Gopal, Direct sunlight enabled photo-biochemical synthesis of silver nanoparticles and their bactericidal efficacy: Photon energy as key for size and distribution control, J. Photochem. Photobiol. B, Biol. 188 (2018) 42–49.

[322] M. Dhiman, Plasmonic nanocatalysis for solar energy harvesting and sustainable chemistry, J. Mater. Chem. A 8 (2020) 10074–10095.

[323] Z. Zhang, A. Zhao, F. Wang, J. Ren, X. Qu, Design of a plasmonic micromotor for enhanced photo-remediation of polluted anaerobic stagnant waters, Chem. Commun. 52 (2016) 5550–5553.

[324] Y. Deng, L. Tang, C. Feng, G. Zeng, J. Wang, Y. Zhou, Y. Liu, B. Peng, H. Feng, Construction of plasmonic ag modified phosphorous-doped ultrathin g-C3N4 nanosheets/BiVO4 photocatalyst with enhanced visible-near-infrared response ability for ciprofloxacin degradation, J. Hard Mater. 344 (2018) 758–769.

[325] Z. Bian, T. Tachikawa, P. Zhang, M. Fujitsuka, T. Majima, Au/TiO$_2$ superstructure-based plasmonic photocatalysts exhibiting efficient charge separation and unprecedented activity, J. Am. Chem. Soc. 136 (2014) 458–465.

[326] S.W. Verbruggen, M. Keulemans, B. Goris, N. Blommaerts, S. Bals, J.A. Martens, S. Lenaerts, Plasmonic 'rainbow' photocatalyst with broadband solar light response for environmental applications, Appl. Catal. B 188 (2016) 147–153.

[327] K.Y. Tang, J.X. Chen, E.D.R. Legaspi, C. Owh, M. Lin, I.S.Y. Tee, D. Kai, X.J. Loh, Z. Li, M.D. Regulacio, E. Ye, Gold-decorated TiO$_2$ nanofibrous hybrid for improved solar-driven photocatalytic pollutant degradation, Chemosphere 265 (2021) 129114.

[328] H.A. Ghaly, A.S. El-Kalliny, T.A. Gad-Allah, N.E.A. Abd El-Sattar, E.R. Souaya, Stable plasmonic Ag/AgCl-polyaniline photoactive composite for degradation of organic contaminants under solar light, RSC Adv. 7 (2017) 12726–12736.

[329] C. Yu, W. Zhou, L. Zhu, G. Li, K. Yang, R. Jin, Integrating plasmonic Au nanorods with dendritic like $\alpha$-Bi$_2$O$_3$/Bi$_2$O$_2$CO$_3$ heterostructures for superior visible-light-driven photocatalysis, Appl. Catal. B 184 (2016) 1–11.

[330] C. Chen, L. Zhou, J. Yu, Y. Wang, S. Nie, S. Zhu, J. Zhu, Dual functional asymmetric plasmonic structures for solar water purification and pollution detection, Nano Energy 51 (2018) 451–456.

[331] G. Baffou, R. Quidant, Nanoplasmonics for chemistry, Chem. Soc. Rev. 43 (2014) 3898–3907.

[332] H. Wei, S.K. Loeb, N.J. Halas, J.H. Kim, Plasmon-enabled degradation of organic micropollutants in water by visible-light illumination of Janus gold nanorods, Proc. Natl. Acad. Sci. 117 (2020) 15473–15481.

[333] S.C. Cai, J.J. Li, E.Q. Yu, X. Chen, J. Chen, H.P. Jia, Strong photothermal effect of plasmonic pt nanoparticles for efficient degradation of volatile organic compounds under solar light irradiation, ACS Appl. Nano Mater. 1 (2018) 6368–6377.

[334] X. Meng, L. Liu, S. Ouyang, H. Xu, D. Wang, N. Zhao, J. Ye, Nanometals for solar-to-chemical energy conversion: From semiconductor-based photocatalysis to plasmon-mediated photocatalysis and photo-thermocatalysis, Adv. Mater. 28 (2016) 6781–6803.

[335] E. Cortes, W. Xie, J. Cambiasso, A.S. Jermyn, R. Sundararaman, P. Narang, S. Schlucker, S.A. Maier, Plasmonic hot electron transport drives nano-localized chemistry, Nature Commun. 8 (2017) 14880.

[336] L. Mascaretti, A. Naldoni, Hot electron and thermal effects in plasmonic photocatalysis, J. Appl. Phys. 128 (2020) 041101.

[337] D. Mateo, J.L. Cerrillo, S. Durini, J. Gascon, Fundamentals and applications of photo-thermal catalysis, Chem. Soc. Rev. 50 (2021) 2173–2210.

[338] H. Huang, L. Zhang, Z. Lv, R. Long, C. Zhang, Y. Lin, K. Wei, C. Wang, L. Chen, Z.Y. Li, Q. Zhang, Y. Luo, Y. Xiong, Unraveling surface plasmon decay in core-shell nanostructures toward broadband light-driven catalytic organic synthesis, J. Am. Chem. Soc. 138 (2016) 6822–6828.

[339] Y. Sivan, Y. Dubi, Recent developments in plasmon-assisted photocatalysis- A personal perspective, Appl. Phys. Lett. 117 (2020) 130501.

[340] P. Christopher, H. Xin, A. Marimuthu, S. Linic, Singular characteristics and unique chemical bond activation mechanisms of photocatalytic reactions on plasmonic nanostructures, Nature Mater. 11 (2012) 1044–1050.

[341] C.J. Murphy, F.A. Ardy Nugroho, H. Harelind, L. Hellberg, C. Langhammer, Plasmonic temperature-programmed desorption, Nano Lett. 21 (2021) 353–359.

[342] J.R. Adleman, D.A. Boyd, D.G. Goodwin, D. Psaltis, Heterogenous catalysis mediated by plasmon heating, Nano Lett. 9 (2009) 4417–4423.

[343] F. Wang, C. Li, H. Chen, R. Jiang, L.D. Sun, Q. Li, J. Wang, J.C. Yu, C.H. Yan, Plasmonic harvesting of light energy for Suzuki coupling reactions, J. Am. Chem. Soc. 135 (2013) 5588–5601.

[344] J. Cui, Y. Li, L. Liu, L. Chen, J. Xu, J. Ma, G. Fang, E. Zhu, H. Wu, L. Zhao, L. Wang, Y. Huang, Near-infrared plasmonic-enhanced solar energy harvest for highly efficient photocatalytic reactions, Nano Lett. 15 (2015) 6295–6301.

[345] A. Naldoni, Z.A. Kudyshev, L. Mascaretti, S.P. Sarmah, S. Rej, J.P. Froning, O. Tomanec, J.E. Yoo, D. Wang, S. Kment, T. Montini, P. Fornasiero, V.M. Shalaev, P. Schmuki, A. Boltasseva, R. Zboril, Solar thermoplasmonic nanofurnace for high-temperature heterogeneous catalysis, Nano Lett. 20 (2020) 3663–3672.

[346] Q. Yang, Q. Xu, S.-H. Yu, H.L. Jiang, Pd nanocubes@ ZIF-8: Integration of plasmon-driven photothermal conversion with a metal-organic framework for efficient and selective catalysis, Angew. Chem. 128 (2016) 3749–3753.

[347] W.H. Hung, M. Aykol, D. Valley, W. Hou, S.B. Cronin, Plasmon resonant enhancement of carbon monoxide catalysis, Nano Lett. 10 (2010) 1314–1318.

[348] X. Huang, S. Tang, X. Mu, Y. Dai, G. Chen, Z. Zhou, F. Ruan, Z. Yang, N. Zheng, Freestanding palladium nanosheets with plasmonic and catalytic properties, Nature Nanotechnol. 6 (2011) 28–32.

[349] D.F. Swearer, H. Zhao, L. Zhou, C. Zhang, H. Robatjazi, J.M.P. Martirez, C.M. Krauter, S. Yazdi, M.J. McClain, E. Ringe, E.A. Carter, P. Nordlander, N.J. Halas, Heterometallic antenna-reactor complexes for photocatalysis, Proc. Natl. Acad. Sci. 113 (2016) 8916–8920.

[350] U. Aslam, S. Chavez, S. Linic, Controlling energy flow in multimetallic nanostructures for plasmonic catalysis, Nature Nanotechnol. 12 (2017) 1000–1005.

[351] A. Marimuthu, J. Zhang, S. Linic, Tuning selectivity in propylene epoxidation by plasmon mediated photo-switching of Cu oxidation state, Science 339 (2013) 1590–1593.

[352] C. Vázquez-Vázquez, B. Vaz, V. Giannini, M. Pérez-Lorenzo, R.A. Alvarez-Puebla, M.A. Correa-Duarte, Nanoreactors for simultaneous remote thermal activation and optical monitoring of chemical reactions, J. Am. Chem. Soc. 135 (2013) 13616–13619.

[353] J.H. Kim, D. Hansora, P. Sharma, J.W. Jang, J.S. Lee, Toward practical solar hydrogen production - An artificial photosynthetic leaf-to-farm challenge, Chem. Soc. Rev. 48 (2019) 1908–1971.

[354] J. Zhang, X. Jin, P.I. Morales-Guzman, X. Yu, H. Liu, H. Zhang, L. Razzari, J.P. Claverie, Engineering the absorption and field enhancement properties of Au-TiO$_2$ nanohybrids via whispering gallery mode resonances for photocatalytic water splitting, ACS Nano 10 (2016) 4496–4503.

[355] S.Y. Tee, K.Y. Win, W.S. Teo, L.D. Koh, S. Liu, C.P. Teng, M.Y. Han, Recent progress in energy-driven water splitting, Adv. Sci. 4 (2017) 1600337.

[356] S.S. Yi, X.B. Zhang, B.R. Wulan, J.M. Yan, Q. Jiang, Non-noble metals applied to solar water splitting, Energy Environ. Sci. 11 (2018) 3128–3156.

[357] S.C. Warren, E. Thimsen, Plasmonic solar water splitting, Energy Environ. Sci. 5 (2012) 5133–5146.

[358] N.L. Reddy, V.N. Rao, M. Vijayakumar, R. Santhosh, S. Anandan, M. Karthik, M.V. Shankar, K.R. Reddy, N.P. Shetti, M.N. Nadagouda, T.M. Aminabhavi, A review on frontiers in plasmonic nano-photocatalysts for hydrogen production, Int. J. Hydrogen Energy 44 (2019) 10453–10472.

[359] Y. Zhang, W. Guo, Y. Zhang, W.D. Wei, Plasmonic photoelectrochemistry: In view of hot carriers, Adv. Mater. (2021) 2006654.

[360] G. Liu, K. Du, J. Xu, G. Chen, M. Gu, C. Yang, K. Wang, H. Jakobsen, Plasmon-dominated photoelectrodes for solar water splitting, J. Mater. Chem. A 5 (2017) 4233–4253.

[361] D.V. Dao, T.T.D. Nguyen, P. Uthirakumar, Y.H. Cho, G.C. Kim, J.K. Yang, D.T. Tran, T.D. Le, H. Choi, H.Y. Kim, Y.T. Yu, I.H. Lee, Insightful understanding of hot-carrier generation and transfer in plasmonic Au@CeO$_2$ core–shell photocatalysts for light-driven hydrogen evolution improvement, Appl. Catal. B 286 (2021) 119947.

[362] J.L. Yang, Y.L. He, H. Ren, H.L. Zhong, J.S. Lin, W.M. Yang, M.D. Li, Z.L. Yang, H. Zhang, Z.Q. Tian, J.F. Li, Boosting photocatalytic hydrogen evolution reaction using dual plasmonic antennas, ACS Catal. 11 (2021) 5047–5053.

[363] Q. Wang, T. Hisatomi, Q. Jia, H. Tokudome, M. Zhong, C. Wang, Z. Pan, T. Takata, M. Nakabayashi, N. Shibata, Y. Li, I.D. Sharp, A. Kudo, T. Yamada, K. Domen, Scalable water splitting on particulate photocatalyst sheets with a solar-to-hydrogen energy conversion efficiency exceeding 1, Nature Mater. 15 (2016) 611–615.

[364] S. Wang, Y. Gao, S. Miao, T. Liu, L. Mu, R. Li, F. Fan, C. Li, Positioning the water oxidation reaction sites in plasmonic photocatalysts, J. Am. Chem. Soc. 139 (2017) 11771–11778.

[365] K. Qian, B.C. Sweeny, A.C. Johnston-Peck, W. Niu, J.O. Graham, J.S. DuChene, J. Qiu, Y.C. Wang, M.H. Engelhard, D. Su, E.A. Stach, W.D. Wei, Surface plasmon-driven water reduction: Gold nanoparticle size matters, J. Am. Chem. Soc. 136 (2014) 9842–9845.

[366] J. Lee, S. Mubeen, X. Ji, G.D. Stucky, M. Moskovits, Plasmonic photoanodes for solar water splitting with visible light, Nano Lett. 12 (2012) 5014–5019.

[367] Z.W. Seh, S. Liu, M. Low, S.Y. Zhang, Z. Liu, A. Mlayah, M.Y. Han, Janus Au-TiO$_2$ photocatalysts with strong localization of plasmonic near-fields for efficient visible-light hydrogen generation, Adv. Mater. 24 (2012) 2310–2314.

[368] K. Song, H. Lee, M. Lee, J.Y. Park, Plasmonic hot hole-driven water splitting on Au Nanoprisms/P-type GaN, ACS Energy Lett. (2021) 1333–1339.

[369] Z. Zhang, L. Zhang, M.N. Hedhili, H. Zhang, P. Wang, Plasmonic gold nanocrystals coupled with photonic crystal seamlessly on TiO$_2$ nanotube photoelectrodes for efficient visible light photoelectrochemical water splitting, Nano Lett. 13 (2013) 14–20.

[370] G. Yu, J. Qian, P. Zhang, B. Zhang, W. Zhang, W. Yan, G. Liu, Collective excitation of plasmon-coupled Au-nanochain boosts photocatalytic hydrogen evolution of semiconductor, Nature Commun. 10 (2019).

[371] N. Keller, J. Ivanez, J. Highfield, A.M. Ruppert, Photo-/thermal synergies in heterogeneous catalysis: Towards low-temperature (solar-driven) processing for sustainable energy and chemicals, Appl. Catal. B 296 (2021) 120320.

[372] S. Guo, X. Li, J. Li, B. Wei, Boosting photocatalytic hydrogen production from water by photothermally induced biphase systems, Nature Commun. 12 (2021).

[373] L. Ma, B. Luo, J. Geng, Z. Huang, L. Guo, Efficient photothermocatalytic hydrogen production performance over a graphene-titanium dioxide hybrid nanomaterial, Int. J. Hydrogen Energy 46 (2021) 2871–2877.

[374] Q. Li, G. Lu, Significant effect of pressure on the $H_2$ releasing from photothermal-catalytic water steam splitting over TiSi$_2$ and Pt/TiO$_2$, Catal. Lett. 125 (2008) 376–379.

[375] M. Cai, Z. Wu, Z. Li, L. Wang, W. Sun, A.A. Tountas, C. Li, S. Wang, K. Feng, A.-B. Xu, S. Tang, A. Tavasoli, M. Peng, W. Liu, A.S. Helmy, L. He, G.A. Ozin, X. Zhang, Greenhouse-inspired supra-photothermal CO$_2$ catalysis, Nat. Energy 6 (2021) 807–814.

[376] C. Mao, L. Yu, J. Li, J. Zhao, L. Zhang, Energy-confined solar thermal ammonia synthesis with K/Ru/TiO$_{2-x}$H$_x$, Appl. Catal. B 224 (2018) 612–620.

[377] J. He, C. Janaky, Recent advances in solar-driven carbon dioxide conversion: Expectations versus reality, ACS Energy Lett. 5 (2020) 1996–2014.

[378] H. Song, X. Meng, Z.J. Wang, H. Liu, J. Ye, Solar-energy-mediated methane conversion, Joule 3 (2019) 1606–1636.

[379] T. Inoue, A. Fujishima, S. Konishi, K. Honda, Photoelectrocatalytic reduction of carbon dioxide in aqueous suspensions of semiconductor powders, Nature 277 (1979) 637–638.

[380] S. Yu, A.J. Wilson, G. Kumari, X. Zhang, P.K. Jain, Opportunities and challenges of solar-energy-driven carbon dioxide to fuel conversion with plasmonic catalysts, ACS Energy Lett. 2 (2017) 2058–2070.

[381] U. Ulmer, T. Dingle, P.N. Duchesne, R.H. Morris, A. Tavasoli, T. Wood, G.A. Ozin, Fundamentals and applications of photocatalytic CO$_2$ methanation, Nature Commun. 10 (2019) 3169.

[382] X. Zhang, X. Li, M.E. Reish, D. Zhang, N.Q. Su, Y. Gutierrez, F. Moreno, W. Yang, H.O. Everitt, J. Liu, Plasmon-enhanced catalysis: Distinguishing thermal and nonthermal effects, Nano Lett. 18 (2018) 1714–1723.

[383] Q. Kang, T. Wang, P. Li, L. Liu, K. Chang, M. Li, J. Ye, Photocatalytic reduction of carbon dioxide by hydrous hydrazine over Au-Cu alloy nanoparticles supported on SrTiO$_3$/TiO$_2$ coaxial nanotube arrays, Angew. Chem. 54 (2015) 841–845.

[384] M. Dhiman, A. Maity, A. Das, R. Belgamwar, B. Chalke, Y. Lee, K. Sim, J.M. Nam, V. Polshettiwar, Plasmonic colloidosomes of black gold for solar energy harvesting and hotspots directed catalysis for CO$_2$ to fuel conversion, Chem. Sci. 10 (2019) 6594–6603.

[385] J.S. DuChene, G. Tagliabue, A.J. Welch, W.H. Cheng, H.A. Atwater, Hot hole collection and photoelectrochemical CO$_2$ reduction with plasmonic Au/p-GaN photocathodes, Nano Lett. 18 (2018) 2545–2550.

[386] G. Kumari, X. Zhang, D. Devasia, J. Heo, P.K. Jain, Watching visible light-driven CO$_2$ reduction on a plasmonic nanoparticle catalyst, ACS Nano 12 (2018) 8330–8340.

[387] W.N. Wang, W.J. An, B. Ramalingam, S. Mukherjee, D.M. Niedzwiedzki, S. Gangopadhyay, P. Biswas, Size and structure matter: Enhanced CO$_2$ photoreduction efficiency by size-resolved ultrafine Pt nanoparticles on TiO$_2$ single crystals, J. Am. Chem. Soc. 134 (2012) 11276–11281.

[388] H. Liu, X. Meng, T.D. Dao, H. Zhang, P. Li, K. Chang, T. Wang, M. Li, T. Nagao, J. Ye, Conversion of carbon dioxide by methane reforming under visible-light irradiation: Surface-plasmon-mediated nonpolar molecule activation, Angew. Chem. Int. Ed. 54 (2015) 11545–11549.

[389] S. Neatu, J.A. Macia-Agullo, P. Concepcion, H. Garcia, Gold-copper nanoalloys supported on TiO$_2$ as photocatalysts for CO$_2$ reduction by water, J. Am. Chem. Soc. 136 (2014) 15969–15976.

[390] R. Li, W.H. Cheng, M.H. Richter, J.S. DuChene, W. Tian, C. Li, H.A. Atwater, Unassisted highly selective gas-phase CO$_2$ reduction with a plasmonic Au/p-GaN photocatalyst using $H_2$O as an electron donor, ACS Energy Lett. 6 (2021) 1849–1856.

[391] J. Zhao, B. Liu, L. Meng, S. He, R. Yuan, Y. Hou, Z. Ding, H. Lin, Z. Zhang, X. Wang, J. Long, Plasmonic control of solar-driven CO$_2$ conversion at the metal/ZnO interfaces, Appl. Catal. B 256 (2019) 117823.

[392] X. Meng, T. Wang, L. Liu, S. Ouyang, P. Li, H. Hu, T. Kako, H. Iwai, A. Tanaka, J. Ye, Photothermal conversion of CO$_2$ into CH$_4$ with $H_2$ over group VIII nanocatalysts: An alternative approach for solar fuel production, Angew. Chem. 53 (2014) 11478–11482.

[393] M. Ghoussoub, M. Xia, P.N. Duchesne, D. Segal, G. Ozin, Principles of photothermal gas-phase heterogeneous CO$_2$ catalysis, Energy Environ. Sci. 12 (2019) 1122–1142.

[394] E.T. Kho, T.H. Tan, E. Lovell, R.J. Wong, J. Scott, R. Amal, A review on photo-thermal catalytic conversion of carbon dioxide, Green Energy Environ. 2 (2017) 204–217.

[395] Y. Li, J. Hao, H. Song, F. Zhang, X. Bai, X. Meng, H. Zhang, S. Wang, Y. Hu, J. Ye, Selective light absorber-assisted single nickel atom catalysts for ambient sunlight-driven CO$_2$ methanation, Nature Commun. 10 (2019) 2359.

[396] J. Jia, H. Wang, Z. Lu, P.G. O'Brien, M. Ghoussoub, P. Duchesne, Z. Zheng, P. Li, Q. Qiao, L. Wang, A. Gu, A.A. Jelle, Y. Dong, Q. Wang, K.K. Ghuman, T. Wood, C. Qian, Y. Shao, C. Qiu, M. Ye, Y. Zhu, Z.H. Lu, P. Zhang, A.S. Helmy, C.V. Singh, N.P. Kherani, D.D. Perovic, G.A. Ozin, Photothermal catalyst engineering: Hydrogenation of gaseous CO$_2$ with high activity and tailored selectivity, Adv. Sci. 4 (2017) 1700252.

[397] A. Alabastri, M. Malerba, E. Calandrini, A. Manjavacas, F. De Angelis, A. Toma, R. Proietti Zaccaria, Controlling the heat dissipation in temperature-matched plasmonic nanostructures, Nano Lett. 17 (2017) 5472–5480.

[398] E. Cortes, F.J. Wendisch, L. Sortino, A. Mancini, S. Ezendam, S. Saris, S.M.L. de, A. Tittl, H. Ren, S.A. Maier, Optical metasurfaces for energy conversion, Chem. Rev. (2022) http://dx.doi.org/10.1021/acs.chemrev.2c00078.

[399] X.G. Zhang, Y. Liu, C. Zhan, X. Jin, Q. Chi, D.Y. Wu, Y. Zhao, Z.Q. Tian, Reaction selectivity for plasmon-driven carbon dioxide reduction on silver clusters: A theoretical prediction, J. Phys. Chem. C 123 (2019) 11101–11108.

[400] B.M. Comer, P. Fuentes, C.O. Dimkpa, Y.H. Liu, C.A. Fernandez, P. Arora, M. Realff, U. Singh, M.C. Hatzell, A.J. Medford, Prospects and challenges for solar fertilizers, Joule 3 (2019) 1578–1605.

[401] J.G. Chen, R.M. Crooks, L.C. Seefeldt, K.L. Bren, R.M. Bullock, M.Y. Darensbourg, P.L. Holland, B. Hoffman, M.J. Janik, A.K. Jones, M.G. Kanatzidis, P. King, K.M. Lancaster, S.V. Lymar, P. Pfromm, W.F. Schneider, R.R. Schrock, Beyond fossil fuel-driven nitrogen transformations, Science 360 (2018).

[402] R. Schlogl, Catalytic synthesis of ammonia-a never-ending story? Angew. Chem. 42 (2003) 2004–2008.

[403] S.D. Minteer, P. Christopher, S. Linic, Recent developments in nitrogen reduction catalysts: A virtual issue, ACS Energy Lett. 4 (2018) 163–166.

[404] L. Wang, M. Xia, H. Wang, K. Huang, C. Qian, C.T. Maravelias, G.A. Ozin, Greening ammonia toward the solar ammonia refinery, Joule 2 (2018) 1055–1074.

[405] R.D. Richter, T. Ming, P. Davies, W. Liu, S. Caillol, Removal of non-CO$_2$ greenhouse gases by large-scale atmospheric solar photocatalysis, Prog. Energy Combust. Sci. 60 (2017) 68–96.

[406] J. Yang, Y. Guo, W. Lu, R. Jiang, J. Wang, Emerging applications of plasmons in driving CO$_2$ reduction and $N_2$ fixation, Adv. Mater. 30 (2018) e1802227.

[407] C. Li, T. Wang, Z.J. Zhao, W. Yang, J.F. Li, A. Li, Z. Yang, G.A. Ozin, J. Gong, Promoted fixation of molecular nitrogen with surface oxygen vacancies on plasmon-enhanced TiO$_2$ photoelectrodes, Angew. Chem. Int. Ed. 57 (2018) 5278–5282.

[408] X. Li, X. Zhang, H.O. Everitt, J. Liu, Light-induced thermal gradients in ruthenium catalysts significantly enhance ammonia production, Nano Lett. 19 (2019) 1706–1711.